

The Role of the  
**Subthalamic Nucleus**  
in the Basal Ganglia

Andrew Jon Gillies

PhD  
University of Edinburgh  
1995



**Declaration**

I have composed this thesis myself and it reports original research that has been conducted by myself unless otherwise indicated.

Edinburgh, 24 November 1995

Andrew Gillies

## Acknowledgements

I would like to thank David Willshaw for being a continual source of guidance and inspiration throughout the last three years. His depth and breadth of knowledge could always point me in the right direction or ward me off dangerous endeavours. He is a great supervisor, always available to listen to new ideas and provides encouragement and wisdom at exactly the right times.

I also wish to thank Gordon Arbutnott whose suggestions and knowledge of the basal ganglia were invaluable. I do not think Gordon realised how much I gained from our discussions. I always seemed to leave the Vet School with many new ideas and references that have significantly shaped the thesis.

Members of David's research group, in particular, Bruce Graham and Martin Simmen have tolerated my many questions and shared in interesting discussions for which I am thankful. I would also like to thank Rosanna for always knowing when I was stressed and for helping with the administration work load during those times.

My friends in Cognitive Science have provided much support that has kept me going over the last three years. Mercè, Ulrike, Holly, And, Possidonia, Catherine, and Alastair have always provided stimulating discussions and kept me focussed on the goals of Cognitive Science.

I wish to thank my family who always encouraged me, whatever research direction I took. In particular, Bruce and Jill who saw through the limitations of dyslexia and showed me what could be achieved.

There were four people that primarily convinced me to come to Edinburgh despite daunting financial and PhD fears. Firstly, Murray Alexander and Anthony Robins who were the source of my original interest in biological models. Secondly, Kaye Saunders and Tracey Cuthbertson who, after pushing me out of my home country, have remained friends and provided support in spite of the distance. They have all made this PhD possible, and I am deeply grateful for their support.

I also wish to thank John Wilson for providing an extended family in Edinburgh, Shari Cohn for her care and wisdom, Martin Mellor for his care and understanding, and Rob, Callum, Steve, and Fred for diversions from Cognitive Science.

Finally, I would like to thank the Committee of Vice-Chancellors and Principals of the Universities of the United Kingdom for providing financial support for this research through the Overseas Research Student Awards scheme.

## Abstract

The basal ganglia are a collection of interconnected subcortical nuclei which have been implicated in motor, cognitive and limbic functions. The subthalamic nucleus is the sole excitatory structure within the basal ganglia. Given its central position influencing many basal ganglia nuclei, it is likely to play an important role in the processing that is performed by the basal ganglia. In this thesis a theoretical analysis of the subthalamic nucleus is presented. In order to explore the multiple facets of processing that may be occurring, models that are designed to capture aspects of the subthalamic nucleus at different levels are developed. These include anatomical, network processing and single neuron multi-compartmental models. Through the integration of the results obtained from these models a new and coherent view of the processing of the subthalamic nucleus is presented.

It is predicted that the subthalamic nucleus be considered as a massively connected excitatory network. Two distinct modes of asymptotic behaviour exist in such a network: a low resting state and a high self-sustained state. The single neuron multi-compartmental model demonstrates that the calcium T-type channel is the primary determinant of characteristic neuron behaviour. Such behaviour includes a slow action potential, initial spike clustering, and a post-response quiescence. The network and single neuron results taken together provide an intrinsic mechanism for termination of uniform high activity generated by the excitatory network. It is therefore predicted that large regions of the subthalamic nucleus respond uniformly to stimuli, in the form of a pulse of activity with a sharp rise and fall. In addition, the single neuron model indicates that pulses will occur in pairs.

It is proposed that the subthalamic nucleus acts as a "braking mechanism". It can induce, via intermediate structures, a wide-spread pulse of inhibition on basal ganglia target nuclei. Furthermore, the sequence of two pulses can generate a window of disinhibition over the basal ganglia targets. The width of this time window may be under direct striatal control. Variable interpulse duration implies a role for the subthalamic nucleus in temporal processing.

# Contents

<b>1 Introduction</b>	<b>1</b>
1.1 Modelling Techniques	2
1.2 Overview of the Thesis	4
<b>2 Background Neurobiology</b>	<b>6</b>
2.1 Historical Introduction	6
2.2 Major Structures of the basal ganglia	7
2.3 Neostriatum	8
2.3.1 Cytology	9
2.3.2 Striatal Afferent Systems	13
2.3.3 Striatal Efferent Systems	14
2.3.4 Organisation	15
2.4 Globus Pallidus	16
2.4.1 Cytology	17
2.4.2 Pallidal Afferent Systems	18
2.4.3 Pallidal Efferent Systems	19
2.4.4 Organisation	20
2.5 Substantia Nigra	21
2.5.1 Cytology	21
2.5.2 Substantia Nigra Afferent Systems	22

2.5.3 Substantia Nigra Efferent Systems	24
2.6 Subthalamic Nucleus	25
2.6.1 Cytology	25
2.6.2 Subthalamic Nucleus Afferent Systems	27
2.6.3 Subthalamic Nucleus Efferent Systems	27
2.7 Summary	29
<b>3 Models of the Basal Ganglia</b>	<b>30</b>
3.1 The Pathways	30
3.1.1 Inhibition and Disinhibition	31
3.1.2 Convergent or Parallel Nuclei	34
3.1.3 Circuit Interaction	37
3.1.4 Direct and Indirect Pathways	39
3.1.5 Summary	42
3.2 From Biology to Simplified Function: The Nuclei	42
3.2.1 The Striatum	44
3.2.2 Sequential Motor Control at the Globus Pallidus	47
3.2.3 Summary	49
3.3 Disorders of the Basal Ganglia	49
3.3.1 An Introduction to Basal Ganglia Disorders	50
3.3.2 Relating the Disorders to the Anatomy	51
3.3.3 Summary	54
3.4 The Role of the STh in the Basal Ganglia	55
<b>4 Dynamic Network Model of the Subthalamic Nucleus</b>	<b>56</b>
4.1 Introduction	56
4.2 Model Derivation	57
4.2.1 Model Units	57

4.2.2	Model Form	60
4.3	Model Constraints	61
4.3.1	Connectivity	62
4.3.2	Firing Rate	73
4.3.3	Cortical Innervation	75
<b>5</b>	<b>Analysis of the Dynamic Network Model</b>	<b>76</b>
5.1	Analytical Results	77
5.1.1	Two Unit Case	78
5.1.2	$N$ Unit Case	83
5.1.3	Summary	85
5.2	Simulation Results	86
5.3	Prebifurcation System	89
5.3.1	Example 1	89
5.3.2	Example 2	91
5.3.3	Summary	93
5.4	Postbifurcation System	94
5.4.1	Example 1	94
5.4.2	Example 2	99
5.4.3	Summary	100
5.5	Discussion	100
5.5.1	Inhibitory Feedback System	102
5.5.2	Intrinsic Membrane Properties	104
<b>6</b>	<b>The Computation of Single Neurons</b>	<b>105</b>
6.1	Introduction	105
6.2	Modelling Neurons of the Subthalamic Nucleus	111
6.2.1	Morphological Considerations	112

6.2.2	Passive Electrical Membrane Properties	120
6.2.3	Membrane Channel Composition	125
6.2.4	Constraining Parameters	131
6.3	Summary: The Development and Specification of a Single Subthalamic Projection Neuron Model	136
<b>7</b>	<b>The Single Subthalamic Nucleus Projection Neuron</b>	<b>138</b>
7.1	Passive Properties	139
7.2	Fast Action Potential	142
7.3	Slow Action Potential	143
7.4	Post Response Quiet	147
7.5	Discussion	150
7.5.1	T Dominance	152
7.5.2	The STh Projection Neuron in Context	153
7.5.3	Conclusion	156
<b>8</b>	<b>The Subthalamic Nucleus Pulse</b>	<b>157</b>
8.1	The Subthalamic Nucleus Pulse Hypothesis	157
8.1.1	Intranuclear Consequences of the Pulse	158
8.1.2	The Long Term Effects of the Intrinsic Properties	160
8.1.3	Are the Intrinsic Properties Sufficient?	161
8.1.4	When Will Pulses Occur?	162
8.1.5	Summary: Artifacts of Modelling	163
8.2	The Role of the STh in the Basal Ganglia	164
8.2.1	The Pathways: Braking Theory	164
8.2.2	The Pathways: Post Brake Window	166
8.2.3	The Pathways: Contemporary Theories	168
8.3	Disorders of the Basal Ganglia	169

8.3.1	The Braking Hypothesis . . . . .	169
8.3.2	The Window Hypothesis . . . . .	171
8.4	Summary . . . . .	172
<b>9</b>	<b>Conclusion</b>	<b>173</b>
	<b>Glossary</b>	<b>176</b>
	<b>Bibliography</b>	<b>184</b>
<b>A</b>	<b>A Multi-level Neural Simulator: Rorohiko</b>	<b>192</b>
A.1	The Single Simulator Formalism . . . . .	192
A.1.1	The Electric Brain . . . . .	193
A.2	The Arbitrary Structure . . . . .	194
A.3	Afferents . . . . .	195
A.4	Conductances . . . . .	197
A.5	Input Files . . . . .	198
A.6	Optimisation . . . . .	199
A.7	Example Simulation . . . . .	199
A.7.1	sth.sim . . . . .	200
A.7.2	reference, numeric, numeric-saved, and sth.log . . . . .	201
A.7.3	setup-simple . . . . .	201
A.7.4	simple.dat . . . . .	202
A.7.5	All other files . . . . .	206
<b>B</b>	<b>Automated Numerical System Solution Search</b>	<b>208</b>
B.1	Recursive Depth Search . . . . .	208
<b>C</b>	<b>Geometric and Spatial Simulator</b>	<b>210</b>
C.1	Immersion . . . . .	211

C.2	Orientation Search . . . . .	211
C.3	Simulation . . . . .	212
C.4	Visualisation . . . . .	213
C.5	Summary . . . . .	213

## List of Figures

2.1	The major nuclei of the basal ganglia . . . . .	9
2.2	Striatal neuron types . . . . .	11
2.3	The major type of projection neuron found in the globus pallidus . . . . .	18
2.4	Neurons of the substantia nigra . . . . .	22
2.5	Two types of projection neurons found in the subthalamic nucleus . . . . .	26
2.6	A summary of the major pathways between the basal ganglia nuclei . . . . .	28
3.1	Major basal ganglia pathways . . . . .	31
3.2	Motor circuit of the basal ganglia . . . . .	36
3.3	Hikosaka model of the basal ganglia . . . . .	39
3.4	Simple model of the globus pallidus . . . . .	47
3.5	Enkephalin/substance P distinction in basal ganglia disorders . . . . .	52
4.1	The sigmoid function . . . . .	59
4.2	A self-excitatory network . . . . .	61
4.3	Position and size of the subthalamic nucleus . . . . .	63
4.4	Geometrical dendritic field and collateral field overlap diagram . . . . .	65
4.5	Example of the visual output of the geometric simulator . . . . .	66
4.6	Geometrical dendritic field and collateral field overlap . . . . .	67
4.7	Geometrical dendritic field and collateral field perpendicular overlap diagram . . . . .	68

4.8	Geometrical dendritic field and collateral field overlap with varying orientation . . . . .	69
4.9	Demonstration of the effect of collateral orientation on intersecting dendritic fields . . . . .	70
4.10	Distribution of weights . . . . .	73
4.11	Fitting the sigmoid from data . . . . .	74
5.1	A simple two-unit self-excitatory network . . . . .	78
5.2	Example phase planes of the dynamic STh network model . . . . .	79
5.3	Stable solution diagrams for the two-unit model . . . . .	80
5.4	Three characteristic model responses . . . . .	87
5.5	Comparing the effect of weak lateral connections . . . . .	90
5.6	Three dimensional response plots . . . . .	91
5.7	Effect of threshold changes in the postbifurcation system . . . . .	95
5.8	Phase planes revealing attractor sizes . . . . .	96
5.9	Inability for localised input to terminate hysteresis . . . . .	97
5.10	Three dimensional response plots illustrating stubborn hysteresis . . . . .	98
5.11	Three dimensional response plots illustrating delays destroying hysteresis . . . . .	99
5.12	The GPe acting as an inhibitory controller preventing states of hysteresis . . . . .	103
5.13	The GPe acting as an inhibitory controller leading to stable oscillations . . . . .	104
6.1	A schematic diagram of a lipid bilayer . . . . .	106
6.2	Electrical circuit diagram of the Hodgkin and Huxley (1952) model of action potentials in the squid giant axon . . . . .	107
6.3	Hodgkin and Huxley example of the S-shaped potassium conductance increase upon membrane depolarisation . . . . .	109
6.4	Hodgkin and Huxley example of the sodium conductance change upon membrane depolarisation . . . . .	110
6.5	Dendritic branching simplifications . . . . .	114
6.6	Schematic drawing of the idealised STh projection neuron . . . . .	115

6.7	Calculated lengths and diameters for the dendritic tree of the idealised STh projection neuron . . . . .	116
6.8	Two cylinder model of a STh projection neuron . . . . .	117
6.9	Compartmental model of a STh projection neuron . . . . .	118
6.10	3D reconstruction of the compartmental model of a STh projection neuron . . . . .	119
6.11	Effects of current injection into the soma of the simulated multi-compartmental neuron . . . . .	125
6.12	Goldman–Hodgkin–Katz example . . . . .	128
7.1	Multi-compartmental model passive properties . . . . .	139
7.2	Calcium T-current leads to post-hyperpolarising spikes . . . . .	141
7.3	Passive properties under conditions of simulated TTX . . . . .	142
7.4	Increasing inter-spike interval of the model . . . . .	143
7.5	The calcium current behind the increasing inter-spike interval . . . . .	144
7.6	Slow action potential . . . . .	145
7.7	Slow action potential simulated with applied TTX and TEA . . . . .	146
7.8	Ca(T) channel kinetics generating the slow action potential . . . . .	147
7.9	Post stimulus hyperpolarisation . . . . .	149
8.1	The effect of changes in sigmoid threshold . . . . .	160
A.1	The design of a dynamic neural network in the <i>Rorohiko</i> simulator . . . . .	194
A.2	The design of a multi-compartmental model in the <i>Rorohiko</i> simulator . . . . .	195
A.3	The design of a multi-compartmental model in the <i>Rorohiko</i> simulator illustrating afferents . . . . .	196
A.4	Example input file structure for the <i>Rorohiko</i> simulator . . . . .	198
A.5	Input file structure used for the dynamic model . . . . .	200
B.1	Example of sector division of phase planes . . . . .	209

## Chapter 1

# Introduction

Deep below the cerebral cortex there are interconnected areas of grey matter collectively known as the “basal ganglia” (basement structures). Recently there has been a surge of interest in these structures, both in the scientific and public arenas. Developments in anatomical and physiological techniques continue to reveal intriguing structural and chemical arrangements. In addition to this, recent developments in surgical procedures directly involving the basal ganglia are found to alleviate certain Parkinsonism symptoms (Bergman et al., 1990). However, despite the recent interest, as with much of the brain, the basal ganglia remain a mystery in both their function and processing properties.

There are a growing number of theoretical studies beginning to address possible functional roles of the basal ganglia, and indeed, making significant contributions to our understanding of the processing properties emerging from certain anatomical arrangements (reviewed in Chapter 3). Most of these focus on the major pathways and primary input or output structures. However, there is a growing realisation that smaller structures within the basal ganglia will also contribute significantly to its overall operation (Kitai & Deniau, 1981; Hikosaka, 1991; Smith et al., 1994). Very few theoretical approaches have been applied to these smaller internal structures. We therefore embark

on a theoretical analysis of one of these internal basal ganglia nuclei. We choose the subthalamic nucleus. The subthalamic nucleus is the only excitatory structure in the basal ganglia, which indicates that it has an important role to play in modulating other basal ganglia structures.

We use theoretical techniques of modelling to discern the types of processing being performed by the subthalamic nucleus. However, techniques of modelling must be applied carefully, as they can easily be too powerful or specific (this is further discussed in Section 1.1 below). We therefore have a two-fold aim:

1. The primary aim is to develop a trenchant account of how the subthalamic nucleus functions. This will take the form of analysing the processing elements, network arrangements, and inputs in order to be able to understand the role it may play in basal ganglia operation.
2. The secondary aim focuses on the development of tools to achieve the first aim efficiently. In particular we require tools and methods of modelling the subthalamic nucleus that limit the caveats of the modelling approach discussed in the following section.

## 1.1 Modelling Techniques

Modelling may be described as a simplification of a system so as to reveal how primary processing elements may generate emergent behaviours. However, this is only one of many definitions, as modelling takes many diverse forms. It is a very powerful tool that can be used to illuminate and describe in simple terms virtually any process. It is also very easy to misuse its power and render any results arbitrary. Therefore we must carefully consider how we will use the technique of modelling to maximise our confidence in its results.

One of the first requirements for modelling is that there is sufficient information about the process under investigation. Wherever possible we would like to add the further, biologically specific, constraint that we draw on experimental observations from a single species. This should eliminate artifacts caused by cross species differences. The subthalamic nucleus is one of the least studied structures of the basal ganglia. Despite increasing interest in this structure and a growing pool of experimental research, there is a significant amount of information required for the construction of models that is simply not known. To limit the effects of this problem we introduce a number of protocols. Firstly, appropriately chosen simplifications allow models to be developed without the need for certain specific details. For example, one of the most difficult properties to determine in any neural network type model of a neurobiological system is the connectivity between neurons. Detailed accounts of connectivity are unavailable. Simplifications must therefore be chosen to overcome this. We introduce layered modelling techniques in order to derive principled simplifications. These techniques involve the development of different types of models that may be used to constrain or provide valid simplifications for each other.

Secondly, parameter independent analysis should be applied wherever possible. In models defined by a tractable mathematical specification, we can apply analysis of asymptotic behaviours in order to determine the range of emergent behaviours that are possible of a particular system. Numerical simulations are also required in order to observe the transient behaviours. For more complex systems, where a mathematical analysis is intractable, we shall use the less rigorous technique of parameter searches to determine behaviour types that may exist.

Finally, if we are to use information from other brain areas or species because such information is not available in the subthalamic nucleus, we introduce a strict procedure for the incorporation of this information into the models. It is hoped the procedure will make explicit any cross species differences so that their effect may be assessed (see Section 6.2.4).



There are two primary consequences of these protocols introduced for constraining the models. Firstly, the simplifications and parameter restriction procedures will allow us to investigate only primary processing functions. For example, we will be unable to effectively model functional processing that may arise from specific connectivity arrangements. Secondly, it is hoped that as a result of the strict protocols the models will be more accurate in capturing and isolating the salient functions of the subthalamic nucleus.

## 1.2 Overview of the Thesis

The research is presented so as to emphasise that we must consider the subthalamic nucleus only in the context of the entire basal ganglia. For this reason, Chapter 2 introduces the primary nuclei of the basal ganglia and briefly reviews their component anatomy. Similarly, Chapter 3 presents an overview of current theories and models of basal ganglia processing. From this, it becomes clear that the subthalamic nucleus may play a major role in modulating basal ganglia functions. Chapter 4 introduces a geometric model with the aim of determining the type of interaction expected between neurons within the subthalamic nucleus. A dynamic network model can then be constructed from the predicted geometric arrangements. The dynamic model reveals intriguing processing properties which are analysed in Chapter 5 both analytically (using bifurcation theory) and through numerical integration. A clear need to investigate the processing properties of single subthalamic nucleus neurons is highlighted. Chapter 6 introduces the technique of multi-compartmental modelling for this purpose. A detailed model of single idealised subthalamic nucleus neurons is developed. The model is analysed by numerical integration in Chapter 7. Finally, Chapter 8 draws the two models together to present a coherent and unique view of the subthalamic nucleus.

In order to simplify the thesis a number of abbreviations will be used for reference to basal ganglia and related nuclei. These will be introduced in the text as needed, but are

Table 1.1: Abbreviations used for reference to basal ganglia and related nuclei. The list is given in alphabetical order.

CD	caudate
CM	centromedian
CTX	cortex
GPe	external segment of the globus pallidus
GPI	internal segment of the globus pallidus
MC	primary motor cortex
PPN	pedunculopontine nucleus
PMC	premotor cortex
PUT	putamen
SC	superior colliculus
SMA	supplementary motor area
SNc	substantia nigra pars compacta
SNr	substantia nigra pars reticulata
STh	subthalamic nucleus
STR	striatum
THAL	thalamus
VA	ventral anterior thalamus
VL	ventral lateral thalamus
VLo	ventral lateral pars oralis
VLpc	ventral lateral pars parvocellularis

also collated in Table 1.1 for reference. A glossary is also included on pages 176—183 to clarify terms that may have particular contextual interpretations or to provide background information.

## Chapter 2

# Background Neurobiology

### 2.1 Historical Introduction

It was as early as 1664 when the first clear identification of distinct subcortical structures was published by the English anatomist Thomas Willis (Parent, 1986). What is now functionally known as the **basal ganglia** was then referred to as the corpus striatum. It held such a central position, striped with a wide range of cortical and brainstem fibres, that at the time it was believed to be the **sensorium commune** as defined by Aristotle (Parent, 1986). It was a structure thought to receive all sensory modalities and to initiate all motor acts. This idea appeared to be anatomically reinforced by its central position and clearly visible ascending and descending fibre systems.

Two subsequent events relegated the corpus striatum to an obscure and less defined position. The attractiveness of the histological organisation of the cortex, and the possibility of localising higher mental functions drew many neurologists of both the 18th and 19th centuries to cortical research. Amongst those who continued studying the corpus striatum, there was a sudden realization that many of the functions originally assigned to it were in fact properties of neighbouring corticospinal paths. As Wilson (1914, page

428) observes, the corpus striatum “seemed to fall from its high estate and depreciate in physiological significance”.

At the beginning of the 20th century there were serious attempts to provide detailed comparative descriptions of the corpus striatum (Wilson, 1914; Cajal, 1911). It began to gain importance once again with the discoveries that lesions of these areas would often result in disorders of motor functions in humans (Wilson, 1914; Vogt, 1911). The corpus striatum came to be viewed as the major components of the “extrapyramidal motor system” (Parent, 1986). This term loosely grouped the corpus striatum with an array of brain stem nuclei and reflected the assumption that this grouping constituted a complete and independent motor unit (Carpenter, 1981). The term “basal ganglia” has been generally used to refer to those major anatomical telencephalic subcortical nuclei at the base of the forebrain. More formally this definition groups the corpus striatum (striatum and globus pallidus) with the substantia nigra and subthalamic nucleus (see Table 2.1).

Significant advances were made in the middle and latter 20th century concurrently with the development of sensitive experimental methods for tracing neuronal connections (Nauta & Mehler, 1966). For example, many techniques based on axon transport of various neural markers (such as horseradish peroxidase) are still invaluable tools in determining the connectivity and morphology of the cells of the basal ganglia nuclei. As the momentum of research builds on these techniques many models and ideas of basal ganglia function are emerging. However, despite the recent developments and surge of research, functionally the basal ganglia remain one of the many mysteries of the brain.

### 2.2 Major Structures of the basal ganglia

The individual nuclei which make up the basal ganglia (Table 2.1) are considered to be histologically distinct and they contain an intriguing array of internuclei pathways. Both the cytology and connectivity prove vital to understanding the functional relationships of the individual structures, and their collective action. The following sections focus on

Table 2.1: The core structures that make up the basal ganglia. From Parent (1986).

Corpus Striatum	
(A)	<b>Striatum</b> <ul style="list-style-type: none"> <li>caudate nucleus</li> <li>putamen</li> <li>ventral striatum (comprising the nucleus accumbens and part of the olfactory tubercle)</li> </ul>
(B)	<b>Pallidum or Globus Pallidus</b> <ul style="list-style-type: none"> <li>external (lateral) segment (or globus pallidus proper in nonprimates)</li> <li>internal (medial) segment (or entopeduncular nucleus in nonprimates)</li> <li>ventral pallidum (comprising part of the substantia innominata)</li> </ul>
Associated Structures	
(C)	<b>Substantia Nigra</b> <ul style="list-style-type: none"> <li>pars compacta</li> <li>pars reticulata</li> </ul>
(D)	<b>Subthalamic Nucleus</b>

each of the major nuclei, exploring both cytology and connectivity to provide a basis for understanding the development of current models and theories of basal ganglia function.

## 2.3 Neostriatum

Early neuroanatomists considered the neostriatum to be a uniform and homogeneous structure. Through the 20th century this idea has been eroded by the growing realization that in fact the striatum conceals a complex heterogeneous composition. Not only has it been found to have a varied and clustered cytology (Mensah, 1977), but also it has become a focus of cytochemoarchitecture research due to its rich neurotransmitter distribution (Graybiel & Ragsdale, 1983).

The neostriatum is by far the largest structure of the basal ganglia. It is divided into two portions, the caudate nucleus and putamen, which are separated by a mass of fibres

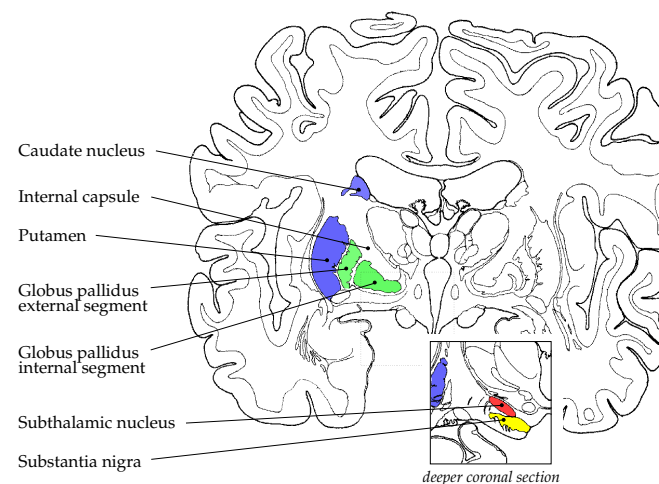


Figure 2.1: A line drawing of a coronal section outlining the major nuclei of the basal ganglia in human. The square insert is of a section projected from the dotted square showing the subthalamic nucleus and substantia nigra. Adapted from Nauta and Feirtag (1986).

called the internal capsule (Figure 2.1). Despite this division, these nuclei form a single anatomical and functional entity. The head of the caudate nucleus lies rostral to the thalamus and bulges into the anterior horn of the lateral ventricle. Its body then extends in a long slender fashion dorsolateral to the thalamus. The putamen lies between the internal capsule and the lateral medullary lamina of the globus pallidus (see Figure 2.1). Rostrally and ventrally, the putamen and the head of the caudate nucleus are continuous, as the internal capsule that anatomically separates the two does not extend into this medial region (Carpenter, 1981).

### 2.3.1 Cytology

The caudate nucleus and putamen may be considered cytologically identical (Carpenter, 1981; DeLong & Georgopoulos, 1981). At least seven types of neurons have been

identified in the mammalian striatum (Parent, 1986). Cells are densely packed and do not exhibit any dominant configurations or laminations (Carpenter, 1981). From studies using the Golgi method (DiFligia et al., 1976), striatal cells may be divided into two categories: those with spiny dendrites, and those with smooth dendrites. Out of all the cells identified, there is one type of spiny neuron which is by far most predominant. The so called “medium spiny” neuron is thought to make up 96% of the neostriatum neuron population (the total caudate–putamen population in rat is approximately 2,800,000 cells, Oorschot, D. E., personal communication) (Carpenter, 1981; Parent, 1986; Groves, 1983). A few of the major types of neurons and their prominent features will be outlined here.

#### *Spiny I or medium spiny*

The medium spiny neuron has an ovoid cell body of medium size ( $20 \times 14\mu\text{m}$ ) from which up to seven or eight primary dendrites extend. These dendrites have smooth surfaces up to or near their first branches, at which point they become profusely covered in spines (Groves, 1983) (see Figure 2.2A). The dendrites radiate into an approximately spherical space about  $300\text{--}400\mu\text{m}$  in diameter (Groves, 1983; Carpenter, 1981; Wickens et al., 1991; Parent, 1986). As these cells are reasonably dense, there is a considerable overlap in the dendritic field of each neuron. Despite this, few dendrodendritic synapses have been located between neighbouring striatal neurons. The axons of the spiny neurons are observed to emit several collaterals before the primary branch extends beyond the striatum. These collaterals usually arise within  $200\mu\text{m}$  of the soma and extend into the parent neuron dendritic field, branching for up to  $400\mu\text{m}$  (DeLong & Georgopoulos, 1981; Groves, 1983). Axodendritic synapses have been identified between collaterals of a medium spiny neuron and its neighbouring neurons overlapping dendrites (Groves, 1983). The primary identified neurotransmitter of the medium spiny neuron is  $\gamma$ -aminobutyric acid (GABA) (Kita & Kitai, 1988; Smith & Bolam, 1990).

#### *Spiny II*

A larger spiny neuron (referred to as spiny II — see Groves, 1983) has been found to be

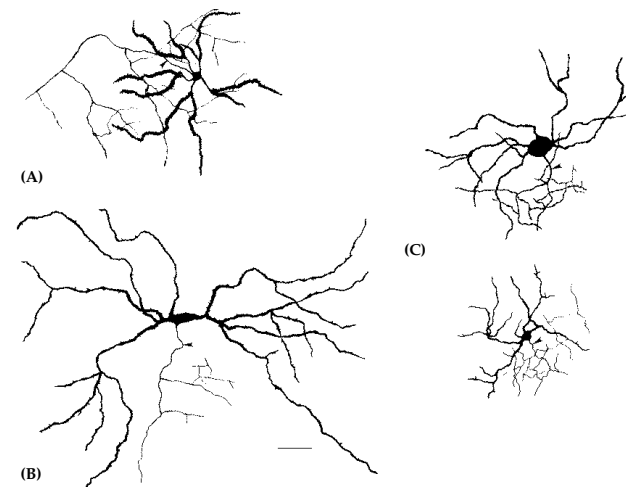


Figure 2.2: Semi-schematic illustrations of the major neurons of the striatum. A. Medium spiny neuron. B. Large spiny II neuron. C. Spiny interneurons. The scale bar represents a length of  $100\mu\text{m}$ . Reprinted from Groves (1983).

distributed fairly evenly throughout the striatum (Graybiel & Ragsdale, 1983). It comprises roughly 1% of striatal neurons (Groves, 1983) and may be characteristically distinguished from the medium spiny neuron by less dense spines distributed over both the soma and dendrites (Groves, 1983; DiFligia et al., 1976). The spiny II neurons typically have an ovoid soma ( $12 \times 15\mu\text{m}$ ) from which four to six dendrites emerge (see Figure 2.2B). These dendrites are generally both thicker and longer than those of the medium spiny, with dendritic fields up to  $1200\mu\text{m}$  in diameter (Kita & Kitai, 1988; DiFligia et al., 1976). The axon of the spiny II, like the medium spiny, extends beyond the striatum to the major striatal output structures (DiFligia et al., 1976). A number of collaterals have been observed to branch orthogonally near the cell body of origin (Groves, 1983).

Together the two types of spiny neurons generate the entire output pathways of the striatum. They have been observed to fire very infrequently and in fact, are silent for much of

the time. Irregularly there occur bursts of high frequency action potential firing which may last 0.1–2.0 seconds (Wilson, 1990).

#### *Aspiny I,II,III*

A number of aspiny types of neurons have also been found in the neostriatum. Generally they are considered to be interneurons, as their axons (if any) are not traced beyond the striatum. However, there is evidence that some of these neurons may receive afferents from beyond the striatum (in particular the cortex, thalamus, and globus pallidus).

The aspiny type I neurons represent about 1% of the striatum (Parent, 1986). These cells are typically spherical (14–15 $\mu$ m in diameter) with five to eight primary dendrites (see Figure 2.2C) (DiFligia et al., 1976). Secondary branches are often thin and varicose. The dendritic radius usually does not exceed 150 $\mu$ m. The axon is short and forms a local plexus at about 40–50 $\mu$ m from the soma (Parent, 1986; DiFligia et al., 1976).

The aspiny type II is the largest cell of the neostriatum (DiFligia et al., 1976), also comprising about 1% of the neuron population. These cells have an ovoid cell body, on average 40  $\times$  30 $\mu$ m for the two longest axes. Ten or more smooth dendrites emerge from the soma, branch many times and extend to within a radius of about 250 $\mu$ m (DiFligia et al., 1976). The axon is thought to be small and profusely arborised around the cell body (Parent, 1986). The aspiny type II striatal neuron has been identified as having the neurotransmitter acetylcholine (Kimura et al., 1980; Lehmann & Langer, 1983).

Finally, the aspiny type III neurons also comprise about 1% of the striatal neuron population (Groves, 1983). These have a small spherical cell body (approximate diameter 12 $\mu$ m) from which usually three to four dendrites radiate. These sparsely branch within a dendritic field of approximately 150 $\mu$ m (DiFligia et al., 1976). A small axon extends up to 20 $\mu$ m from the soma before arborising profusely in a restricted section of the parent neuron's dendritic field.

Interneurons that are thought to contain the neuropeptide somatostatin have also been found in the cat and primate striatum (Chesselet & Graybiel, 1987). These were found to

have mean soma diameters of 20 $\mu$ m, and axons that are generally restricted to specific zones within the striatum (in particular, the matrix compartments, see Section 2.3.4).

### 2.3.2 Striatal Afferent Systems

The neostriatum is considered to be the principal input gateway to the basal ganglia (Parent, 1990). Afferents arising from the cerebral cortex, intralaminar thalamic nuclei, and the substantia nigra are profuse and are projected topographically over much of the striatum (Carpenter, 1981).

The neostriatum appears to receive input from almost the entire cortical mantle (Parent & Hazrati, 1993). Most regions of the cortex project to the striatum and most regions of the striatum receive fibres from the cortex. The projection of the sensory motor cortex in primates is almost exclusively to the putamen (Künzle, 1975; Flaherty & Graybiel, 1991). These projections are organised somatotopically with oblique strips representing leg, arm, and face independently (DeLong & Georgopoulos, 1981; Carpenter, 1981). In the primate, the prefrontal cortex projects solely to the caudate nucleus (DeLong & Georgopoulos, 1981; Carpenter, 1981). Autoradiographic studies have demonstrated that the cortical afferents are not uniformly distributed across the striatum, but rather appear as patches or clusters of various size (Künzle, 1975). It has also been observed that the cortical fibres terminate principally on the dendritic spines of the medium spiny and spiny type II cells (Smith & Bolam, 1990). It is likely that the primary neurotransmitter of the cortical afferents is glutamate, thus exerting an excitatory influence over the striatal cells (Carpenter, 1981; Parent, 1986).

Projections from the thalamus are the second most prominent striatal afferent. Thalamostriate fibres arise from all intralaminar thalamic nuclei and are also considered to be organised topographically (Carpenter, 1981). The afferents, like cortical afferents, appear to terminate primarily on the medium spiny striatal neurons (Carpenter, 1981). The intralaminar projections form a patchy, yet ordered pattern across the neostriatum. These

nuclei also project sparsely to the cortex, possibly through collaterals from the thalamo-striate projections (Carpenter, 1981; Graybiel & Ragsdale, 1983). Other thalamic nuclei (in nonprimates) such as the ventral anterior, ventral lateral, and lateral posterior also have projections to the neostriatum. Thalamic projections are thought to be excitatory (Parent, 1986; Graybiel & Ragsdale, 1983).

Projections from the substantia nigra to the striatum were first noted in 1895 by von Monakow (Carpenter, 1981). The majority of the pathway arises from the dopaminergic neurons of the pars compacta and the projection appears to be topographically organised (Carpenter, 1981). Most of these afferent fibres are thought to carry dopamine to the striatal neurons. At the neonatal stage, these may be observed terminating across both the caudate nucleus and putamen in a patchy island-like fashion (Graybiel & Ragsdale, 1983). The dopaminergic afferents appear to terminate primarily on the spiny neurons (Lehmann & Langer, 1983; Smith & Bolam, 1990). The effects of dopamine are unclear and are reviewed in Wickens and Alexander (1993), Servan-Schreiber et al. (1990) and Graybiel and Ragsdale (1983).

Although the corticostriate, thalamostriate, and nigrostriate projections make up the majority of striatal afferents, pathways from brainstem structures, the pallidum, and the subthalamic nucleus have also been proposed. For example, the dorsal raphe nucleus projects serotonergic fibres to the putamen (Carpenter, 1981). Sparse projections from the external segment of the globus pallidus to the striatum have also been identified (Parent, 1986). The effect of these sparse connections is poorly understood.

### 2.3.3 Striatal Efferent Systems

The medium spiny and spiny type II neurons generate the output pathways of the striatum. These project primarily to only two major structures: the globus pallidus and the substantia nigra. Both the striatopallidal and striatonigral projections are topographically organised (Carpenter, 1981). The putamen and caudate nucleus project to these

structures with little, if any, overlap in their termination sites. The division of the striatal output neurons by target structure seems to be reflected in their respective neurotransmitters. Although all striatal output neurons are GABAergic, those that project to the substantia nigra and the internal segment of the globus pallidus are found to also express substance P (Gerfen, 1992). Neurons that project solely to the external segment of the globus pallidus appear to coexpress enkephalin (Graybiel & Ragsdale, 1983). The functional significance of this neurochemical division is not yet fully understood (see the Organisation section below).

Parent and Hazrati (1993) describe multiple collaterals, and thus multiple termination sites of the striatal efferent fibres in the output structures. This has given rise to the idea that the striatum projects multiple representations over the globus pallidus and substantia nigra (Parent & Hazrati, 1993). The consequences of this are as yet unexplored.

### 2.3.4 Organisation

There are a number of ways that the heterogeneous striatal structure may be organised in order to reflect important divisions. The first level of striatal organisation is reflected in striatal projection sites of the output neurons. There appears to be a compartmental organisation in those medium spiny neurons that project to the substantia nigra, and those that project to the globus pallidus (in rat there is also a significant population of neurons that project to both structures, see Parent, 1986). The two major output pathways have approximately an equal number of projection neurons (Gerfen & Young, 1988).

A second organisational division is the **patch/matrix** distinction between the striatonigral cells. Traditionally, neurochemical markers divided them into those that contained  $\mu$  opiate receptors (patch) and those without these receptors (matrix) (Pert et al., 1976). This patch/matrix organisation correlates with: striatal neurons that project to the substantia nigra pars compacta (patch) and those that project to the pars reticulata (matrix) (Gerfen, 1992). It appears that neurons belonging to patches are clustered in groups throughout the striatum, maintaining a compartmentalisation that is segregated from

the wider matrix distribution. Neurons associated with patches are found to receive input from deep layer V and layer VI of the cortex, whereas matrix compartments appear to receive inputs from the superficial layer V (Gerfen, 1992). A small projection to the striatum from cortical layer III is also found (McGeorge & Faull, 1989). In the primate putamen, only matrix areas are observed to receive projections from the somatosensory cortex (Flaherty & Graybiel, 1991). The patch/matrix organisation has been related to limbic/nonlimbic functions (Gerfen, 1992).

On top of this organisation, there is the neuropeptide division previously described. This may be related to dopamine receptor types. A majority of striatal projection neurons express only one of the receptor subtypes, D<sub>1</sub> and D<sub>2</sub>. Striatal neurons that project to the globus pallidus express the neuropeptide enkephalin and the D<sub>2</sub> dopamine receptor (Gerfen et al., 1990). Other studies have indicated that enkephalin and the D<sub>2</sub> receptor types may be restricted to only striatal neurons projecting to the external segment of the globus pallidus (Albin et al., 1989). Striatal neurons projecting to the substantia nigra (and possibly the internal segment of the globus pallidus) express substance P and the D<sub>1</sub> dopamine receptor (Gerfen, 1992). This division has been hypothesised to play an important role in the description of many dopamine-related striatal disorders (see Section 3.3).

## 2.4 Globus Pallidus

In primates the globus pallidus is divided into two anatomical segments: internal (GPi) and external (GPe) (Figure 2.1). Although these segments are separated by the medial medullary lamina, the pallidal neurons from each segment are extremely similar, and for the most part morphologically indistinguishable (Carpenter, 1981). In nonprimates the anatomical structures usually have a larger separation and are referred to as the pallidum and entopeduncular nucleus (corresponding to the external/lateral and internal/medial segments respectively). In humans the external segment constitutes 70% of

the total volume of the globus pallidus. The mean volume of neurons, though, is 19% higher in the internal segment (Carpenter, 1981).

As with the neostriatum, the globus pallidus appears to have topographically organised afferents (Parent, 1986). It receives its predominant input from the striatum and forms a major component of the output pathways of the basal ganglia (forming much of the ansa lenticularis). The two segments of the globus pallidus are also topographically connected to each other. The GPe has been observed to have a point to point topographic relation with the GPi (Smith et al., 1994). It has also been suggested that there is a reciprocal GPi → GPe connection (Pert et al., 1976).

### 2.4.1 Cytology

Two types of pallidal neurons are revealed by Golgi studies (Carpenter, 1981). The majority are large ovoid neurons (20–60 μm maximum soma diameter) with four to five thick dendrites radiating outwards (Figure 2.3). The dendrites can extend up to 1000 μm in length. On a single neuron some dendrites may be smooth while others exhibit spines (DiFiglia et al., 1982). Large neurons have also been found with spines on the soma. In rodents the dendrites form a discoidal dendritic field (Parent, 1990) with the longest axis lying perpendicular to the incoming striatal afferents (i.e. parallel to the lateral medullary lamina separating the globus pallidus from the putamen). This positions the dendritic fields so as to intercept maximal numbers of striatal afferents (Park et al., 1982). The large pallidal neurons have thin axons that extend beyond the pallidum with a few collaterals that branch sparsely near the soma (Parent, 1986). Virtually all pallidal output neurons are GABAergic (Parent & Hazrati, 1993). There is also some evidence that neurons in the external segment may coexpress substance P (Parent, 1986).

Small interneurons (12–21 μm in diameter) are observed less frequently. These have few dendrites that extend only up to around 150 μm (Parent, 1986). Occasionally these are identified with short sparsely branching axons. Tracing experiments in the cat entopeduncular nucleus (the cat equivalent of the primate GPi) have indicated that these small

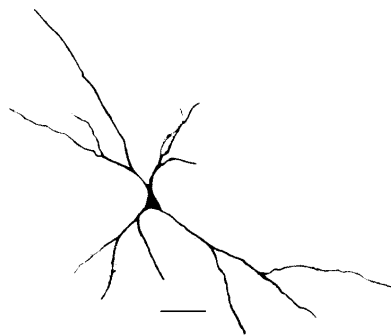


Figure 2.3: Semi-schematic illustration of the major type of neuron found in the monkey globus pallidus. The scale bar represents a length of  $100\mu\text{m}$ . Adapted from Carpenter (1981).

neurons may in fact project beyond the pallidum (Moriizumi et al., 1987). In the macaque monkey medium sized neurons ( $23\text{--}34\mu\text{m}$ ) have also been found, and may be associated with the pallidal projections to the lateral habenular nucleus.

#### 2.4.2 Pallidal Afferent Systems

The majority of projections to the globus pallidus arise from the striatum and subthalamic nucleus. The largest of these is from the striatum and projects in a topographic manner to both pallidal segments (Carpenter, 1981; Parent, 1990). The projections from the caudate nucleus and putamen remain segregated in the pallidum (Parent, 1986). Striatal fibres descend into the globus pallidus perpendicular to the lateral medullary lamina. At certain points the fibres are observed to emit orthogonal collaterals extensively from the main axon (DiFiglia et al., 1982). These then arborise and terminate in the form of bands parallel to the lateral medullary lamina. The collaterals thus heterogeneously arborise in parallel and in synaptic contact with the discoidal dendritic fields of the large pallidal neurons (Parent & Hazrati, 1993). It has been proposed that there is only limited synaptic contact between the main nonarborising striatal fibres and the pallidal cells, whereas at collaterals and terminal arborisation sites, the striatal fibres closely intertwine

the pallidal dendrites (Parent & Hazrati, 1993; Parent, 1986). Collaterals are found at multiple points along the striatal axons path in both segments of the pallidus. This reinforces the idea of multiple representations of striatal input in the globus pallidus (Parent & Hazrati, 1993).

Striatal innervations of the internal and external segments are thought to originate from distinct striatal matrix regions (Parent & Hazrati, 1993; Parent, 1990). Striatal neurons projecting to the external segment are found to express enkephalin while those projecting to the internal segment express substance P (see Section 2.3.4).

A subthalamopallidal projection has been demonstrated in both segments of the globus pallidus. Anterograde tracing from injection sites in the subthalamic nucleus (STh) reveal rich bands in both pallidal segments (Smith et al., 1994). Subthalamopallidal fibres were first observed in the internal segment (Carpenter, 1981). It has been suggested that fibres coursing from the STh to the internal pallidal segment continue to the external segment leaving extensive collaterals in both segments (Smith et al., 1994; Carpenter, 1981). Fibres from the STh are found to arborise in the form of multiple elongated terminal bands. The STh is considered to exert a powerful glutaminergic excitatory influence over its target structures (Parent, 1990).

In addition to these major afferents, the globus pallidus is found to receive much smaller projections from the brain stem structures: substantia nigra, dorsal raphe nucleus, and pedunculopontine nucleus (Parent, 1986). Evidence for these smaller pathways have been reinforced with the findings of dopaminergic and serotonergic innervations of the pallidum.

#### 2.4.3 Pallidal Efferent Systems

The internal and external segments of the globus pallidus have distinct projection sites. Fibres arising from the internal segment form a major output pathway of the basal ganglia. Most of this pathway terminates in the thalamus (Carpenter, 1981). In particular



the GPi has a massive topographic projection to the ventral tier thalamic nuclei, lateral ventral, lateral anterior, and a small part of the centromedian intralaminar nucleus (Carpenter, 1981; Parent, 1990). The pallidothalamic termination sites are fairly segregated from the nigrothalamic termination sites, and probably project to the frontal premotor cortical areas (Künzle, 1975). Some researches have posited the importance of the GPi output projection to the lateral ventral, since it has been suggested that the lateral ventral nucleus may be viewed as an interface or convergent point between cerebellum and basal ganglia output (Desiraju & Purpura, 1969). Yet evidence for this possible integration is by no means established.

The GPi also sends projections to the lateral habenular and pedunculopontine nucleus (Parent, 1990). The lateral habenular connection is small in monkey, yet suggests the GPi may play some role in the limbic system (Carpenter, 1981).

The external segment of the globus pallidus projects primarily to the subthalamic nucleus, again in a topographic manner (Carpenter, 1981; Parent, 1990). Yet it is also observed to yield sparser efferents to the substantia nigra (Parent & Hazrati, 1993) and the striatum (Parent, 1986). Note that the major GPe projection completes a pallidal subthalamic loop; such loops are considered characteristic of the basal ganglia (Parent, 1986). As with the pallidothalamic projections, the pallidosubthalamic fibres are GABAergic.

#### 2.4.4 Organisation

One of the clearest functional divisions seen in the pallidum arises from the striatal input. As previously mentioned, projections from the caudate nucleus and putamen remain segregated in the pallidum. In monkeys, as the caudate nucleus is thought to primarily receive cortical input from association areas, whereas the putamen receives cortical input from sensorimotor areas, this sensorimotor/association division is maintained in the pallidum. In anatomical terms this separation in the pallidum is caudoventral/rostrodorsal. As we shall see, this separation appears maintained throughout the entire basal ganglia.

## 2.5 Substantia Nigra

The substantia nigra, a midbrain structure, is considered part of the basal ganglia complex due to its close ties with the striatum (see Section 2.3.3). Classically it has been divided into two components: the pars compacta (SNc), and the pars reticulata (SNr). The pars compacta is a cell-rich region that in humans is composed of large pigmented neurons. The pars reticulata is less rich in cells, and contains morphologically similar neurons deeply entangled in the striatonigral projections (Carpenter, 1981). In monkeys the pars compacta contains 85% of the total nigral neuron population. However, the division into these two components can be unclear in primates. Despite this, the division is important for revealing a neurotransmitter and projection separation for the nigral neuron population.

### 2.5.1 Cytology

Cells in both the pars compacta and pars reticulata exhibit a triangular (fusiform) shape. These cells have traditionally been divided into two types. Small neurons (10–12 $\mu$ m in diameter) with short axons are considered to be the major nigral interneurons (Parent, 1986). These (in rodents) average at 10% of the total neurons in the SNc and 40% in the SNr (Carpenter, 1981). The second type of neuron is larger (15–20 $\mu$ m in diameter) and constitute the nigral output neurons. In some animals (for example, humans and squirrel monkeys) the large nigral neurons exhibit a characteristic black pigmentation; hence the origin of the structure's name.

The projection neurons are closely grouped in the SNc, yet separated by astrocytic sheaths (Juraska et al., 1977). They display three to five long smooth dendrites orientated in two main directions and with few branches (Figure 2.4) (Juraska et al., 1977). A close similarity has been drawn with the GPi output neurons (Tokuno & Takada, 1993). Neurons in the pars compacta and pars reticulata share many morphological features,

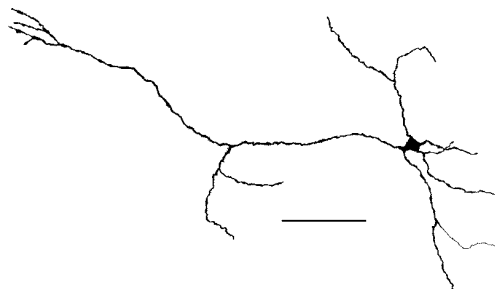


Figure 2.4: Semi-schematic illustration of an output neuron of the substantia nigra pars compacta. The scale bar represents a length of  $100\mu\text{m}$ . Adapted from Juraska et al. (1977).

yet one of the important distinctions found in rat is in their dendritic branching pattern. Most neurons in the pars compacta send 1–2 dendrites deep into the pars reticulata (Juraska et al., 1977). This often creates a lopsided appearance in the dendritic trees of compacta neurons. The dendrites are covered in boutons with increasing density from the soma (Carpenter, 1981). Most synapsing boutons are thought to be of striatal origin.

Axons of the output neurons are often found to yield dense collateral arborisations that extend into the parent neuron's dendritic field and possibly beyond (Juraska et al., 1977). This has been considered as one of the most important intranigral features. What is more interesting is that in the pars reticulata it has been found that these collaterals form significant synapses on the dendrites of their parent neuron (Karabelas & Purpura, 1980).

Neurons of the pars compacta have a high concentration of dopamine, and are considered to be the major supplier of dopamine to the striatum (Carpenter, 1981). The pars reticulata neurons have a similarly high concentration of GABA.

## 2.5.2 Substantia Nigra Afferent Systems

The afferent and efferent connections of the substantia nigra have been the subject of controversy for many years, although recently a greater understanding has been achieved

(Carpenter, 1981). Striatonigral projections are by far the most predominant. These projections are topographic and maintain the caudate/putamen segregation (Carpenter, 1981). As previously mentioned, the striatal afferents are observed to innervate multiple sites of the substantia nigra. Striatal axons emit collaterals at up to four locations through their course in the nigra (Parent & Hazrati, 1993). As with the pallidum, this introduces the idea of multiple representations of striatal activity.

Conventionally it was thought that the striatal afferents were restricted exclusively to the pars reticulata (Carpenter, 1981). This has been questioned, given that some putamen projections are now known to pass through the SNr (possibly emitting collaterals) and sweep across into the pars compacta (Parent, 1986). Similar linkages have been indicated with caudate projections. As previously discussed (Section 2.3.3), these striatal fibres are primarily GABAergic. Neuropeptide substance P and enkephalin are also found in nonoverlapping areas of the nigra, although this distribution varies significantly across animal species (Parent, 1986).

Minor projections are also found from the pallidum (see Section 2.4.3). These are almost exclusively from the external segment and contain both substance P and GABA. In rats these probably terminate more on the areas of the pars compacta (Bunney & Aghajanian, 1976).

A similar minor projection is found from the subthalamic nucleus (Hammond & Yelnik, 1983; Parent, 1990). These fibres terminate in both the pars reticulata and pars compacta (Carpenter, 1981). In rats they arise from collaterals of subthalamic neurons projecting to the GPi (Parent, 1986). In monkeys these afferents arise from separate subthalamic populations. Subthalamonigral neurons have been demonstrated to exert an excitatory influence, probably through the neurotransmitter glutamate (see Section 2.6.1).

The substantia nigra also receives a number of projections from various other midbrain structures. These include the raphe nucleus and the pedunculopontine nucleus. The raphe nucleus provides a major source of serotonin to the pars reticulata, whereas the pedunculopontine nucleus is thought to have a cholinergic influence over the pars compacta (Parent, 1986).

### 2.5.3 Substantia Nigra Efferent Systems

The axons from nigral cells are highly collateralised and may project to many output structures. It is convenient to review the organisation of the nigra efferent systems independently for the pars compacta and pars reticulata.

#### *Pars Compacta*

The pars compacta produces the major nigrostriatal dopaminergic pathway. The neurons primarily project to localised regions of the striatum (Carpenter, 1981). The medial pars compacta may also project dopaminergic efferents to various parts of the cortex, along with dopaminergic efferents from the tegmentum. Nigral dopaminergic projections are also found to a much lesser degree in the globus pallidus and subthalamic nucleus (Cambell et al., 1985).

The pars compacta also has a significant non-dopaminergic population that projects to the amygdala (Parent, 1986).

#### *Pars Reticulata*

The pars reticulata generates the second major output pathway of the basal ganglia. It is divided into three major projection systems: nigrothalamic, nigrotectal, and nigrotegmental. Neurons projecting to these differing sites have been reported to have distinct morphological characteristics (Parent, 1986). The nigrothalamic projections are the most abundant. These projections are topographic (Ilinsky et al., 1985) and terminate in the ventral anterior (pars magnocellularis), ventral lateral (pars medialis) and mediodorsal (pars paralaminae) thalamic areas (Carpenter, 1981). Nigral innervations have also been found in the centromedian–parafascicular complex (Carpenter, 1981). As previously mentioned, little, if any, overlap in the termination sites of the GPI and SNr are found in the monkey thalamus (Ilinsky et al., 1985), although common areas have been found in rat (Carpenter, 1981). The nigrothalamic projections are primarily GABAergic.

The nigrotegmental efferent system is the second most abundant, with the majority of fibres terminating in the pedunculopontine nucleus. The nigrotectal projections arise exclusively from the rostral pars reticulata, and terminate primarily in the deep and middle layers of the superior colliculus (Carpenter, 1981). These projections are also topographically organised (Carpenter, 1981), and as with the nigrotegmental efferents, exhibit GABA as a neurotransmitter.

## 2.6 Subthalamic Nucleus

The subthalamic nucleus (STh) is the final major component of the basal ganglia. It is a small lens-shaped nucleus lying on the dorsomedial surface of the internal capsule. Like the substantia nigra, the STh is a midbrain structure that is included in the definition as a result of its close ties with other basal ganglia components.

### 2.6.1 Cytology

The diversity of STh cytology is still under question. Early studies revealed a homogeneous structure (Yelnik & Percheron, 1979). Currently, it is considered that there may be up to three principal varieties of neurons in the subthalamic nucleus. Two of these constitute projection neurons. Generally authors classify a difference between projection neurons based on dendritic morphology and soma size. For example, one type is described as having an elongated triangular soma with four to nine dendrites radiating outwards (Afsharpour, 1985a; Hammond & Yelnik, 1983). These dendrites are sparsely covered in spines and give rise to tapering branches that extend beyond 400 $\mu$ m (Carpenter, 1981). The second type of projection neuron are a similar size, yet with polar dendrites (see Figure 2.5). Axons of both of these neuron types are found to emerge from the proximal dendrites or somas and branch into two fibres either inside the STh or ventral to it (Hammond & Yelnik, 1983). This implies that (in rat) single STh neurons probably project to at least two output structures. However, other divisions into multiple neuron



Figure 2.5: Reconstructed drawings of two prominent types of projection neuron found in the subthalamic nucleus. **A.** A neuron with radiating dendrites. **B.** A neuron with bipolar dendrites. The scale bar represents a length of 50 $\mu$ m. Reprinted from Afsharpour (1985a).

types have been made. For example, differences in the population of projection neurons have been found solely on the basis of axon morphology (Kita et al., 1983a). In particular, a distinction can be made on the basis of the presence or absence of intranuclear terminating axon collaterals.

A small interneuron has also been observed (Carpenter, 1981). It has only a few long dendrites, with as yet, no clearly identified axon.

Subthalamic neurons were originally thought to exert an inhibitory influence over the globus pallidus (Carpenter, 1981; Hammond et al., 1983). This has conflicted with its proposed excitatory influence over the substantia nigra (Hammond et al., 1983). Contemporary studies have more conclusively demonstrated that STh neurons are primarily excitatory (Smith & Parent, 1988; Albin et al., 1989). Evidence for this arises from a

number of observations. Firstly, cell bodies of STh neurons do not demonstrate GABA immunoreactivity, but, virtually all neurons were found to exhibit strong immunoreactivity to glutamate (Smith & Parent, 1988). Secondly, *in vitro* intracellular recordings confirm the excitatory nature of subthalamonigral (Nakanishi et al., 1987b) and subthalamopallidal pathways (Kitai & Kita, 1987). Thirdly, *in vivo* chemical stimulation of the STh leads to significant enhancement of activity in its target structures (Féger et al., 1991). Together this is convincing evidence for the excitatory nature of STh neurons.

## 2.6.2 Subthalamic Nucleus Afferent Systems

As mentioned in Section 2.4.3 the external segment of the globus pallidus provides a massive projection to the STh. This is topographically organised and observed in all parts of the nucleus. A second, but less intense afferent arrives from the cortex (Afsharpour, 1985b; Parent & Hazrati, 1993). It has been demonstrated that the STh receives a somatotopic projection from the precentral motor cortex (Carpenter, 1981). Regions within the supplementary motor and frontal eye field areas were also found to project to selective subthalamic areas (Künzle & Akert, 1977). The cortex is likely to exert an excitatory (glutamate) influence over the STh (Parent & Hazrati, 1993). Actual cortical innervation of the STh appears to arise from the cerebral peduncle or internal capsule (Afsharpour, 1985b; Kitai & Deniau, 1981). There is some indication that cortical innervation arises from collaterals emitted from corticospinal neurons (Afsharpour, 1985a).

In addition to these two major afferents, the STh also receives projections from the pedunculopontine nucleus and the centromedian–parafascicular complex (Hammond et al., 1983). The intralaminar thalamic afferents are proposed to be collaterals from thalamostriate neurons (Sugimoto et al., 1985).

## 2.6.3 Subthalamic Nucleus Efferent Systems

As previously mentioned, the STh projects massively in a topographic manner to both segments of the globus pallidus (see Section 2.4.2). It also projects in a more minor fash-

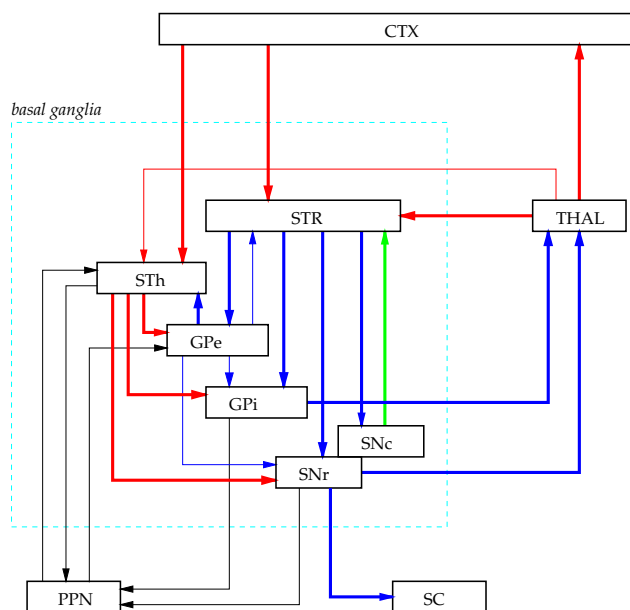


Figure 2.6: A summary of pathways involving the basal ganglia nuclei. Thick lines indicate major projections and thin lines represent minor or less well established connections. Red represents pathways which have glutamate as a primary transmitter, blue represents pathways which have GABA as a primary transmitter and green indicates projections with dopamine as the primary transmitter. Black lines indicate minor connections where the transmitters are not well established.

ion to the substantia nigra pars reticulata (see Section 2.5.2). These projections are found to terminate on regions of the GPi and SNr which are also influenced by topographically similar regions of the neostriatum. Apart from these pathways already discussed, the STh also has minor projections to the pedunculopontine nucleus of the midbrain. Thus the STh forms recurrent connections with the pedunculopontine nucleus. Sparse projections have also been found to the thalamus and putamen (Carpenter, 1981).

## 2.7 Summary

We have presented some of the current and detailed findings of basal ganglia anatomy and cytochemistry. Although our focus of attention is the subthalamic nucleus, by presenting a comprehensive review of all the associated structures, we will be able to consider how the STh may play a role in the functions of the basal ganglia as a whole. One of the most striking observations highlighted in the review is that the STh is the only excitatory structure in the basal ganglia. Considering also that it directly influences both output pathways (GPi, SNr) and receives direct cortical input, it is in a central position for controlling basal ganglia processing.

Figure 2.6 summarises the major projections of the various basal ganglia nuclei. Glutamatergic projections are shown in red, GABAergic in blue, and dopaminergic in green. The connectivity between basal ganglia nuclei is complex, with numerous recurrent circuits evident. This illustration highlights the central position of the subthalamic nucleus.

Before we undertake an analysis of the STh, it would be advantageous to consider current theories and models of the basal ganglia. There are currently **no** model of the subthalamic nucleus itself. However, there are an increasing number of models and theories of the basal ganglia which reference the STh as an integral part. In the following chapter we will review a majority of these models and begin to illuminate the current perception of the role of the STh in basal ganglia function.

## Chapter 3

# Models of the Basal Ganglia

We divide the theoretical approaches of basal ganglia research into three general types, concerning Pathways, Individual Nuclei and Disorders. Firstly, a systems analysis of the primary pathways between the various nuclei reveals interesting paradoxes of basal ganglia processing. We also present some contemporary theories that begin to address these apparent paradoxes. Secondly, theories of the processing of individual nuclei will be introduced. Understanding how individual nuclei process information is crucial for understanding cooperative processing. Finally, we describe theories of basal ganglia disorders and their consequences for normal functional processing. It is hoped that from this review and analysis of current theories we may not only reveal the current views of the role of the STh in the basal ganglia, but also gain insight into the information processing of the basal ganglia as a whole.

### 3.1 The Pathways

What is the general anatomical circuitry or connectivity of the basal ganglia nuclei? From the previous chapter describing the various primary efferents and afferents, a diagram of the predominant pathways can be drawn (Figure 3.1). These apparently com-

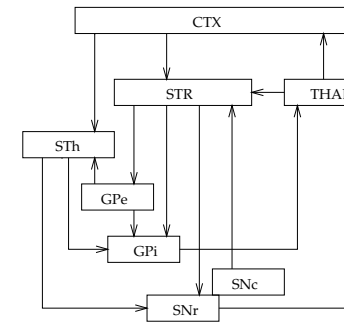


Figure 3.1: The major pathways of the basal ganglia. For abbreviations used see Table 1.1.

plex pathways may be simplified further<sup>1</sup> to reveal four major basal ganglia corticothalamic routes (For abbreviations used see Table 1.1):

$$\begin{aligned} \text{CTX} &\rightarrow \text{STR} \rightarrow \text{SNr} \rightarrow \text{THAL} \\ \text{CTX} &\rightarrow \text{STR} \rightarrow \text{GPe} \rightarrow \text{STh} \rightarrow \text{GPi} \rightarrow \text{THAL} \\ \text{CTX} &\rightarrow \text{STR} \rightarrow \text{GPe} \rightarrow \text{GPi} \rightarrow \text{THAL} \\ \text{CTX} &\rightarrow \text{STR} \rightarrow \text{GPi} \rightarrow \text{THAL} \end{aligned}$$

These four pathways form the basis for many of the generalisations and theories of basal ganglia function. Although many of the small and intricate circuits are excluded, and may be highly significant in the operation of the basal ganglia, by initially investigating only these massive pathways some revealing generalisations of basal ganglia function can be formed.

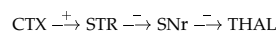
#### 3.1.1 Inhibition and Disinhibition

Given these four simple pathways, we can now consider the accumulative physiological effect of the neurotransmitter properties of each of the routes. Again if we ignore intranuclear effects and further assume transmitters are either excitatory or inhibitory, we

<sup>1</sup>Corticothalamic projections are omitted here for simplicity, but will be introduced in Sections 3.1.3 and 3.1.4.

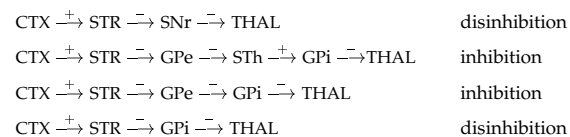
can begin to assess the effect a simple and straightforward basal ganglia circuit may have on the corticothalamic pathways.

Cortical afferents to the striatum are glutaminergic and thus may be assumed excitatory. Striatal, pallidal, and nigral efferents are GABAergic, and may be assumed inhibitory. The subthalamic nucleus is found to primarily exhibit glutamate as its transmitter and may also be attributed an excitatory role. Given these general, either excitatory or inhibitory effects, what sort of influence should we expect cortical activity to exert over the thalamus through the basal ganglia? Consider the first pathway:



Here,  $\xrightarrow{+}$  represents an excitatory influence, and  $\xrightarrow{-}$  represents an inhibitory one. Activity in the cortex should excite striatal neurons. The phasic activity in these neurons inhibit the tonically active substantia nigra neurons. Under normal conditions, and with no striatal activity, neurons of the SNr (and GPi) fire at a regular and sustained rate of about 100 spikes per second (Chevalier & Deniau, 1990). Given that these neurons are GABAergic, this would maintain a constant inhibitory influence over the thalamus (and their other target structures). When activity occurs in the striatum, the regular firing of the nigral neurons would be suppressed. This in turn would release the thalamus from the strong nigral inhibition. Under these conditions the thalamus is referred to as being **disinhibited**.

The other primary pathways may be considered in a similar manner, to reveal the following:



It appears that cortical activity projected through the basal ganglia may induce a combination of inhibition and disinhibition at the thalamus. This combination, though, is observed only in the pathways involving the GPi.

The primary nigrothalamic pathway is solely disinhibitory. Disinhibition can have **no** effect on neurons of the thalamus that are currently receiving no other input. It is a process that only works in cooperation with concurrent excitatory input. This implies that areas of the thalamus under disinhibitory control, must also be receiving other, probably excitatory, afferents. This has implications for issues such as whether the basal ganglia are responsible for “triggering” motor operations. It is possible that they do, since if the thalamic neurons were to be tonically active in the absence of basal ganglia afferents, then disinhibition could indeed activate selective thalamic areas. Experimentally, such triggering may be induced by the introduction of GABA agonists into the SNr of rodents (Chevalier & Deniau, 1990). In monkeys, however, disinhibition alone is not sufficient to “trigger” movements (Chevalier & Deniau, 1990). This may imply the basal ganglia have a regulatory or gating control over the thalamus (and its other output targets, such as the superior colliculus). The basal ganglia may allow, or disallow any activity that occurs at its target structures, but have no effect when these structures are silent.

Of course, we may have known that the influence of the basal ganglia over the thalamus would either be inhibitory or disinhibitory, as both of the basal ganglia output structures (i.e. the GPi and SNr) are GABAergic. As mentioned above only the generalised routes that include the GPi exert a combination of effects over the thalamus. This dual influence has interesting implications, as it implies that either the internal pallidal segment projects to multiple thalamic sites or it exhibits a complex timing variation in its innervations (i.e. inhibition and disinhibition occurring in some temporal order). A combination of these is also possible. Although organisation of the GPi is not well established, it does comprise two of the major basal ganglia thalamic pathways (ansa lenticularis and lenticular fasciculus). These are thought to project from differing regions of the GPi, and possibly terminate at different thalamic areas (Carpenter, 1981). A rostral/caudal separation of projections sites is also indicated (Carpenter, 1981).

So far, the high level systems considerations that have been discussed are at a very global and generalised level, and pose more questions than provide possible solutions. Looking at the global connectivity and its accumulative effects has provided a potential constraint on basal ganglia function, but cannot answer the important questions of how the multiple pathways may interact, and what are the signal transformations that inevitably occur within the nuclei. Theories and models of how the pathways may interact (both within and between routes) will be considered in the following sections.

### 3.1.2 Convergent or Parallel Nuclei

It has been previously mentioned that the striatum is by far the largest structure in the basal ganglia. Given also that approximately 96% of its neurons are projection neurons, one could hypothesise that in each pathway there may be some convergence of striatal fibres within its target structures. In particular, the striatum has many more projection neurons than the total populations of neurons in its output targets (GPi and SNr) combined. This “cardinal convergence” argument provided the basis for many early theories of the basal ganglia (Alexander et al., 1990). The findings of large dendritic fields in both the globus pallidus and substantia nigra, orientated in such a way as to maximally intercept striatal fibres reinforced the ideas of widespread convergence. The basal ganglia might thus be looked upon as a centre for convergence of its diverse cortical input. Since it receives input from across the entire cortical mantle, it could integrate oculomotor, motor, limbic and cognitive information (Percheron & Filion, 1991).

This hypothesis of widespread convergence has lost favour in view of recent findings and proposals. As mentioned in Section 2.4.2, striatal fibres are found to arborise in parallel with the dendritic fields of pallidal neurons. What has also become apparent is that the striatopallidal axons remain myelinated as they course through the pallidum, with few synapses en route (Alexander & Crutcher, 1991). Thus the “optimally orientated” dendritic fields are optimally innervated by the arborisations of only a few striatal afferents. Given the topographical distribution of striatal afferents, it is unlikely that widespread integration of oculomotor, motor and limbic functions occurs, at least at this

level of the basal ganglia pathways (i.e. excluding intranuclear interactions). From the morphological and anatomical similarity of the GPi and SNr, these arguments may also be applied to the striatal innervation of the SNr.

Alexander et al. (1990) present a view of parallel segregated circuits for the motor, oculomotor, prefrontal, and limbic functions of the basal ganglia. Within each of these parallel circuits, there may also be a number of segregated subcircuits. For example, in the “motor circuit” there is a defined topography that may lead to channels specific for “arm”, “leg”, etc.. The parallel circuits may also be associated with different types of behaviour, such as motor preparation or execution. The parallel circuit hypothesis predicts that there is a limited and specific interaction only within a channel or circuit in the various nuclei. To explore this further, we consider the motor circuit as presented by Alexander et al. (1990).

As previously described (Section 2.3), motor pathways in primates are focused on the putamen. It receives somatotopic projections from the primary motor and somatosensory cortices (Künzle, 1975; Jones et al., 1977). Alexander et al. propose that the somatotopic segregation of arm, leg, etc. is enforced in the striatum (see Section 3.2.1) and maintained through the pallidum/nigra and onto the thalamus. Evidence for the segregation of the “motor” circuit can be gained by looking at the different routes to the thalamus. The GPi, which receives topographic projections from the putamen, projects to the thalamic ventral lateral (pars oralis) and lateral ventral anterior (pars principalis) nuclei. However, lateral portions of the SNr which receive inputs from the putamen project to the ventral anterior nucleus (pars magnocellularis) (Alexander et al., 1990). These thalamic nuclei are thought to project back to the primary cortical motor areas, closing the basal ganglia “motor” loop. Thalamostriate projections from these areas are also observed to terminate exclusively onto the putamen, indicating a “motor” segregation. Figure 3.2 illustrates the “motor” circuit of the basal ganglia as described by Alexander et al. (1990).

If there is parallel segregation of the circuits as suggested, what may its purpose involve? To consider this, we need to look further than the apparently parallel anatomy by incor-



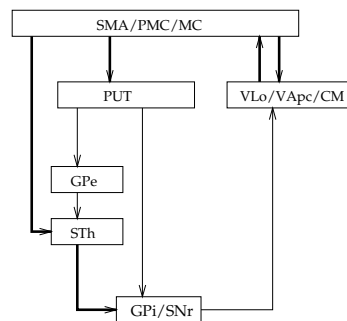


Figure 3.2: The motor circuit of the basal ganglia as defined by Alexander et al. (1990). Thick lines represent excitatory connections, whereas thin lines are presumed inhibitory. For a list of abbreviations used, see Table 1.1.

porating observed physiology. Firstly, it appears that the cortex is responsible for initiating motor signals in the basal ganglia. In the basal ganglia corticocortical loop, physiological timing experiments indicate activity in the cortex prior to basal ganglia activity (Crutcher & Alexander, 1990). Within the basal ganglia, and in particular, the “motor” circuit of the putamen, there is a somatotopic cortical innervation. If we were simply to consider a one to one correspondence of neuron (or cell assembly) to muscle in the somatotopic map, then it is clear, that whatever the basal ganglia are doing with the map, many muscle combinations should work in parallel. From this perspective alone, the necessity for a degree of parallelism is implied. Furthermore, the fact that most structures of the basal ganglia are made up primarily of inhibitory neurons also supports the idea of parallel pathways. As Hikosaka (1991) points out, **selective** motor control cannot be formulated by any combination of excitatory connections. The ability to selectively control specific muscles, inhibitory interactions, and parallel pathways are all mutually supportive.

It appears that there are many other operations occurring within this motor circuit, not just a pattern of sequential/parallel motor selections. Different cell populations in the putamen appear to respond to differing functions such as “direction of movement” (Crutcher & Alexander, 1990). In fact, experiments involving the presentation of a target

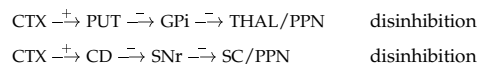
to cue specific learned movements, have demonstrated that some cell populations are active immediately after target appearance, and well prior to the initiation of the motor action (Crutcher & Alexander, 1990). Thus, in broad terms there appears to be a functional division into motor planning (involving preparatory and direction cells) and motor execution. If we take parallelism to its extreme here, and separate the planning and preparation pathways, then this has severe implications for the role of the basal ganglia. Such a parallel segregation would imply the basal ganglia are not directly responsible for the transformation of motor planning into motor action. Although it is unlikely to have sole responsibility for this, it is also very likely to be involved in this transformation (Marsden, 1982). From a functional view alone, there should occur significant, yet specific, interaction between certain circuits.

### 3.1.3 Circuit Interaction

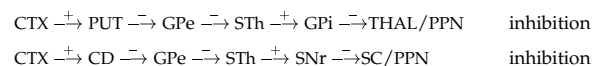
If parallel circuits are to interact, what may this interaction look like? Hikosaka (1991) presents a theory for interaction between the basal ganglia motor and oculomotor circuits. Experiments involving the micro-stimulation of cat caudate nucleus result in **coordinated** movements of eye and head, providing evidence for a possible connection between the two circuits (Hikosaka, 1991). Oculomotor circuits differ from the motor circuits by entering the basal ganglia through the caudate nucleus (rather than the putamen) and terminating through the basal ganglia output structures on the superior colliculus (see Section 2.5.3). Since the two circuits have differing input and termination sites, it would seem logical that interaction should occur in the basal ganglia (Hikosaka, 1991).

Hikosaka proposes a view of the basal ganglia where suppression and activation of motor movements must coexist (Hikosaka, 1991). The subthalamic nucleus is attributed a role of motor suppression, while the cortex, through disinhibition, initiates the activation and preparation. Cortical projections excite the striatum, which in turn inhibits the basal ganglia output nuclei (GPi and SNr). This inhibition results in the disinhibition of

their output targets (thalamus, superior colliculus, etc.) which is the means for controlling the activation of these target sites (see Section 3.1.1). In this model the motor and oculomotor activation circuits take different routes:



(Additional abbreviations, PUT = putamen, CD = caudate nucleus, PPN = pedunculo-pontine nucleus, SC = superior colliculus). Suppression is proposed to be generated through the pathways that pass through the GPe and STh. Again, cortical stimulation of the striatum inhibits the tonically active GPe neurons, which in turn disinhibits the STh. This allows the STh to exert a more powerful excitatory influence over its output structures, the GPi and SNr. The increased activity in these structures results in stronger inhibition of the basal ganglia output targets:



What is the effect of these two opposing influences on the interaction of the motor and oculomotor circuits? Figure 3.3 illustrates the entire circuitry of the model proposed by Hikosaka (1991). It is clear that if the two circuits interact then it should be in the common suppressing GPe  $\rightarrow$  STh link. This is simply due to the fact that this link is the only one in common to the two oculomotor and motor routes. Hikosaka proposes that, although we do not understand this interaction well, it is possible that the oculomotor/cognitive<sup>2</sup> and motor pathways are **antagonistic**. For example, cortical stimulation of the caudate nucleus in order to perform some cognitive/oculomotor task may suppress or “gate” the opposing motor pathway through the GPe  $\rightarrow$  STh inhibition. This possible antagonistic operation is hypothesised to play a focusing role. For example, oculomotor activity does not eliminate motor activity, rather as Hikosaka proposes, the basal ganglia in some way gate their multiple inputs, focusing on a dominant operation. Although these ideas are speculative and are backed by only limited evidence (see Hikosaka 1991), they introduce interesting possibilities as to how circuits may interact.

<sup>2</sup>In this context, the term “cognitive” refers to the cortical innervation from prefrontal areas (Alexander et al., 1990). This is thought to enter the basal ganglia through the caudate nucleus and is thus grouped with the oculomotor circuit.

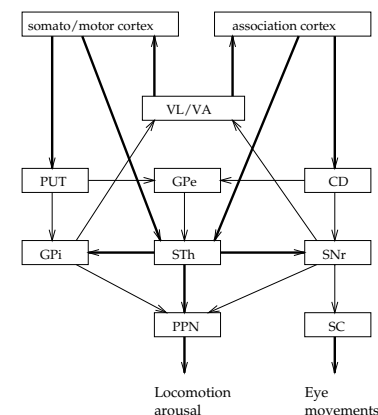


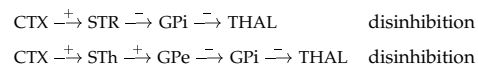
Figure 3.3: The interactions of the circuits as defined by Hikosaka (1991). Thick lines represent excitatory connections, whereas thin lines are presumed inhibitory. For abbreviations used see Table 1.1.

### 3.1.4 Direct and Indirect Pathways

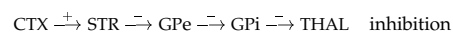
Smith et al. (1994) propose a division of pathways, which they term “direct” and “indirect”. The direct pathway comprises connections between the striatum and the basal ganglia output structures (GPi and SNr). The indirect pathway involves the GPe and STh routes. The model, called the “focusing model”, illustrates a possible interplay between these parallel pathways. It demonstrates how an interaction between the indirect and direct pathways can provide a possible explanation for a common electrophysiological effect observed in the basal ganglia output nuclei. When a pool of GPi neurons (in monkey) are suppressed from firing via striatal inhibition, the activity of neighbouring cells increases (Chevalier & Deniau, 1990). This has led to the idea that striatofugal inhibition is tightly **focused** onto a small population of pallidal and nigral neurons.

The model illustrates how the motor pathways may be split to achieve this focusing effect in the GPi. Consider, for example, the operations required to achieve a fast movement of the arm. For such a task it is important that the appropriate muscles are strongly

activated and the antagonistic muscles are inactive. Since there is a somatotopic organisation within much of the basal ganglia, it is likely that neural areas representing antagonistic muscles are close together. Thus it is vital that the initiating cortical activity cannot spread, but is focused onto only the appropriate neural populations. Consider the contracting muscles. An appropriate neural impulse from the primary motor cortex activates a population of striatal neurons that in turn project directly to the GPI. Simultaneously, movement related cortical projections stimulate the dorsal lateral part of the STh. This in turn stimulates the GPe which also inhibits the GPI neurons. These two pathways lead to the appropriate thalamic disinhibition.



Both of these pathways induce GPI inhibition, possibly in the same pool of neurons (Smith et al., 1994). Note that the corticosubthalamic projection has been included in this model as a functional component of the basal ganglia. As mentioned in Section 2.6.2, this projection is somatotopic and is likely to play an important role in motor functions. These authors further suggest that, in parallel with the cortical activity representing the correct movement, there is activity in neighbouring areas representing the antagonistic motor operations. It is proposed that this paradoxical antagonistic activity projects to an adjacent, yet separate population of striatal neurons (Flaherty & Graybiel, 1991). These in turn project to the GPe which disinhibits the GPI:



The GPI disinhibition is thought to occur in neighbouring regions surrounding the pool of inhibited neurons. It is this interaction of opposing pathways that may enforce the focusing of thalamic disinhibition. GPI neurons responding to the correct muscle movement are strongly inhibited (via the STR and STh), whereas neighbouring regions responding to the antagonistic muscle operations are strongly disinhibited (via STR  $\rightarrow$  GPe).

Although this proposal can provide an adequate description of the observed physiology, it also raises a number of issues. For example, what is the necessary internal organisation of the striatum, to account for the division of projection sites of the neighbouring regions. If adjacent regions of the striatum represent antagonistic muscles, as its topology implies, and these regions project to different targets, then multiple representations of muscles may be required. Muscles which are antagonistic at one point, eventually must play an active role, thus requiring a nonantagonistic projection. Such multiple representations and distinct clusters that may project to different targets have been implicated (Flaherty & Graybiel, 1991). This model thus imposes certain restrictions on the internal organisation of the striatum.

As Smith et al. (1994) point out, there is also a range of other mechanisms that may account for this physiological effect. For example, Chevalier and Deniau (1990) suggest the interactions that occur within the GPI (and SNr) provide a sufficient mechanism for achieving the observed focusing. Simply, the striatal inhibition of a small population of pallidal (or nigral) output neurons suppresses their activities. If these neurons were inhibiting their neighbouring neurons, this inhibition would now be released and the neighbouring neurons activities are increased. One of the important points that can be drawn from these two possible explanations is that the interactions and processing that may occur within a nucleus are as important as interactions between nuclei. Section 3.2 considers models of internal processing.

Another proposal to account for the paradoxical opposing pathways is called the “scaling model”. In this proposal, the parallel pathways work through a temporal interplay in order to scale the activity in basal ganglia output targets (Wichmann et al., 1994). Disinhibitory pathways allow an increase in the target structure activity (positive scale) whereas inhibitory pathways dampen target activity (negative scale). In this scenario, if the pathways are active at different times they can bidirectionally modulate output targets (for example, the thalamus or superior colliculus). This thesis would place the basal ganglia in a pure modulatory, rather than initiation role.

### 3.1.5 Summary

The pathways of the basal ganglia cannot tell us the full story. However, they do provide some insights into how the basal ganglia may function. It is generally accepted that the global effect of disinhibition on basal ganglia target structures places a bound on its possible role. For example, disinhibition only works in cooperation with other excitatory activity and thus may provide a means for gating the thalamic and superior colliculus operation.

The fact that there are multiple corticothalamic routes through the basal ganglia immediately implies a complex interplay between cortical information. Within each route, though, there is much evidence for a large degree of parallelism. In particular, it is likely that the functionally distinct motor, oculomotor, and cognitive information remain largely segregated<sup>3</sup>. How the segregated circuits within each pathway and the multiple routes interact, remains an important issue still to be resolved.

It is becoming apparent that the subthalamic nucleus is in such a position (connectivity wise) to provide regulation and gating within much of the basal ganglia. Both Hikosaka (1991) and Smith et al. (1994) stress that through its widespread gating ability it may play an important role in integrating information. It is also stressed that the globus pallidus external-to-internal projection may be more massive than originally indicated and thus also partake significantly in basal ganglia processing (Smith et al., 1994).

## 3.2 From Biology to Simplified Function: The Nuclei

As we have seen, the internal processing performed within each of the major nuclei of the basal ganglia must be considered in any accurate description of its function. Analysis of the pathways only provide absolute limitations on the effect the basal ganglia may have

<sup>3</sup>Note that most of the theories discussed focus on the pathways involving the matrix compartments of the dorsal striatum, and thus do not address possible limbic roles.

on their output targets. The isolation and simplification of the type of processing that occurs within each nucleus is not nearly as simple as those that were performed on the pathways. Structure within the nuclei is complex, and much less understood than the major efferent and afferent systems.

We can begin to analyse the internal structure of the nuclei by dividing the processing likely to be performed into a number of specific types. Firstly, processing must depend on the afferents received by a particular structure. This involves the types and distribution of afferents, the types of neurons they terminate on, and the types of signals they carry. For example, within the cat entopeduncular nucleus (the cat equivalent of the GPI in primates) both subthalamic and striatal terminals are found. If they were to terminate on neurons in different areas of the nucleus this would possibly imply a division in the processing of these afferents. However, it is found that they probably terminate on the same neurons (Moriizumi et al., 1987). This reveals an important insight into the type of processing that may occur. Afferent convergence implies that some form of integration of striatal and subthalamic information is likely to be performed in the entopeduncular nucleus of the cat.

A second type of processing is the interaction of neurons within a single nucleus. This may involve interaction between all, or any, of the different types of neurons found. The connectivity of neurons within a structure can easily dictate the integration or segregation of information that arrives through the afferents. Consider, for example, neurons of the striatum. Synapses are found between neighbouring GABAergic medium spiny neurons indicating that some sort of lateral inhibition may occur (Groves, 1983). Yet interaction between the cholinergic interneurons and the medium spiny is also found (Smith & Bolam, 1990) which complicates such straightforward assumptions.

A third type of processing that plays an equally important role is the chemoarchitecture of the nuclei. The significance of a synapse between two neurons may only be properly considered in the context of the neurotransmitters involved. The basal ganglia contains a rich pool of neurotransmitters, including glutamate, GABA, dopamine, serotonin, acetylcholine, enkephalin, substance P, somatostatin, and many more (for a review of

neurotransmitters of the striatum see Graybiel and Ragsdale, 1983). It immediately becomes apparent that classifying these as either excitatory or inhibitory will distort much of the processing that may be occurring. For example, catecholamines such as dopamine have neither a clear excitatory or inhibitory effect (Servan-Schreiber et al., 1990). Yet it plays such a vital role in basal ganglia function that processing is drastically altered upon changes in its distribution (see Section 3.3).

Not only does such a variety of neurotransmitters complicate the synaptic interactions, but the effect of different neurotransmitters may be realised in different ways. For example, often a distinction is made between neurotransmitters and neuromodulators. The latter are usually associated with widespread tonic influences, that can affect large populations of neurons. This differs from neurotransmitters, which generally have a localised effect, usually at a synapse.

The task of simplifying the many types of processing that may occur within a single nucleus is much more formidable than that of simplifying the pathways. This is complicated further by the fact that much of the neural connectivity and chemoarchitecture of many structures is currently undetermined or speculative. For these reasons, very few models of basal ganglia components exist. Two very different models will be briefly introduced here. The first attempts to address much of the intranuclei processing mentioned above for the neostriatum, whereas the second model is more abstract and focuses on observed electrophysiology of the globus pallidus.

### 3.2.1 The Striatum

Wickens et al. (1991) present a descriptive model of the neostriatum. It explores anatomical, neurochemical, and electrophysiological aspects of how the striatum's internal structure may process the information passed through it. The model is based on the electrical simplifications of a neuron made by Hodgkin and Huxley (1952b) (see Chapter 6). In particular it characterises a slice of medium spiny membrane which also incorporates the possible effects of striatal cholinergic interneurons. At least two dynamic modes of

behaviour are predicted to emerge from a network composed of this type of simplified neuron. The dynamics of the model will be described briefly before its implications for basal ganglia function are examined.

The medium spiny membrane is simplified to contain five conductance types, each associated with a single (or group of) membrane channel type(s). The conductances are classified as excitatory, inhibitory, leak, after-hyperpolarising potassium (AHP), and potassium muscarinic (potassium channels affected by acetylcholine). Excitatory conductances may be activated by cortical input and yield an alpha function response (an exponential with a time constant; see Rall 1967, 1989). Inhibitory conductances are activated by a neighbourhood of striatal neurons through GABAergic synapses. A voltage-sensitive potassium channel was included to simulate the observed after-hyperpolarisation in the medium spiny neurons after an action potential. Finally, a second potassium channel is included in the model to reflect the muscarinic activity induced by acetylcholine released by the large aspiny interneurons. Since these interneurons are thought to exert a widespread modulatory cholinergic influence, the channels are tonically activated in a diffuse manner. This plays an important role in simulating dopamine effects on the striatum, as a strong antagonism between dopamine and acetylcholine has been postulated (Lehmann & Langer, 1983; DeLong & Georgopoulos, 1981).

Although this is a complex description of the striatal medium spiny neurons, it can begin to reveal how the striatum may process cortical information. The network dynamics of the system are as follows. An appropriate connectivity of the simulated striatal neurons is calculated in such a way so as to represent the overlap of the neighbouring neurons dendritic fields with the parent neuron's axon collaterals (see Section 2.3.1). Using parameter values that represent a normal biologically realistic situation, a state of "competition" is observed in the presence of random cortical stimulation. In particular, there exists a neighbourhood of neurons in which usually there will be a single dominant neuron in the active state (Wickens et al. 1991, refer to this neighbourhood as a "domain of inhibition"). This has important consequences for the issues that have been looked at in Section 3.1. Firstly, it further demonstrates that the internal processing of the individual nuclei play a crucial part in the operation of the basal ganglia. Within the striatum

tum itself, there is a mechanism that adequately performs striatal focusing of cortical inputs. It has been electrophysiologically demonstrated that neighbouring neural regions within the striatal matrix may be associated with muscle representations, usually of a single joint (Alexander & Delong, 1985). This implies that representations of antagonistic muscles may be in neighbouring regions. If this is the case, then a neighbourhood of cells, with the dynamics as predicted by the model would ensure neurons representing antagonistic muscles are not active at the same time. A parameter independent mathematical analysis was also used to demonstrate the modes of network operation independent of any specific parameter selections. See Wickens et al. (1991) and Wickens and Alexander (1993) for a more detailed description. Secondly, the model can be used to investigate basal ganglia disorders, which are discussed more fully in Section 3.3. When parameter conditions are changed so as to reflect the accumulative effect of the loss of dopamine (through a change in the tonic muscarinic activity), the network undergoes a transition towards a mode of coactivation. Cortical input, which was previously focused onto single cells through neighbourhood competition is now free to coactivate neighbouring neurons. If, as previously indicated, adjacent neural populations represent antagonistic muscles, then their coactivation may be associated with the symptoms observed in disorders involving dopamine loss, such as rigidity (stiffness and difficulty in initiating motor actions – see Section 3.3).

As the internal processing of individual nuclei plays an important role in the operation of the basal ganglia, how may the dynamics predicted by this model influence the striatum's target structures? Although, to a large degree, this also depends on the processing performed by the target structures, striatal dynamics as presented by this model reinforces the parallel pathways hypothesis (Section 3.1.2). Under normal conditions of competition the model exhibits a mechanism that enforces segregation of neighbouring regions, rather than facilitating integration. This does not rule out integration at other sites, or between the direct and indirect routes. It simply indicates that structures receiving striatal input in a topographic manner probably receive segregated zones of activity.

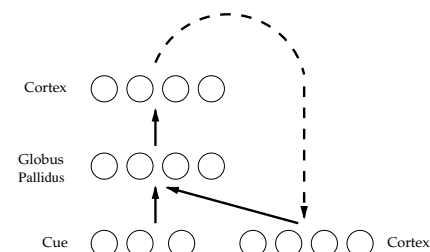


Figure 3.4: This is a simple model of predicted interactions between the globus pallidus and the cortex. The layer representing the globus pallidus receives input from both the cortex and “cue” units (representing signals from the body). The two layers representing the cortex should be considered as one layer since the connections between the two simply copy (not modify) the activity between both layers (the “copying” of activity is indicated by the dashed line). See text and Brotchie et al. (1991c) for further details.

### 3.2.2 Sequential Motor Control at the Globus Pallidus

Brotchie et al. (1991c) present a very simplified model to explore the possibility of a role for the globus pallidus in controlling the **sequential** operation of cortically initiated motor patterns. It has been proposed that the cortex sequentially initiates each motor act required for a specific motor sequence (Marsden, 1982). The initiation of an individual motor act must occur in perfect synchronisation with the physical completion of the previous act. Brotchie et al. propose that the basal ganglia, and in particular the globus pallidus, may be responsible for this synchronisation and control of cortically initiated motor sequences. Of particular interest, is how the firing patterns observed in the globus pallidus may relate to this function. Two general types of firing patterns have been observed in the pallidum (Brotchie et al., 1991b, 1991a). The first is a “movement related” phasic discharge that occurs in relation to current body movements. The second is sustained activity, often observed prior to the movement. This latter activity they call “set-related activity” and occurs in a much smaller population of neurons (18%). Brotchie et al. (1991c) construct a simplified model of a hypothetical corticopallidocortical circuit to explore the possible role of these two types of activity in the sequential switching of cortical motor patterns.

The model (see Figure 3.4) is based on the Jordan sequential network (McClelland & Rumelhart, 1988). It is effectively a three layer network that possesses a copy of the output layer as part of the input layer (through recurrent connections). The back propagation algorithm is used to learn the sequential patterns representing motor acts required for a specific motor sequence. The network was trained to maintain a stable pattern of activation over the units representing the cortex until a phasic cue indicates that the current cortical pattern representing a motor act has been completed. This allows the selection of a second pattern in the sequential set, which also has to be maintained, until a relevant cue for it is received. This sequential pattern selection may be continued many times. What is of interest to Brotchie et al. is the representation required in the network at the pallidal level to achieve this sequential switching. In this model, the globus pallidus receives input from units representing the "body" and the cortex. Its purpose here is to maintain the cortical motor pattern until a cue indicating the completion of the current motor pattern has been received. Upon learning this task, representations found at the pallidal level were of two types. Firstly, units that had a constant sustained activity were found responsible for maintaining the cortical pattern. Secondly, phasic units that respond solely to the input cues were found responsible for switching patterns at the cortical level. Brotchie et al. (1991c) draws a parallel between these two types of activities and the electrophysiological results observed in the globus pallidus of the monkey (Brotchie et al., 1991b). This parallel is difficult to justify due to the level of simplification in the model (i.e. reducing the basal ganglia down to a single layer overlooks a large amount of processing), although the model introduces an interesting possibility for the function of the loops of the basal ganglia. Small loops between structures are one of the interesting characteristics of the basal ganglia (Parent, 1986). From the small and varied exploration of simplified loops (called recurrent networks) that has been made in the field of neural networks it is becoming apparent that such loops are important in learning and performing sequential operations (for example, Elman 1990). As Brotchie points out, motor operations have a distinct serial component.

### 3.2.3 Summary

It is important to consider how each individual nucleus within the basal ganglia may be processing information. However, such processing involves a complex interaction of anatomical, electrophysiological and chemical aspects of the internal structure. Modelling such complexity is difficult and restrained by the amount of information which is as yet unknown. Despite this, models based on the electrical nature of neurons with acceptable simplifications have achieved some success in describing the processing that may be occurring. Higher level models, that make gross simplifications, are harder to relate to the function of the basal ganglia. Yet, they may also provide useful insights at an abstract level. It is clear that there is a need for more models to address processing within basal ganglia nuclei.

## 3.3 Disorders of the Basal Ganglia

It was observed in the early 20th century that lesions involving the basal ganglia often resulted in motor related disorders in humans (Wilson, 1914; Vogt, 1911). Currently a role for the basal ganglia in movement disorders such as akinesia, rigidity, chorea, and athetosis is widely accepted (DeLong & Georgopoulos, 1981). The relationship of the basal ganglia to these disorders has led to much speculation about its function. For example, the difficulty of initiating movements observed in Parkinson's disease has led to the hypothesis that the basal ganglia may be involved in automatic execution of learned movements (Albin et al., 1989; Marsden, 1982). Similarly, many of the theories and models so far discussed propose explanations as to how certain disorders may arise within the basal ganglia.

It should be noted that there are disadvantages in viewing disorders of the basal ganglia as a means of isolating or determining its functions. Lesions and disorders can yield a broad spectrum of clinical phenomena with no guarantee that the major areas

of damage or degradation are the areas responsible for the observed symptoms. For example, degeneration of the pars compacta neurons of the substantia nigra, as observed in Parkinson's disease (DeLong & Georgopoulos, 1981) diminishes the major dopamine pathways, which seriously affects *other* basal ganglia nuclei.

### 3.3.1 An Introduction to Basal Ganglia Disorders

Albin et al. (1989) divides the observed movement disorders into three categories: hyperkinetic, hypokinetic, and dystonia. **Hyperkinetic** disorders, as the name implies, characterises an excess of movement, often rapid and continuous. Chorea is probably the most common of these uncontrolled movements. "Chorea" is derived from the Greek word for dance and generally involves rapid and fluid movement of the trunk, head, and limbs. It is often associated with athetosis, which has a slower withering character (Albin et al., 1989). Huntington's disease is the prototype choreoathetoid disorder and is pathologically characterised by severe loss of neurons in the striatum (Breakfield & Bressman, 1987). This has often led to the implication that the striatum plays a major role in such disorders. Ballism is a rare, but severe form of choreoathetosis which almost exclusively results from lesions of the subthalamic nucleus (Albin et al., 1989). It is distinguished by a much more violent flinging motion of the extremities.

**Hypokinetic** disorders involve a reduced ability to move or initiate movements. The most predominant in this category are akinesia and rigidity. In humans, akinesia is seen most frequently in patients with Parkinson's disease (DeLong & Georgopoulos, 1981). It is often characterised by slowness of movement, increased muscle tone, reduced spontaneous movement and tremor (Albin et al., 1989). The most common cause of this is thought to involve the impairment of the nigrostriatal dopamine transmission. For example, Parkinson's disease involves the degeneration of the nigrostriatal, mesocortical and hypothalamic dopaminergic systems (Jellinger, 1987). It is found that there is a 50–85% decrease in the pigmented neurons of the substantia nigra (Jellinger, 1987). Effects of the degeneration of the dopamine systems are by no means clear. Induced lesions to

the ascending dopamine system in experimental animals has led to a variety of effects from akinesia to sensory neglect (DeLong & Georgopoulos, 1981).

Muscular rigidity, which often features in Parkinson's disease, is also thought to be related to the dopamine systems, particularly within the striatum (DeLong & Georgopoulos, 1981). Conventional lesioning techniques in animals have been largely unsuccessful in its replication. However, neuroleptics such as reserpine, which depletes dopamine from synaptic terminals, has reproduced a form of muscular rigidity in animals (DeLong & Georgopoulos, 1981).

**Dystonia**, the third category of disorders, is characterised by spontaneous sustained muscle contractions that cause unusual postural positions which may be maintained for some time (Albin et al., 1989). There are different forms of dystonia, such as flexion dystonia observed in Parkinson's disease or torsion dystonia (see Rothwell and Obeso 1987). It may be induced by a wide array of lesions in the thalamus, striatum, or globus pallidus (Rothwell & Obeso, 1987).

### 3.3.2 Relating the Disorders to the Anatomy

How may the anatomy and chemoarchitecture of the basal ganglia be related to such disorders? Albin et al. (1989) have proposed a model of the basal ganglia to provide an explanatory account of various movement disorders. It incorporates a number of different aspects involved in basal ganglia operation, including limited chemoarchitecture, predominant connectivity of the major structures, and specific interneurons. Figure 3.5 illustrates the model under normal anatomical and chemical conditions. One of the particular distinctions made is between the different projection sites for the neurons of the striatum expressing enkephalin and substance P (see Section 2.3.4). As seen in Figure 3.5, the SNc, GPI, and SNr receive afferents from neurons expressing substance P, whereas the GPe predominantly receives afferents from neurons expressing enkephalin. This plays an important role as the striatal populations which generate these different pathways are thought to be related to different dopamine receptor types. Striatal neurons expressing



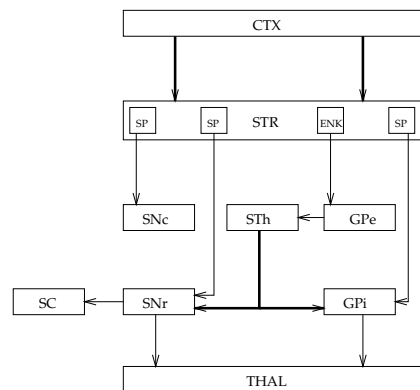


Figure 3.5: The enkephalin/substance P distinction as described by Albin et al. (1989). This distinction is thought to play an important role in basal ganglia disorders involving dopamine. Thick lines represent excitatory connections and thin lines represent inhibitory ones. Extra abbreviations used: ENK = neurons expressing enkephalin, SP = neurons expressing substance P.

enkephalin are considered to be associated with the D<sub>2</sub> dopamine receptor type, whereas neurons expressing substance P are associated with the D<sub>1</sub> type (Gerfen, 1992). Changes in the dopamine levels of the striatum are thought to have different effects on the different receptor types (Gerfen et al., 1990). This can be observed artificially by the effects of D<sub>2</sub> antagonists on the striatum. With the application of such antagonists, a marked increase in the synthesis of enkephalin and preproenkephalin mRNA is observed (Albin et al., 1989; Gerfen et al., 1990). It is predicted that this reflects an increase in the activity of neurons expressing enkephalin. Conversely, lesions of the nigrostriatal dopamine pathway caused by 6-hydroxydopamine results in a reduction of the specific mRNAs encoding the D<sub>1</sub> receptor and substance P (Gerfen et al., 1990).

Consider how this model may begin to account for Parkinsonism symptoms. As Albin et al. (1989) stress, such an explanation would primarily involve a description of the action of dopamine on striatal neurons. If, as predicted, the impairment of striatal dopaminergic afferents increases activity in neurons expressing enkephalin while decreasing activity in neurons expressing substance P, then what may the accumulative ef-

fects of this distortion be on the basal ganglia target structures? If we assume dopamine loss only occurs in the striatum, then we can predict how such changes may alter the normal operation of the rest of the basal ganglia. As the striatum is predominantly stimulated by cortical afferents, we will assume that some of these afferents are active in the initiation of some motor movement. Cortical stimulation under the abnormal dopamine conditions is likely to produce excessive activity in the neurons of the striatum which express enkephalin. These project predominantly to the GPe and would result in increased inhibition. This would then decrease its tonic inhibition of the STh, allowing increased excitation of the SNr and GPi:

$$\begin{aligned}
 & \text{CTX} \xrightarrow{+} \text{STR} \xrightarrow{-} \text{GPe} \xrightarrow{-} \text{STh} \xrightarrow{+} \text{GPi} \xrightarrow{-} \text{THAL} && \text{increased inhibition} \\
 & \text{CTX} \xrightarrow{+} \text{STR} \xrightarrow{-} \text{GPe} \xrightarrow{-} \text{STh} \xrightarrow{+} \text{SNr} \xrightarrow{-} \text{THAL} && \text{increased inhibition}
 \end{aligned}$$

Here,  $\xrightarrow{+}$  represents an increased excitatory influence,  $\xrightarrow{-}$  represents an increased inhibitory influence, and  $\xrightarrow{-}$  represents a reduced inhibitory influence. The resulting increased inhibition on the thalamus (and other output structures) would predict some form of reduced movement (Bergman et al., 1994).

Consider now the decreased activity expected in the subpopulation of neurons in the striatum expressing substance P. Cortical activity projected to these neurons is likely to have a reduced effect, producing less striatal inhibition along the associated striatal efferent pathways. Direct projection to the GPi is thus expected to be less inhibitory, as would those to the SNr and SNc. Reduced inhibition of the GPi (in the extreme) allows it to retain its tonic activity, and to continue or increase its sustained inhibition on the basal ganglia output targets:

$$\begin{aligned}
 & \text{CTX} \xrightarrow{-} \text{STR} \xrightarrow{-} \text{GPi} \xrightarrow{-} \text{THAL} && \text{reduced disinhibition} \\
 & \text{CTX} \xrightarrow{-} \text{STR} \xrightarrow{-} \text{SNr} \xrightarrow{-} \text{THAL} && \text{reduced disinhibition}
 \end{aligned}$$

While the overall increased inhibition on basal ganglia output targets by both pathways may be associated with some of the akinesia symptoms found in Parkinson's disease, it is apparent that the processes are very complex and must ultimately involve the dopamine related changes that may occur within each nucleus. However, predictions relating to

the expected levels of the neuropeptides in the intermediate structures (for example, expected decreases in substance P levels in the SNr and GPi) have generally concurred with experimental findings (Albin et al., 1989).

The same model can be used to examine the hyperkinetic disorder, ballism. This is one of the few disorders with a well established anatomical localisation. Destruction or lesions of the subthalamic nucleus will usually result in this syndrome (Albin et al., 1989). If the STh is removed from the model this will predominantly affect both the major output components of the basal ganglia (GPi and SNr). Each would be predicted to undergo a massive reduction of excitatory input. Evidence for the STh providing a tonic excitatory activity to these output structures can be found in experiments involving chemical inhibition of the STh (Robledo & Féger, 1990). If the STh plays an active role in the sustained tonic activity of both the GPi and SNr, then we should consider the effects of overall reduced activity expected in the absence of the STh. For both structures, reduced activity means widespread reduced inhibition of the basal ganglia output targets (thalamus, superior colliculus etc.). If in normal operation, selective reduced inhibition (i.e. disinhibition) is the means of **controlling** specific muscle operations (see Section 3.1.1) then massive reduced inhibition, as predicted here, would result in target structures that are effectively uncontrolled. Parallels between this predicted widespread lack of control and the symptoms of ballism may easily be drawn (Albin et al., 1989).

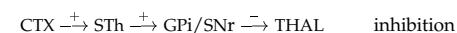
### 3.3.3 Summary

Forming conclusions about how certain disorders arise is very difficult and caution should be taken in drawing broad inferences. Although the known connectivity and limited chemoarchitecture allows parallels to be drawn between lesions and the symptoms found in associated disorders, there is still a considerable amount of processing and mechanisms that are not well understood. For example, the simple distinction between D<sub>1</sub> and D<sub>2</sub> receptors may overlook many synergistic and autoreceptor interactions that may occur (Pantelis et al., 1992). However, the functional associations that can be made

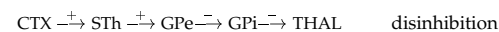
between localised disorders and predicted mechanisms may provide limited insights into the basal ganglia's function.

### 3.4 The Role of the STh in the Basal Ganglia

We have presented a selected number of models from each of the theoretical approaches. These reflect the primary and current views of basal ganglia function. We can also use some of these models to form a number of views of the function of the STh in the basal ganglia. Firstly, as indicated by Hikosaka (1991) the STh should be responsible for some form of motor suppression. This arises from its direct influences over basal ganglia output structures:



However, Smith et al. (1994) highlight that the STh is also involved in paradoxical and opposing pathways. In particular, its projection to the GPe allows it to have a disinhibitory influence over the thalamus:



Finally, Albin et al. (1989) suggests that the STh is the driving force behind the tonic GPi/SNr activity (also see Robledo and Féger 1990). Thus lesions of the STh should result in a significant drop in the ability of the basal ganglia to tonically inhibit their output targets (for example, the thalamus, and superior colliculus).

Reviews of the theoretical basal ganglia literature reveal that the STh is in a prime position to influence both output pathways (GPi and SNr). Despite this, very little is known about subthalamic nucleus processing itself. Is it a structure that simply provides tonic excitation to sustain activity in the output structures, or will it take an active role from its direct cortical and thalamic input? In the following chapters we present an analysis of the STh to begin to reveal the type of processing it may be performing, and how this will influence its primary output targets.

## Chapter 4

# Dynamic Network Model of the Subthalamic Nucleus

### 4.1 Introduction

The subthalamic nucleus (STh) is the only glutaminergic structure within the basal ganglia. It is likely that it plays a crucial role in the neural processing performed by the basal ganglia as a whole. For example, there is a large recurrent projection to the GPe. Thus the GPe is not only a major source of STh afferents, but also a major receptor for STh efferents. The existence of this recurrent loop elicits intriguing possibilities for the cooperative processing of these structures. However, before we begin to address how the STh will influence its neighbouring structures it is necessary to determine the type of information processing it is performing. For example, how will the STh respond to cortical or thalamic excitation? Moreover, a significant proportion of STh projection neurons are found with internal axon collaterals (approximately 50% in rat and 8% in monkey - see Kita et al., 1983a). It is very possible these internal collaterals form synapses with other STh projection neurons, introducing a greater complexity in the neural processing being performed. Understanding how the STh is likely to respond to its environment is the key to understanding its role in the basal ganglia.

To explore these computational questions a dynamic network model was constructed. It is the purpose of this model to investigate intrinsic *network* STh processing capabilities. As the emphasis is on the cooperative parallel processing of many neurons, a single STh neuron will be modelled simplistically. We will refer to the simplified model neuron as a “unit”.

### 4.2 Model Derivation

#### 4.2.1 Model Units

To examine STh network processing capabilities we are required to simplify the properties of an STh neuron into an appropriate mathematical model. In particular we choose a model following Shamma (1989). The major computational properties of an STh neuron we wish to capture are:

1. bounded firing rate — in rat this can reach a maximum of 500Hz (Kita et al., 1983b).
2. firing threshold.
3. simple integration of afferents following an alpha type function (Rall, 1967).

The bounded firing rate is exhibited by STh projection neurons in *in vitro* current injection experiments (Nakanishi et al., 1987a). The firing rate progressively and smoothly approaches a maximum of around 500Hz. Rather than a binary threshold, STh neurons exhibit a smooth and continuous increase of firing rate in response to current injection. The steepest gradient of the experimentally observed current/firing rate relation appears to occur at lower current injections (see Figure 2B of Nakanishi et al., 1987a). This indicates that there may be a fast threshold like transition from rest firing rates<sup>1</sup>. Finally, the integration of afferents following an alpha type function allows modelling of typical synaptic responses (see Shamma, 1989). The integration of these three simplified properties into a single model will be considered below.

<sup>1</sup>The experimental observations require a constant hyperpolarising current injection to eliminate spontaneous firing. The effect of this on the observed relation is unclear.

Inputs to a single neuron (both external and lateral) may be considered as trains of spikes, mathematically represented by delta functions:

$$x_i(t) = \sum_k \delta(t - \tau_k)$$

where  $x_i(t)$  is the output of unit  $i$  at time  $t$ , and  $\tau_k$  are the times at which spikes occur (see Shamma, 1989). How such input spikes ( $x_i(t)$ ) affect the artificial cell potential, or activity ( $y_i(t)$ ), can be modelled by an alpha type transfer function,  $h_{ij}(t)$ , specifying the effect of unit  $j$  on unit  $i$  (see Rall, 1967). The accumulative effect of many spikes along a single input line (i.e. the accumulation of the alpha function responses) can be simply modelled by the convolution of the spike train and transfer function:

$$y_i(t) = \sum_{j=0, j \neq i}^N (h_{ij}(t) * x_j(t)) + h_{ik}(t) * I_i(t) \quad (4.1)$$

where  $I_i(t)$  is the external input (in the form of a spike train),  $N$  is the number of units in the network and  $*$  is the convolution symbol. The alpha function is not the only transfer function that may be used. A similar, yet simpler, function<sup>2</sup> that will be used here is an exponential decay.

A unit's potential provides an indication of its average firing rate ( $\sigma_i$ ). This should at least include the biologically observed properties of threshold and saturation. A descriptive account of these properties is given by a sigmoid function:

$$\sigma_i(t) = \frac{Z_{max}}{1 + e^{-b(y_i(t) - y_0)}} \quad (4.2)$$

The characteristics of the thresholding may be described using the parameters  $b$  and  $y_0$ , whereas saturation occurs at the maximum firing rate  $Z_{max}$ . For very low potentials the firing rate,  $\sigma_i(t)$ , reaches zero and for high potentials it reaches  $Z_{max}$ . Figure 4.1 illustrates a sigmoid function for specific parameters.

Given the average firing rate of a unit (Equation 4.2) we could generate its output train of spikes stochastically. However, it is more convenient to replace the stochastic spike trains by the firing rate itself. By redefining the potential  $y_i(t)$  as the ensemble mean

<sup>2</sup>By eliminating the reference to time outside the exponential, the dynamic equations directly reduce to an autonomous system.

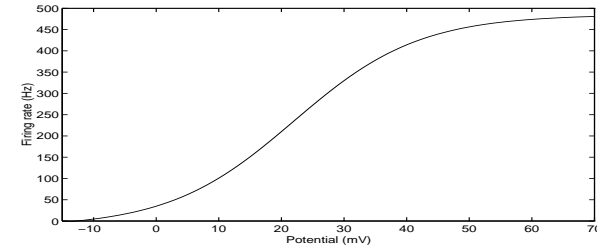


Figure 4.1: The firing rate/potential relation based on the assumption that the relation found experimentally can be fitted with the sigmoid function given in equation 4.2 (see Section 4.3.2). Both the potential and firing rate should be interpreted only in terms of the dynamic model, and its associated assumptions. Parameters are  $b = 0.1$ ,  $y_0 = 22.0$ , and  $Z_{max} = 500$ . Resting potential is defined at 0mV. A small negative vertical shift in the sigmoid has also been made — see Figure 4.11 for details.

of the instantaneous unit potential, and defining the expected value (denoted by  $E$ ) of a spike train as the firing rate ( $E(x_i(t)) = \sigma_j(t)$ ) we eliminate all spike trains from the system (see Shamma, 1989):

$$\begin{aligned} y_i(t) &= E \left( \sum_{j=0, j \neq i}^N (h_{ij}(t) * x_j(t)) + h_{ik}(t) * I_i(t) \right) \\ &= \sum_{j=0, j \neq i}^N (h_{ij}(t) * E(x_j(t))) + h_{ik}(t) * E(I_i(t)) \\ &= \sum_{j=0, j \neq i}^N (h_{ij}(t) * \sigma_j(t)) + h_{ik}(t) * e_i(t) \end{aligned} \quad (4.3)$$

where  $e_i(t)$  is the external input, represented now as a firing rate.

We choose our transfer function  $h_{ij}(t)$  to be a connection-specific synaptic efficiency ( $w_{ij}$ ) multiplied by an exponential decay function with a time constant,  $\tau$ :

$$h_{ij}(t) = \frac{w_{ij}}{\tau} e^{-t/\tau} \quad (4.4)$$

Using this transfer function we can calculate the change in potential that occurs over time ( $\dot{y}_i(t)$ ):

$$\begin{aligned} y_i(t) &= \sum_{j=0, j \neq i}^N (h_{ij}(t) * \sigma_j(t)) + h_{ik}(t) * e_i(t) \\ &= \sum_{j=0, j \neq i}^N \left( \int_{-\infty}^t w_{ij} \frac{e^{-(t-v)/\tau}}{\tau} \sigma_j(v) \, dv \right) + \int_{-\infty}^t \frac{e^{-(t-v)/\tau}}{\tau} e_i(v) \, dv \end{aligned}$$

Differentiating:

$$\begin{aligned} \dot{y}_i(t) &= \frac{1}{\tau} \left[ \sum_{j=0, j \neq i}^N w_{ij} \sigma_j(t) - \sum_{j=0, j \neq i}^N w_{ij} \int_{-\infty}^t \frac{e^{-(t-v)/\tau}}{\tau} \sigma_j(t) \, dv \right. \\ &\quad \left. + e_i(t) - \int_{-\infty}^t \frac{e^{-(t-v)/\tau}}{\tau} e_i(v) \, dv \right] \\ \tau \dot{y}_i(t) &= -y_i(t) + \sum_{j=0, j \neq i}^N w_{ij} \sigma_j(t) + e_i(t) \end{aligned} \quad (4.5)$$

We are assuming here that the weight (synaptic efficiency) on the external input  $e_i$  is unity. Equation 4.5 describes the change in potential of each unit, and how it is affected by the activity of neighbouring units. The term summing over all units is easily reduced to local neighbourhoods if we set the weights ( $w_{ij}$ ) to zero for large distances between  $i$  and  $j$ .

#### 4.2.2 Model Form

In a dynamic network model of the STh we assume each unit receives external input from the cortex ( $e_i$ ) and also neighbourhood inputs from other STh units with axon collaterals ( $\sum_j w_{ij} \sigma_j(t)$ ). Figure 4.2 illustrates this network. The form and extent of the lateral connections and other model parameters will be considered in the next section. We desire the initial model to be simple and tractable, so we will restrict the main investigation to a one dimensional array of units (as shown in Figure 4.2). This simplifies both analysing the network and deriving the necessary parameters such as connectivity. Further we assume this array does not necessarily represent the ‘‘physical’’ placement of units, rather that it represents a collection of units that are laterally and recurrently connected. In particular, it represents an extracted sample of recurrent circuits from the STh. The size and

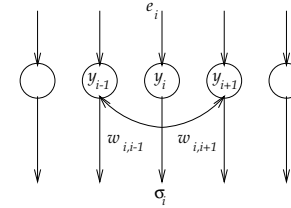


Figure 4.2: Each unit receives an external input ( $e_i$ ) and lateral input from its neighbours. All inputs are considered to be excitatory. The immediate collateral connections from only one unit are shown here. All units have an average output firing frequency  $\sigma_i$ .

type of such circuits will be addressed in the following section. Finally, all units in the network are considered to have lateral connections. Units without axon collaterals play no active role in the internal STh dynamics and therefore may be excluded from the system.

### 4.3 Model Constraints

There are a number of parameters in the system that directly affect the model’s behaviour. The most obvious are  $Z_{max}$ ,  $w_{ij}$ ,  $y_0$ , and  $b$ . We wish to consider how these parameters may be constrained, albeit loosely, to biologically realistic ranges of values. It is indeed very difficult to form clear relations between such an abstract model and specific biological properties. Nevertheless, there are some biological constraints that may be placed on most of the parameters. As much of the experimental research into the STh is performed in rat, the model will be orientated to capturing the primary features of rat STh. All referenced experimental observations are from rat, unless explicitly stated otherwise.

### 4.3.1 Connectivity

Explicit connectivity between neurons is one of the most difficult parameters to constrain to biologically realistic values. Computational models require complete specification of which units connect to which other units, and how much they will computationally influence each other (an explicit weight). However, current anatomical and physiological research can only provide such information either in small particular instances, or in general unspecific terms. For example, the detailed extent and branching of internal axon collaterals observed in the STh is unknown. Furthermore, there is no direct evidence that these form synapses on other STh projection neurons. The situation becomes even more complex since the concept of computational connectivity through a “weight” has no single biological equivalent. Due to the abstract level of the model the term “weight” encompasses many biophysical processes<sup>3</sup>. It is therefore very difficult to choose specific connectivity and weight values required in a computational model with clear biological motivation. In this subsection we introduce the lengthy procedure of geometric modelling in order to begin to address the extent of lateral connectivity present in the STh.

It is first useful to take an anatomical perspective of the subthalamic nucleus. The STh is roughly a disk shaped nucleus with the two longest axes in the rostrocaudal and dorsolateral–ventromedial orientations. Afsharpour (1985a) observes that the two longest axes are equal in length and approximately 1–1.5mm long. The shorter axis was observed to be 250–300 $\mu$ m. From Kita et al. (1983a) the longest rostrocaudal and dorsolateral–ventromedial lengths are approximately 1.6mm and 1.1mm respectively, with the widest mediadorsal–ventrolateral width (the shortest axis of the disk) approximately 400 $\mu$ m. From these observations we simplify the nucleus to an oblate spheroid with dimensions and orientations given in Figure 4.3. We take conservative estimates of axis lengths, since the STh is observed to have sharper edge tapering than an oblate spheroid. From these idealisations we can estimate the volume of the subthalamic nucleus to be around 0.131mm<sup>3</sup>.

<sup>3</sup>For example, the term “weight” may encompass post-synaptic efficiency, synaptic vesicle release, number of synapses between two neurons, etc..

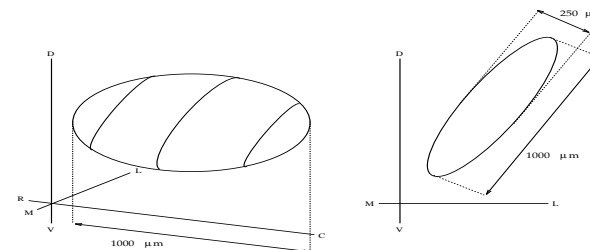


Figure 4.3: The idealised orientation, size, and shape of the rat subthalamic nucleus. It is idealised to a disk shape, with the two longest axes of equal length in the rostrocaudal and dorsolateral–ventromedial orientations. R=rostral, C=caudal, M=medial, L=lateral, D=dorsal, V=ventral.

If we assume that the density of neurons in the rat STh is similar to that in mouse (numbers taken from Sturrock, 1991) then we estimate there to be in the order of 16,000 rat STh neurons. However, recent research reveals a figure of  $13,560 \pm 1,410$  (Oorschot, D.E., personal communication). The difference is most likely to be due to the oblate spheroid assumption, producing an over estimation of volume. From the neuron density, it is possible to gauge the approximate degree of the lateral connectivity. By making assumptions about dendritic and axon collateral field shapes we may begin to put limits on the extent of lateral connections that may occur in the rat STh.

The dendritic field of a single STh neuron is difficult to approximate. Afsharpour (1985a) describes the dendritic fields of a majority of neurons as “a flat oval dendritic field such that the long axis is parallel to the long axis of the nucleus” (p. 3). The observations of Kita et al. (1983a) from all three planes of view agree with the idea that the majority of dendritic fields are oval with an orientation parallel to that of the nucleus itself. The dendritic tree structure is explored in more detail in Chapter 6, but for the purposes of the current simplified model we will consider the dendritic field as a homogeneous volume. Dendrites can extend over 500 $\mu$ m, and on average there are 3–4 primary dendrites extending from the soma. Given such lengths, it is possible for a dendritic field to extend across 1,000 $\mu$ m. Indeed, Kita et al. (1983a) report “the largest extent of the dendritic field would usually cover about half the area of STh in every plane of view” (p. 247). However,

since we assume that the dendrites form a uniform and calculable *field* for the purposes of estimating lateral connectivity, a more conservative estimate may be profitable. We assume that the dendritic fields are similar in shape to the nucleus itself, i.e. roughly a disk with the two longest axes  $500\mu\text{m}$ , and the shorter axis of  $125\mu\text{m}$ . These dimensions were chosen to allow the mean longest dendrites to course a real distance of  $250\mu\text{m}$  in one direction, absorbing  $250\mu\text{m}$  in other directions. This provides a conservative approximation of dendritic field size. We will use the oblate spheroid with the above dimensions as an approximation of dendritic field volume. Therefore the estimated volume of a dendritic field is calculated to be  $1.6 \times 10^7 \mu\text{m}^3$  ( $0.016\text{mm}^3$ ).

About 50% of STh neurons in rat are reported to have internal axon collaterals, and many of these were observed in the rostral half of the nucleus (Kita et al., 1983a). The majority of collaterals within the STh were observed to terminate *outside* the parent's dendritic field (although not all observed examples did so). Examples of neurons located in the rostral half of the nucleus with collateral terminals in the caudal half were also observed. We can make some general conclusions about these axon collaterals. Firstly, with only two or three collateral branches observed to arise from the main axon (Kita et al., 1983a), a uniform field surrounding the parent's dendritic field is unlikely. Such a field would require a massive arborisation. Secondly, the terminal arborisations of these internal axons "consisted of intermittent varicosities along collateral branches and short filaments with beaded endings" (Kita et al., 1983a, p. 247). Extensive arborisation is not observed; rather it is expected that over the length of the collateral and outside the parent's dendritic field, small occasional branches and filaments extend locally around the collateral. Thirdly, as there are generally two to three such collaterals extending from the main axon, we can expect distinct and possibly isolated zones of distal neurons to be influenced. Finally, as there are few interneurons, we assume that the primary synaptic targets of the collaterals are other STh projection neurons. If we simplify the collaterals in a similar manner to how we simplified the dendritic fields, we can use the volume overlap between the dendritic and collateral fields to estimate expected connectivity (see below). We choose a cylinder as a simple geometric simplification of a collateral. This allows the primary features, such as limited branching, to be captured by the geometric representation. We assume the collaterals extend an average distance of  $200\mu\text{m}$ , and

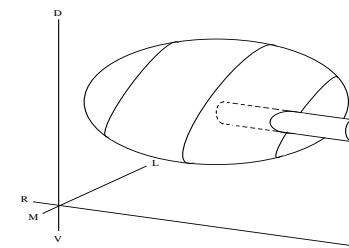


Figure 4.4: A schematic of intersecting dendritic and axon collateral fields. With simple geometric assumptions, we may use the overlap of dendritic and axon collateral fields to estimate the extent of lateral connectivity in the subthalamic nucleus. Here a dendritic field is represented as an oblate spheroid, and the intersecting axon collateral field is represented as a cylinder. It is assumed that the possible extent of synaptic contact is proportional to the volume of intersection.

synapse uniformly within a radius of  $20\mu\text{m}$ . This yields a single collateral field volume (using the cylinder geometry) of  $25,100\mu\text{m}^3$ .

All of these assumptions have been made to allow us to investigate the type of interconnectivity expected within a simplified STh structure. Given a prototypical dendritic field (in particular an oblate spheroid), a simplified single collateral field (a cylinder), and an estimate of neuron density, we may calculate how many dendritic fields may be influenced by a single collateral. For example, if we consider a single dendritic field and a single collateral field belonging to different neurons, we can calculate the volume of intersection between the two solid geometric representations (Figure 4.4). If we assume that the number of synapses that occur between the two neurons is proportional to the volume of intersection, we are able to gauge the relative influence the single collateral field may have over a unit with an intersecting dendritic field.

In order to compute the volume intersections for large populations of dendritic fields and collaterals a geometric volume simulator was constructed. The simulator was designed to calculate overlapping volumes between populations of arbitrarily orientated dendritic fields and collaterals (in this case spheroids and cylinders). All the subsequent calculations were performed using the simulator, and conformation of the geometric ar-

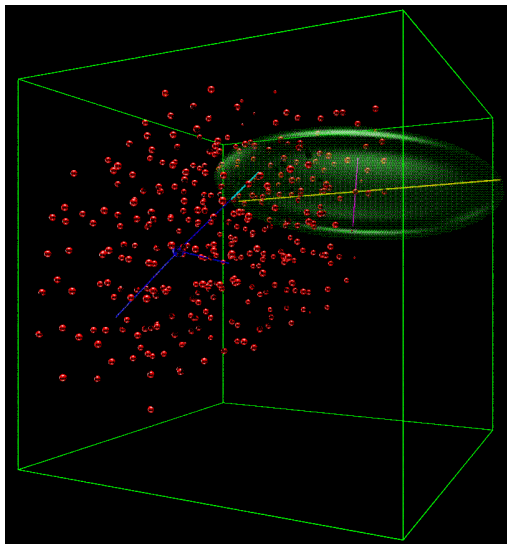


Figure 4.5: The visual output of the geometric simulator. The cube represents the spatial limits within which units are placed. In this example, 1000 units are simulated. The blue sphere represents the unit of interest. Its three collaterals are also shown in blue (note the cylinders emerging from the blue sphere). All the red spheres are the neighbouring units in the space whose dendritic fields significantly intercept any of the blue collaterals. To confirm intersection, the dendritic field of one of the red spheres is chosen at random and shown in green (the oblate spheroid). This particular intersection is highlighted in turquoise. It can be seen in this example that a large number of units have significant overlap with the unit of interest. For a more detailed description of the geometric simulator see Appendix C.

rangements and resulting field interactions could be made visually. An example visual display is illustrated in Figure 4.5.

The relative orientation of the dendritic and collateral fields in 3D space will certainly influence the possible intersections. Afsharpour (1985a) found that a majority of dendritic fields had their longest axis parallel to the longest axis of the nucleus. Initially we will assume all dendritic and collateral fields have the same orientation, that is, that they have their longest axis in the rostrocaudal direction (Figure 4.4).

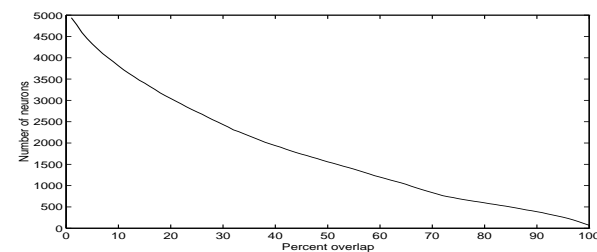


Figure 4.6: The number of units that have *at least* a certain percentage overlap with a given collateral field. Values are averaged over 5 trials, with  $2\mu\text{m}$  standard deviation variation from a uniform dendritic field placement. See text for field sizes and general procedure.

Assuming that units are regularly spaced in a cubic lattice with only a little variation from a perfect uniform distribution<sup>4</sup>, we calculate from the above estimated neuron density of  $138,000 \text{ cells}/\text{mm}^3$  the number of units that a single collateral field will intersect (Figure 4.6). The arrangement is such that a single collateral field is immersed in a 3D population of dendritic fields. At this stage we are only interested in situations where the collateral field remains within the confines of a nucleus with near uniform cell density. The number of units shown for a given percentage of field overlap is the total number of units that have *at least* that percent intersection (100% intersection would be where a collateral was completely immersed in the dendritic field). As shown in Figure 4.6 an average of 4939 units in the 3D arrangement have at least 1% overlap with the collateral field, whereas 1557 units intersect  $\geq 50\%$  volume of the given collateral field.

We must interpret these values very carefully. A large number of assumptions were made (albeit necessarily) in order to derive them, so equally we can expect a large range of possible values around those calculated. By no means can we use these calculations as definitive connectivity specifications. Rather, the volume field formalism allows us to begin to explore the possible extent of connectivity within the nucleus.

Let us first limit the side effects of assuming that the fields are homogeneous volumes

<sup>4</sup>Spacing of units is slightly randomised, such that units vary with a Gaussian distribution from the position that would yield a perfect uniform arrangement. A random variation in dendritic field position reduces artificial effects that can arise from a uniform arrangement of dendritic fields of identical shape and volume.



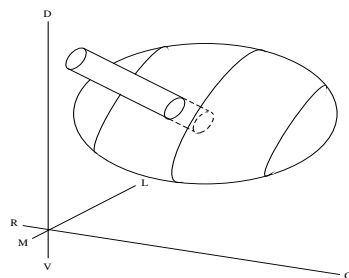


Figure 4.7: A schematic of intersecting dendritic and axon collateral fields. Here, the collateral is perpendicular to the face of the dendritic field.

by considering a 50% overlap between a collateral field and a dendritic field as the point where the unit owning the collateral field has synaptic innervations extensive enough to begin to influence the unit belonging to the intersecting dendritic field. All ramifications of this imposed limit are as unclear as the volume simplifications themselves. However, a primary consequence is likely to be a reduction in spurious connections that result from the use of homogeneous volumes alone. By considering such a large overlap as the point where one unit begins to *affect* another we increase the confidence in the likelihood of real connections between neurons of a similar arrangement in the nucleus.

A further assumption we wish to address is the relative orientation of the dendritic and axon collateral fields. The orientations chosen in the above calculations (both fields with their long axes in the rostral–caudal direction) allows for large overlaps, but due to the relative size and shapes of the fields, fewer dendritic fields are intersected by a collateral of this orientation. This is because a collateral in, say, a dorsomedial–ventrolateral orientation (i.e. perpendicular to the face of the disk – see Figure 4.7) allows significantly more dendritic fields to intersect it due to the nature of the dendritic fields being effectively skewed spheres (oblate spheroids). Figure 4.8A illustrates the dramatic effect that orientation can have on the number of intersecting units. This figure shows the same plot as Figure 4.6 except over collateral orientation varying from 0 (rostrocaudal) to  $\pi/2$  (dorsomedial–ventrolateral) radians (rotation about a medial–lateral axis). It is worth noting that a single collateral at an orientation perpendicular to the face of the dendritic

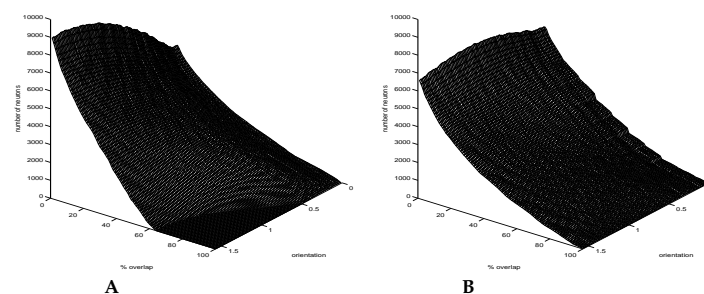


Figure 4.8: The number of units that have *at least* a certain percentage overlap with a given collateral field. The numbers are counted both for percentage overlap and collateral field orientation with respect to the dendritic fields. Dendritic fields are uniformly orientated and positioned with a random spatial variation given by a Gaussian distribution with a  $2\mu\text{m}$  standard deviation. A. Collateral length  $200\mu\text{m}$  and radius  $20\mu\text{m}$ . B. Collateral length  $100\mu\text{m}$  and radius  $40\mu\text{m}$ . The stepping observed around zero orientation is a side effect of imposing uniform field sizes.

fields can intercept around 9000 units. This appears extremely high considering that there are only around 13,500 units in the nucleus. However, we have assumed that collaterals are completely immersed in a near uniform distribution of dendritic fields. Figure 4.9 illustrates that, given the dimension of the nucleus and the dendritic field sizes, this is possible for straight collaterals in such a situation. If we perform the same calculations with a collateral of half the length ( $100\mu\text{m}$ ) and twice the radius, the number of intersected units is roughly the same over all orientations (Figure 4.8B).

Figure 4.8A shows that at greater orientations (i.e. the collateral tending more towards the perpendicular with respect to the disk face) high percentage overlap is simply not possible. The maximum width of a dendritic field is less than the length of the collateral extent, allowing only limited overlap between two fields at near perpendicular angles. However, for lower percentage overlaps there are a greater number of dendritic fields intersecting the collateral. Table 4.1 lists some of the specific values. Note that the number of intersecting dendritic fields with  $\geq 50\%$  overlap with the collateral field vary less with change in collateral orientation than lower percentage overlaps (0.8 fold decrease over orientation compared to 1.8 fold increase).

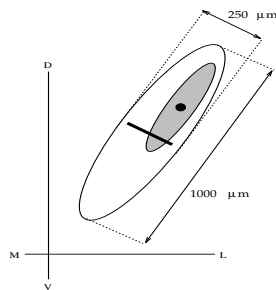


Figure 4.9: A 200  $\mu\text{m}$  collateral is shown as the thick line in the centre of the nucleus and is contained completely within the nucleus. This collateral is also perpendicular to the face of the dendritic fields. One example dendritic field is shown in grey; it is clear that this collateral could intersect a large proportion of all the dendritic fields in the nucleus.

It is possible that there are recurrent circuits within the STh. Addressing the issue of the connectivity allows us to address the possible extent of recurrent circuits, and from this we can consider their effect on the computational processing being performed.

We will take the smallest number of units with  $\geq 50\%$  overlap from the range of orientations considered for use in further calculations. This will allow us to place a minimum bound on the possible connectivities independent of orientation<sup>5</sup>. Approximately 1000 units have  $\geq 50\%$  volume intersection with a given collateral field in the dorsomedial-ventrolateral orientation. This orientation yields the lowest number of calculated intersecting units. If a given unit has approximately three collaterals (Kita et al., 1983a) then that unit theoretically has the ability to affect one quarter of the entire nucleus (given that each collateral may independently affect approximately 1000 units). Of the units contacted, 50% are expected to have collaterals themselves. Therefore, in theory *each* can contact an independent quarter of the nucleus. Thus we have a high degree of first order recurrence (direct recurrent connections between two units), and massive higher order recurrence (i.e. with intervening units in the recurrent circuit). It is very clear that the nucleus is extremely well connected. Even if we assume that only 10% of the significantly overlapping collaterals form synapses (as opposed to 50% in the above calculations), the

<sup>5</sup>This will only make calculations independent of orientations involving rotation about a medial-lateral axis. More complex orientations are assumed to have similar effects.

Table 4.1: Example of calculated values of the number of dendritic fields that intersect a collateral field for varying collateral orientation and percentage overlap. Note that these examples are drawn from a single calculation, so the values may differ from the means given in the text and Figure 4.6.

Orientation	Percent Overlap				
	1	25	50	75	100
0	4925	2705	1552	690	61
$\pi/8$	6453	3385	1995	971	30
$\pi/4$	7866	3942	1854	320	0
$3\pi/8$	8780	4342	1467	0	0
$\pi/2$	8989	4496	1241	0	0

network is still tightly interconnected, and is likely to contain massive recurrent circuits.

It is clear from this anatomical analysis that recurrent circuits are likely to occur, and in fact may be quite extensive throughout the STh. However there is little anatomical data available exploring the nature and extent of the intranuclei axon collaterals themselves; in particular, how they course and branch, what distances they extend, and what directions they follow. Despite this, it is primarily the large dendritic fields of STh neurons that leads to such high connectivity. As we observed, orientations and shapes of the collaterals played little role in the numbers of dendritic fields significantly influenced ( $\geq 50\%$ ).

Having predicted from the geometric simulations massive connectivity, the network model still requires the specification of an explicit weight between connected units. There are two approaches we could take to achieve this. We could use the relative volume intercepts between a given collateral and dendritic field as a measure of the weight. For example, the complete dendritic and collateral fields of a population of neurons could be geometrically simulated to generate a specific instance of connectivity. Alternatively, we could assume a generic Gaussian weight distribution such that the weight between two units is given as a function of some measure of distance between them. Both of these approaches produce relative weights based on well defined formalisms. Yet both specify only *relative* weights. For example, until we assign a physical weight to a 100% collateral dendritic field overlap or to the peak of the Gaussian, all the weights

remain unspecified. Once the point of reference is established, both approaches are sufficient for a complete specification of model connectivity.

This “peak” weight parameter is effectively undefined, as influences between neighbouring STh neurons are unmeasured. However, if we continue to use a simplified neuron, we can use mathematical and numerical integration techniques to observe the effect of different peak weight values. We therefore chose the Gaussian distribution as a more generic approach. The geometric simulations produce specific instances of a connectivity distribution and would require large numbers of simulations to discern average properties. Furthermore, as large geometric simulations are computationally intensive (consider 500 units, each with three collaterals all positioned in 3D space) and may produce simulation artifacts (for example, complex edge effects) the simpler Gaussian distribution may allow for a clearer analysis<sup>6</sup>.

The only limiting factors in the choice of the peak and shape of the Gaussian distribution used are the following two observations

1. Weights must not exist beyond the estimated connectivity calculated above. However, this places little constraint on the weights, as the STh has been calculated to be massively connected.
2. The chosen weights should not cause the resting firing rate to exceed realistic observed bounds. Here we require that the level and extent of weights included in the model maintain a resting firing rate less than 50Hz.

Figure 4.10 illustrates a Gaussian distribution used for the weights of unit 1 in a 500 unit network torus. It should be noted that the distance between two units in the array does not necessarily correspond to the physical distance that separate the units in the theoretical nucleus, rather it is related to the strength of recurrent connections between two units.

<sup>6</sup>Weight distributions from volume intersection calculations were used in simulations (not shown) and edge effects were found to be a considerable problem. As these weight distributions are generated from specific random placement of a population of units, a simple torus could not easily be adopted as in the Gaussian distribution case.

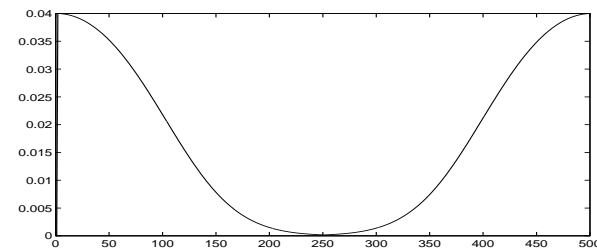


Figure 4.10: Weight distribution for unit 1 in a 500 unit one dimensional torus of units. The Gaussian has a peak of 0.04 and a spread ( $\beta$ ) of 0.0001. Note that the connection from unit 1 to itself has zero weight.

This is the primary feature we wish to capture at this stage, as the purpose of this model is to investigate the nature and effect of such recurrent connections, and infer how such connections may affect cortical–basal ganglia influences that occur through the STh.

### 4.3.2 Firing Rate

The maximum firing rate ( $Z_{max}$ ) of a STh projection neuron has been found to be near 500Hz (Kita et al., 1983b). We can use the current/voltage and current/firing-rate relations observed in STh neurons (Nakanishi et al., 1987a) to estimate the sigmoid threshold,  $y_0$ , and the sigmoid gain,  $b$ , in the model. Here, “current” refers to intracellular current injection in *in vitro* slices. It is assumed there is a sigmoidal relation between voltage and resulting firing rate. A derivation of the estimated experimental voltage/firing-rate relation is undertaken and then fitted with a sigmoidal function. Both the sigmoid gain and threshold are then determined from the resulting fit. Data was taken from Nakanishi et al. (1987a) and a voltage/firing-rate relation was generated (Figure 4.11). Added hyperpolarising currents (used to suppress spontaneous firing) were subtracted from the calculations. The resulting curve is considered accurate only over the ranges of injected current common to both the current/firing-rate and current/voltage relations. As there is possibly a large degree of error in the data (resulting from the sparseness of data points and transformations into the voltage/frequency form) we may only place bounds on the

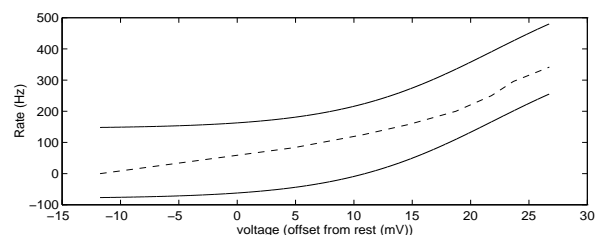


Figure 4.11: The data and sigmoid approximation bounds for the voltage/firing-rate relation. We can predict that the sigmoid threshold lies within  $15 \leq y_0 \leq 22$  and sigmoid gain  $0.1 \leq b \leq 0.3$ . The data is given as a dashed line, and the sigmoid bounds are given as solid lines. Notice that as the parameters  $b$  and  $y_0$  primarily effect the sigmoid shape/form, the bounds illustrate outer limits of the sigmoid contortions and not example sigmoid functions. Small negative vertical shifts may be included in the simulations to enforce zero firing rates at negative potentials.

primary sigmoid parameters. We can expect the sigmoid threshold to lie between 15 and 22mV. As this parameter moves outside these bounds the sigmoid functions at higher voltage become very distorted. Similarly we expect the sigmoid gain,  $b$ , to lie between 0.1 and 0.3. For gains outside these limits the curvature of the sigmoid deviates significantly from the experimental values. Figure 4.1 illustrates an example sigmoid function generated from parameters lying within the above bounds.

The resulting parameter constraints give a very large range of values from which to choose. However, we can be reasonably confident that realistic values do not lie outside this range. It is important to emphasize that this model introduces many simplifications that may lump together biologically distinct functions (for example, the voltage–firing rate relation describes a broad observation influenced and generated by many independent processes, see Chapter 6). In fact, the sigmoid assumption is itself likely to be inaccurate (higher order functions undoubtedly may be fitted to the relation more accurately). Yet, by fixing all the parameters so as to capture the *characteristic* experimental observations, it is hoped that the model will reflect the consequential characteristic network behaviour.

### 4.3.3 Cortical Innervation

Finally, we need to consider the cortical innervation of the STh. Note at this simplified model stage, we will only consider the cortical STh afferents. Brief cortical stimulation appears to produce widespread prolonged subthalamic activation (Fujimoto & Kita, 1993). It is unclear as to whether the spread and increase in duration occurs within the cortex, STh, or a combination of the two. Cortical innervation in most simulations followed a Gaussian distribution, such that a central unit is maximally stimulated while units more distal to this chosen central unit receive less stimulation. The use of a generic distribution allows both peak and spread effects to be explored numerically in the simulations.

## Chapter 5

# Analysis of the Dynamic Network Model

In this chapter we aim to explore the types of behaviours exhibited by the dynamic network model presented in the previous chapter. Two approaches will be used to accomplish this. Firstly, a mathematical analysis of the model will be undertaken using bifurcation theory. Secondly, numerical integration allows us to simulate the model under specific input and parameter conditions. The *combination* of these two methods is important. The mathematical analysis allows us to identify what general types of asymptotic behaviours exist in such a system, and within which parameter bounds these will occur. However, this analysis requires unrealistic model simplifications. Therefore numerical integration allows us to investigate the system under more realistic conditions and further explore transient as well as asymptotic behaviours. *Together*, these approaches provide a powerful tool in the investigation of the dynamic model.

The numerical integration of the model is performed using the simulator *Rorohiko*, described in Appendix A. This provides a single formalism for both this network model

and the more complex models presented in later chapters. All simulations were performed on a DEC *alpha* 3500S. A single simulation of 500 units for 300msec with full connectivity (250,000 connections) required 30–40 minutes<sup>1</sup>. Numerical calculation of phase plots and all graphical results are produced using the mathematical package MATLAB®. The numerical calculation of the stable equilibrium solution spaces were produced using a dedicated program written in C (see Appendix B).

### 5.1 Analytical Results

We can use techniques of bifurcation theory and stability theory (for an introduction to these see Guckenheimer and Holmes, 1983) to discern the *asymptotic* behaviours of the dynamic system. These are behaviours such that once the system has reached an asymptotic behaviour, it remains in that behaviour unless externally disturbed. For example, once the systems shown in Figure 5.5 reach their respective resting potentials, they remain at those potentials unless externally acted upon (here, by cortical stimulation). The *transient* behaviour of the system is the behaviour that occurs as the system moves to and from asymptotic states. This behaviour is much more difficult to qualitatively characterise (if at all possible), and generally techniques of numerical integration are used in a quantitative analysis (see Sections 5.3 and 5.4 below). However, analysis of the asymptotic behaviour allows us to determine whether distinctly different behaviours occur, and under what parameter ranges these are possible. We choose to undertake the mathematical analysis prior to the numerical integration so as to guide the parameter selections of the simulations to explore behaviours of interest. Using the analytical results we may focus the simulations onto the different types of asymptotic behaviours the system can produce. This in turn will allow us to address all the possible behaviours the system can produce in terms of the types of processing the subthalamic nucleus may be performing.

<sup>1</sup>The simulation time could be dramatically reduced by decreasing the accuracy of the Runge–Kutta algorithm. However, this time was necessary for high accuracy.

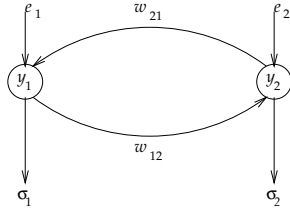


Figure 5.1: A two unit simplification of the dynamic network model. Each unit receives an external input ( $e_i$ ) which is considered constant over the period of analysis. Recurrent lateral connections have a uniform weight value  $w_{12} = w_{21} = w$ . In addition to this all units share common parameters  $\tau$ ,  $Z_{max}$ ,  $y_0$ , and  $b$ , and the external inputs are the same ( $e_1 = e_2$ ).

### 5.1.1 Two Unit Case

We begin by introducing a number of simplifications to make the analysis both tractable and as straightforward as possible. At this stage we reduce the model to the two-unit case, as illustrated in Figure 5.1. Firstly, it is assumed that the input  $\{e_1, e_2\}$  is constant over the period of analysis. Secondly, we assume a fully symmetrically connected network (with no self-connections), such that  $w_{12} = w_{21} = w$ . Thirdly, we assume all units have identical core parameters  $\tau$ ,  $Z_{max}$ ,  $b$ , and  $y_0$ . Finally, we assume that there are zero delays between connected units (for an analysis of a morphologically similar network with lateral delays, see Marcus and Westervelt 1989).

The two-unit system may be written as

$$\begin{aligned}\tau \dot{y}_1 &= -y_1 + w_{21} Z_{max} \sigma_2 + e_1 \\ \tau \dot{y}_2 &= -y_2 + w_{12} Z_{max} \sigma_1 + e_2\end{aligned}\quad (5.1)$$

where  $\sigma_i$  is given by

$$\sigma_i = \frac{1}{1 + \exp(-b(y_i - y_0))}\quad (5.2)$$

We may intuitively infer that a bifurcation of system behaviour exists under certain conditions by drawing phase planes of the two-unit network for example parameters. Figure 5.2 illustrates two phase planes of the dynamic network for different parameter sets.

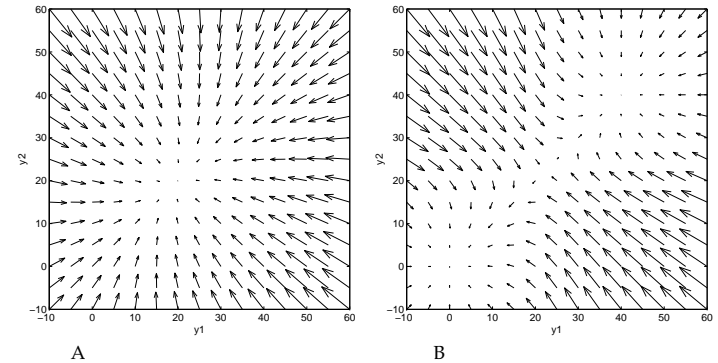


Figure 5.2: **A.** Phase plane for the Equations 5.1 with parameters  $w_{21} = w_{12} = 80.0$ ,  $Z_{max} = 500\text{Hz}$ ,  $b = 0.02$ , and  $y_0 = 22.0$ . **B.** Phase plane with  $b = 0.3$ ; otherwise the parameters are the same as in **A.**

Given a parameter condition that contains small sigmoid gradient  $b$  (Figure 5.2A) the phase plane indicates that only one solution with medium voltage ( $y$ ) exists. With larger sigmoid gradient (Figure 5.2B) the phase plane indicates two stable solutions, implying that a bifurcation has taken place during the transition of  $b$  to a higher value.

There is an alternative way of viewing multiple solutions, and in particular changes in solutions, over varying parameters. If we plot numerically calculated points of stability, extracted from phase plane type information (see Appendix B), we may watch solution changes as we vary a parameter. Since in our simple two-unit model the solutions will always lie on the diagonal of the phase plane (i.e.  $y_1 = y_2$  since  $w_{21} = w_{12} = w$  and  $e_1 = e_2$ ) we need only consider one of the voltage variables. Thus we can plot stable solution points (of  $y$ ) versus a parameter of interest (e.g.  $w$ ). This is essentially the same as a bifurcation diagram, except we do not plot unstable solutions. Figure 5.3A illustrates the change in solutions as we vary the parameter  $b$  from a low to high value, with all other parameters remaining constant. We see the emergence of two stable solutions about the  $b \approx 0.15$  value. However,  $b$  is not the only parameter whose alteration can cause a change in the number of stable solutions. Figure 5.3B illustrates changes in solutions as we vary only the parameter  $w$ . We will explore the relationship between the

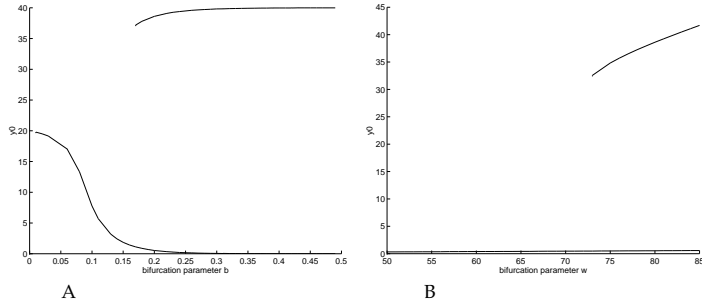


Figure 5.3: **A.** Stable solution diagram demonstrating the split into two solutions as the parameter  $b$  is increased. Unstable solutions are not shown. Other parameters,  $Z_{max} = 500\text{Hz}$ ,  $w = 80$ , and  $y_0 = 22.0$ . **B.** A similar diagram illustrating the split into two stable solutions as the weight  $w$  is increased. Parameters as for **A** with  $b = 0.2$ .

parameters and the changes in the system behaviour using bifurcation theory.

The system is nonlinear, and in this form an analysis is very difficult. However, under certain conditions, a suitably linearised system is morphologically similar (homeomorphic) in the vicinity of the equilibrium points (see the Hartman–Grobman Theorem, in Guckenheimer and Holmes 1983). At equilibrium (i.e.  $\dot{y}_i = 0$ ) the system (5.1) becomes:

$$\begin{aligned}\bar{y}_1 &= w_{21}Z_{max}\bar{\sigma}_2 + e_1 \\ \bar{y}_2 &= w_{12}Z_{max}\bar{\sigma}_1 + e_2\end{aligned}\quad (5.3)$$

where the bar represents the value of the system variable (or function) at the equilibrium point. The linearised system may be constructed from the Jacobian matrix of Equations 5.1 calculated at the equilibrium point:

$$L = \begin{bmatrix} -\frac{1}{\tau} & q \\ r & -\frac{1}{\tau} \end{bmatrix}\quad (5.4)$$

where

$$\begin{aligned}q &= \frac{1}{\tau}w_{21}Z_{max}b\bar{\sigma}_2(1 - \bar{\sigma}_2) \\ r &= \frac{1}{\tau}w_{12}Z_{max}b\bar{\sigma}_1(1 - \bar{\sigma}_1)\end{aligned}\quad (5.5)$$

such that the linearised system is given by

$$\dot{y} = Ly\quad (5.6)$$

If we could calculate an equivalent diagonal matrix of  $L$

$$L_d = \begin{bmatrix} \lambda_1 & 0 \\ 0 & \lambda_2 \end{bmatrix}\quad (5.7)$$

then the Equations 5.6 would become uncoupled and solutions of the linearised system could be calculated directly. In fact we do not need to diagonalize the matrix, rather we need only investigate the eigenvalues of the matrix  $L$ . These may be found from the roots of the characteristic equation (given by  $\det |\lambda I - L| = 0$ )

$$\begin{aligned}\left(\lambda_i + \frac{1}{\tau}\right)^2 - qr &= 0 \\ \lambda_i + \frac{1}{\tau} &= \pm\sqrt{qr} \\ \tau\lambda_i &= \pm wZ_{max}b\bar{\sigma}(1 - \bar{\sigma}) - 1\end{aligned}\quad (5.8)$$

The eigenvalues of the linearised matrix reveal important characteristics of the system about the equilibrium points. We are particularly interested in situations where a parameter change leads to distinct changes in the asymptotic solutions. The solutions of the linearised system take the form of

$$y_i(t) = k e^{\lambda_i t}\quad (5.9)$$

where  $k$  is a constant. Since it has been shown that the linear system chosen above is morphologically similar to the nonlinear system about the equilibrium points (see Guckenheimer and Holmes 1983) we can therefore also characterise the types of asymptotic behaviours the nonlinear system exhibits. Noting the phase diagram (Figure 5.2B) it would be advantageous to find parameter conditions that lead to the generation of an unstable solution (in this case a saddle point). If we could find the parameter changes that lead to the system developing this unstable point, we would have found the critical point leading to the bifurcation.

The system has a single stable solution when

$$\lambda_i < 0, \quad i = 1, 2.\quad (5.10)$$

However, when one of the eigenvalues becomes greater than zero, we have an unstable solution and thus a bifurcation has taken place (consider a positive eigenvalue in Equa-

tion 5.9). In our model,  $\tau$ ,  $w$ ,  $b$ ,  $Z_{max}$ , and  $\bar{\sigma}$  are all greater than zero by definition. Furthermore, the sigmoid function  $\bar{\sigma} \leq 1$ . Therefore, it is only possible that one of the two eigenvalues may become positive, in particular, the eigenvalue given by

$$\tau\lambda_1 = wZ_{max}b\bar{\sigma}(1 - \bar{\sigma}) - 1 \quad (5.11)$$

This will occur under the parameter conditions

$$wZ_{max}b\bar{\sigma}(1 - \bar{\sigma}) > 1 \quad (5.12)$$

i.e. an equilibrium condition which satisfies this is *unstable*. The point at which the system becomes unstable is called the *critical point* and, for this model, it occurs when

$$wZ_{max}b\bar{\sigma}(1 - \bar{\sigma}) = 1 \quad (5.13)$$

This condition for bifurcation, (i.e. a change in equilibrium states) reveals important facts about the system. Firstly, note that  $0 < \bar{\sigma}(1 - \bar{\sigma}) \leq 0.5$ . This directly places constraints on the condition for bifurcation. The critical point may only be reached (i.e. a bifurcation may only occur) given that

$$wZ_{max}b \geq 2.0 \quad (5.14)$$

We can therefore begin to see why changes in different parameters, such as  $b$  and  $w$  can both lead to bifurcations as illustrated in Figures 5.3A, B. For a system with a single equilibrium point, increases in either of these parameters can independently force the eigenvalue given in Equation 5.11 to become positive, thus generating an unstable solution and leading to a distinctly different asymptotic behaviour.

If the inequality (5.14) does not hold, a bifurcation will not be possible and the system will reside (asymptotically) in the single solution state. However, if it does hold for a certain equilibrium point and parameter regime, there may be other equilibrium points under the same parameter regime where  $\bar{\sigma}(1 - \bar{\sigma})$  is exceedingly small. This leads to alternative stable solutions in addition to the unstable one. The function  $\bar{\sigma}(1 - \bar{\sigma})$  becomes very small for  $y \gg y_0$  or  $y \ll y_0$ . Thus there may be two stable solutions beyond the critical point. The unstable equilibrium point lies where  $\bar{\sigma}(1 - \bar{\sigma})$  is maximised, which occurs when  $y$  is near  $y_0$ .

What are the consequences of the two-unit analysis for the dynamic STh model? Firstly, depending on the parameters, we can expect two dramatically different asymptotic behaviours. Parameters producing a system that resides below the critical point lead to a situation where a *single* stable equilibrium exists and the system will always return to that one asymptotic behaviour. Alternatively, parameters producing a system that resides beyond the critical point may have two stable solutions, whereupon the system could rest in either one. Secondly, the system is critically dependent on the parameters  $w$ ,  $b$ , and  $Z_{max}$  as these will determine which of the two behaviours are possible. As discussed in Chapter 4,  $Z_{max}$  is possibly the only parameter of the three that can be confidently constrained. The sigmoid gain,  $b$ , may vary between 0.1 and 0.3 and the weight magnitude,  $w$ , is unknown. Therefore, at this stage it is difficult to predict on which side of the critical point the behaviour of the dynamic model should reside. We must emphasise, however, that the above analysis only applies to the two-unit case. In the following section we extend the analysis into the  $N$ -unit case to determine the effect of an arbitrarily large number of units on the system dynamics. This may also provide an indication as to which side of the critical point the system may reside.

### 5.1.2 $N$ Unit Case

By continuing the assumption that all units in the network are interconnected by a constant weight  $w$ , with the exception of self connection, and further, that all units are identical, a simple  $N$ -unit analysis is possible. We take the same approach as for the two-unit case, where we use the eigenvalues of the Jacobian matrix about the equilibrium points. In  $N$ -dimensions the Jacobian matrix becomes

$$\mathbf{L} = \begin{bmatrix} -\frac{1}{\tau} & q_2 & q_3 & \cdots & q_N \\ q_1 & -\frac{1}{\tau} & q_3 & \cdots & q_N \\ q_1 & q_2 & -\frac{1}{\tau} & \cdots & q_N \\ \vdots & & & \ddots & \vdots \\ q_1 & q_2 & q_3 & \cdots & -\frac{1}{\tau} \end{bmatrix} \quad (5.15)$$



where  $q_i$  is given by

$$q_i = \frac{1}{\tau} w Z_{max} b \bar{\sigma}_i (1 - \bar{\sigma}_i) \quad (5.16)$$

and  $\bar{\sigma}_i$  is  $\sigma_i$  (given by Equation 5.2) at the equilibrium point  $\bar{y}_i$ . This matrix can be simplified into the form

$$L = \frac{1}{\tau} (qS - I) \quad (5.17)$$

where

$$S = \begin{bmatrix} 0 & w & w & \cdots & w \\ w & 0 & w & \cdots & w \\ w & w & 0 & \cdots & w \\ \vdots & & & \ddots & \vdots \\ w & w & w & \cdots & 0 \end{bmatrix} \quad \text{and} \quad I = \begin{bmatrix} 1 & 0 & 0 & \cdots & 0 \\ 0 & 1 & 0 & \cdots & 0 \\ 0 & 0 & 1 & \cdots & 0 \\ \vdots & & & \ddots & \vdots \\ 0 & 0 & 0 & \cdots & 1 \end{bmatrix} \quad (5.18)$$

Assuming identical units and starting point,  $q$  takes the generic form,

$$q = Z_{max} b \bar{\sigma} (1 - \bar{\sigma}) \quad (5.19)$$

If the simplified matrix S has eigenvalues  $\alpha$  and eigenvectors  $\mathbf{v}$ , such that

$$S\mathbf{v} = \alpha\mathbf{v}$$

then, defining  $M = qS$ , the eigenvalues of M are given by  $M\mathbf{v} = qS\mathbf{v} = q\alpha\mathbf{v}$ . The eigenvalues of matrix L directly follow

$$\begin{aligned} L\mathbf{v} &= \frac{1}{\tau} (qS - I)\mathbf{v} = \frac{1}{\tau} (M - I)\mathbf{v} \\ &= \frac{1}{\tau} (M\mathbf{v} - I\mathbf{v}) = \frac{1}{\tau} (q\alpha\mathbf{v} - \mathbf{v}) \\ &= \frac{1}{\tau} (q\alpha - 1)\mathbf{v} \end{aligned}$$

Thus we need only calculate the eigenvalues  $\alpha$ , of the simplified matrix S. This matrix has eigenvalues

$$\alpha = \begin{cases} w(N-1) & \text{once} \\ -w & (N-1) \text{ degenerate} \end{cases} \quad (5.20)$$

The eigenvalues of L are then

$$\lambda = \begin{cases} \frac{1}{\tau} ((N-1)w Z_{max} b \bar{\sigma} (1 - \bar{\sigma})) - \frac{1}{\tau} & \text{once} \\ \frac{-1}{\tau} (w Z_{max} b \bar{\sigma} (1 - \bar{\sigma})) - \frac{1}{\tau} & (N-1) \text{ degenerate} \end{cases} \quad (5.21)$$

It can be seen that this collapses into Equation 5.8 for the  $N = 2$  case. Furthermore, we still only have one eigenvalue that may become positive, yielding a morphologically similar system to the two-unit case. We therefore need only consider the parameter conditions that will result in this eigenvalue becoming positive. The eigenvalue of interest is given by

$$\tau\lambda = (N-1)w Z_{max} b \bar{\sigma} (1 - \bar{\sigma}) - 1 \quad (5.22)$$

The only difference to the two-unit case is the presence of the factor  $(N-1)$ . For a large number of units in a fully connected circuit, it is more likely that the system will contain a positive eigenvalue and thus an unstable equilibrium state. In general terms, the greater the interconnectivity the more likely a given parameter system will sit beyond the critical point. As we have demonstrated in Chapter 4, the interconnectivity is likely to be large as predicted from geometric simulations. Thus for reasonable  $b$ , and  $w$  we may expect the system to reside *beyond* the critical point.

### 5.1.3 Summary

We have shown that the dynamic network model of the STh may produce one of two distinctly different system behaviours. Firstly, the *prebifurcation* system results from parameters  $N$ ,  $w$ , and  $b$  satisfying the condition

$$(N-1)wb Z_{max} \bar{\sigma} (1 - \bar{\sigma}) < 1 \quad (5.23)$$

for all equilibrium points  $\bar{y}_i$ . This system produces behaviours that will always return to a single stable resting point. Secondly the *postbifurcation* system results when

$$(N-1)wb Z_{max} \bar{\sigma} (1 - \bar{\sigma}) > 1 \quad (5.24)$$

for any equilibrium point<sup>2</sup>. This system will generate behaviours that may reside in one of possibly two states. Perturbations of the system (for example, changes in external input) may move the system from one state to another. Once the system is in a new state it will reside there until again externally acted upon. The two states may be described as high activity and low activity.

We are confident that the parameter  $N$  is large in the STh (see Section 4.3.1), i.e. that there is a large degree of lateral connectivity. Thus for the prebifurcation system to exist, the parameter  $w$  would be required to be very small (even given the minimal estimate of parameter  $b$ ). If this is the case we need to address what functions a highly connected network with extremely small connection weights will be performing. Similarly, if it is more likely the postbifurcation system exists, we need to explore what type of functions emerge from a multiple equilibrium state system.

As we have pointed out, the analytical results are restricted by unrealistic simplifications. In particular, we have assumed a fully connected network with each connection of uniform weight  $w$ . It would be advantageous to consider, for example, what dynamics occur for more realistic weight distributions based on distance between units. Thus to complete the analysis we describe in the following sections numerical simulations of such a network.

## 5.2 Simulation Results

We initially use numerical integration techniques to confirm the analytical results of Section 5.1 under more realistic connection and weight distributions. We use a network of 500 units connected as outlined in Chapter 4. For the range of realistic parameters it is found the system exhibits *three* distinctly different asymptotic behaviours: one which

<sup>2</sup>When the condition  $(N-1)wbZ_{max}\bar{\sigma}(1-\bar{\sigma}) = 1$  is satisfied, the Hartman–Grobman Theorem no longer holds and we cannot guarantee that the linear and nonlinear systems are morphologically similar about the equilibrium points.

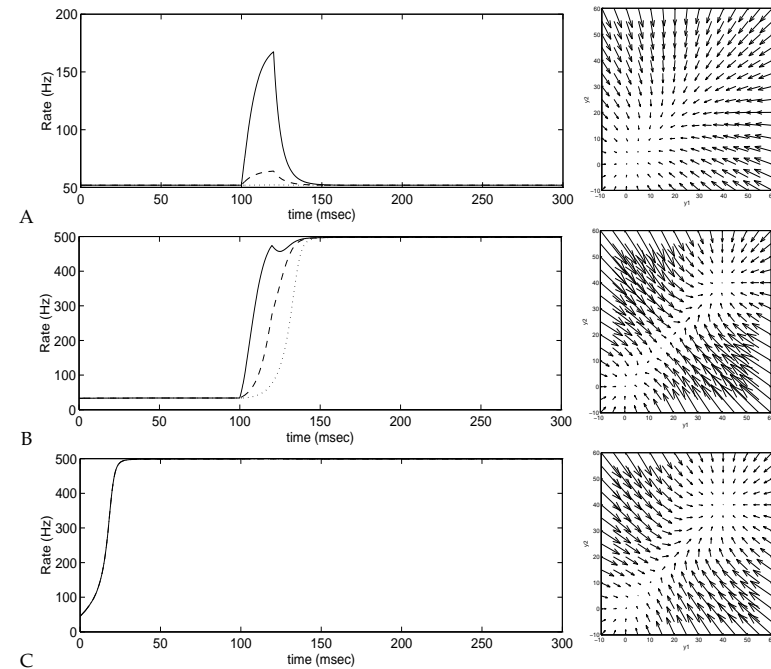


Figure 5.4: Examples of three distinctly different behaviours of the dynamic network model. In each case an example 500 unit simulation result is presented, along with a two-unit phase plot exhibiting the same behaviour. The input to each system has a strength given by a Gaussian distribution centred at unit 250. Response plots are shown for units 250, 300, and 400 (solid, dashed and dotted lines respectively).

may be classified analytically as prebifurcation, and two that may be classified as postbifurcation. Figure 5.4 illustrates simulations of all the behavioural types. Firstly, the prebifurcation system (Figure 5.4A) has only one equilibrium point. This equilibrium point is stable, and thus external input acting on the system (beginning at  $t = 100$  msec in the Figure) will only yield transient responses. At the end of the external stimulus (at  $t = 120$  msec) the system returns to the single stable equilibrium point. A two-unit phase plot with compatible parameters is also given in Figure 5.4A to illustrate the single

equilibrium point.

A two-state postbifurcation system is also clearly exhibited by the 500 unit model (Figure 5.4B). This system has two stable equilibrium points (and one unstable one) at high and low firing rates ( $\sim 35\text{Hz}$  and  $\sim 500\text{Hz}$  respectively). External input can drive this system between the two states. Figure 5.4B illustrates the same excitatory input used in Figure 5.4A pushing this system to a new equilibrium state. Once the new state is reached the system will permanently reside there unless further (in this example, inhibitory) input pushes the system back to the low state.

Finally, a one-state postbifurcation system is exhibited by the model (Figure 5.4C). This system has only one stable equilibrium state, yet has parameters that place it beyond the critical point (see Equation 5.24). In the example presented in Figure 5.4C, the only stable state is the high state. The system, without the need of external input, moves directly into the high equilibrium state and permanently resides there. As in the prebifurcation system, external input would not affect the final asymptotic resting state. As shown in the associated phase plane, the second state exists, but has merged with the unstable state. It is the system parameters (in particular  $y_0$ ) that determine which of the states becomes unstable.

In the following two sections we explore the prebifurcation and postbifurcation systems independently. We will not consider the single state postbifurcation system as the parameters used in its generation are outside our constraints (see Section 4.3.2). In particular,  $y_0$  was required to be very large to yield a single low stable state or very small to yield a single high stable state.

We will explore the two different systems with the aim of discerning what processing advantage or functions the different network dynamics produce. As we cannot exhaustively explore all the parameters we rely on the analytical results having isolated the system's primary behaviours. Within each behaviour we can only present examples of how such a system may respond to external input.

### 5.3 Prebifurcation System

We consider here the question "If STh intraconnectivity is profuse, yet so weak as not to lead to the possible two-state system, what could the function of this interconnectivity be?". In particular, we approach this question by addressing the related one, "what do *weak* profuse lateral connections add to the processing performed by the STh that would be absent in a system without such lateral connections?". We will explore this by considering two example situations. Firstly, we compare a network with weak lateral connections with a network that has no lateral connections. Secondly, we introduce more realistic connectivity delays into the system and consider their effect on the functional roles found for the weak laterally connected network.

#### 5.3.1 Example 1

A number of interesting observations may be made by comparing the response properties of the network under the conditions of weak lateral excitatory connections (WLC) with the responses generated without lateral connections (NLC). In this way important functional roles for the weak lateral connections may be discerned. Figure 5.5 illustrates the firing rates of the two networks, and in particular, their responses to identical brief external stimulation. Internal collaterals allow the network to produce a much larger and more pronounced response. Note also that, as expected, the resting firing rate of the WLC network has increased to near 50 spikes per second. This reflects the increased resting potential of each unit (not shown). The ratio of peak firing rates of the two networks is 148 : 86 (WLC:NLC). This near two-fold increase shows the dramatic effect that weak lateral connections spread over a reasonably wide area can have on response properties, despite not being large enough to alter the network's asymptotic behaviour. Furthermore, the larger resting potential of each unit increases their sensitivity to input, as each now lies closer to its threshold.

A second observation is the extension in the response duration for the WLC network. Note that this effect may be influenced by temporal delays in the lateral weights that are

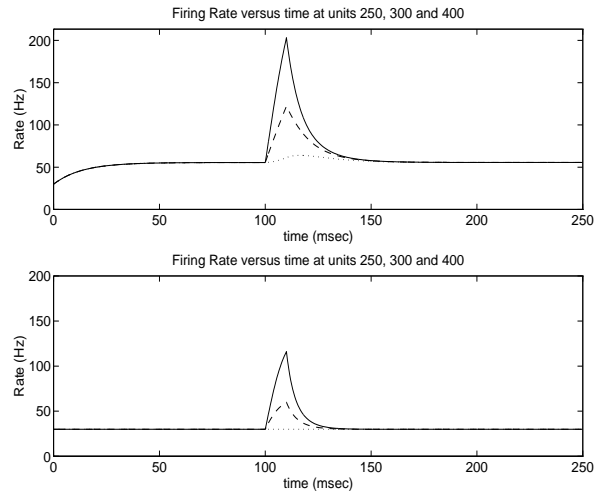


Figure 5.5: A. The top response plot shows the firing rate for units 250, 300, and 400 in a network with weak lateral connections. The connections have a Gaussian distribution with peak weight strength of 0.08. The plot shows the response to 10msec external stimulation at  $t = 100$ msec. B. A plot showing the response of a network with no lateral connections to the same excitatory input. See Figure 5.4 for the plot key.

not modelled in these simulations. The half-height width for the NLC network is 9msec, while for the WLC it is 11msec. This stretch in response duration is likely to be due to both a slower decay (as inputs from neighbouring units prolong the exponential decay) and a larger peak. A further, yet related, effect is a change in rise time. The gradient of the firing rate immediately after the presentation of the external stimulus is significantly larger for the WLC network. This is again due to the feedback from neighbouring units which contributes to a larger net input for each unit, forcing a faster increase in firing rate (see Equation 4.5). It would be more appropriate to investigate such temporal effects in simulations that include lateral delays. Such delays may extend the former observed effect, and reduce the latter. These will be explored in Example 2.

So far we have observed the effects of weak lateral connections on individual unit responses. There are also effects on the network as a whole. An indication of this is seen

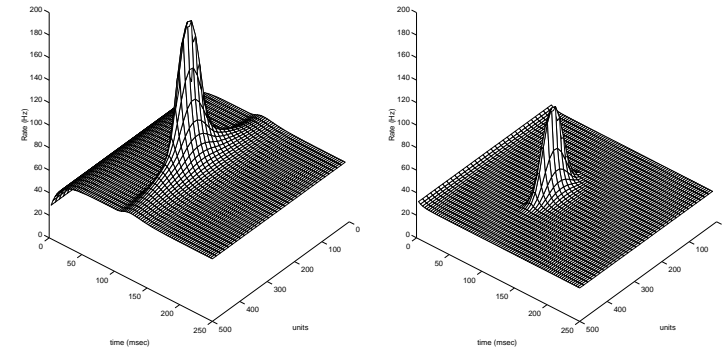


Figure 5.6: Response plots for all units over time. A. The left plot shows the same simulation of the WLC network as in Figure 5.5A for all units. Peak cortical response occurs at unit 250. B. The right plot shows the corresponding response of the NLC network. In both cases, the responses of all 500 units are not shown, rather the responses of individual units chosen at regular intervals are shown to clarify the diagram.

by looking at the response of unit 400 (dotted line) in Figure 5.5. In the WLC network there is a distinct, albeit weak, response in this unit compared to the absent response of the equivalent unit in the NLC network. Figure 5.6 shows the two network responses over all units. The shape of the Gaussian input is clearly observable. The response to this input, however, extends across a larger number of units in the WLC network. Weak lateral connections create a large neighbourhood of units that are primed (subthreshold) after a central stimulus. This effect is quite pronounced, and extends beyond the excitatory domain of 500 units<sup>3</sup>.

### 5.3.2 Example 2

Two types of lateral delays were introduced into the network. The first type is a constant delay associated with each lateral connection (this delay type will be referred to

<sup>3</sup>This effect is artificially enhanced as a result of using a network torus. However, due to the small value of the activities at the edges, such enhancement is minimal.

Table 5.1: The effect of LD and ESD delays at 1msec and 5msec (LD and max ESD). The resting firing rate, peak firing rate and half-height width of the response are given for unit 250 for each delay condition.

	Rest (Hz)	Peak (Hz)	$\frac{1}{2}$ HW (msec)
no delays	55.5	203.2	10.8
ESD (1 msec)	55.5	202.0	10.9
LD (1 msec)	55.5	195.9	11.0
ESD&LD (1 msec)	55.5	194.9	11.0
ESD (5 msec)	55.5	197.3	11.1
LD (5 msec)	55.5	177.3	11.2
ESD&LD (5 msec)	55.5	174.4	10.0

as LD). In these simulations this delay did not depend on the connection distance as it was assumed that for the average collateral distances ( $200\mu\text{m}$ ) such differences would be minimal. The second form of delay is an external input delay from the cortex. It was assumed that the first external stimulus arrival occurred at a central location (usually the same location as the maximum stimulus), and at further distances from this location the stimulus became more and more delayed. External stimulus delay (ESD) increased with distance following a Gaussian function up to a maximum. Simulations were performed with one, or both types of signalling delay at 1msec (LD and max ESD) and 5msec.

Table 5.1 lists the results of simulations for the 500 unit network under the various delay conditions. Values are given for unit 250, which received peak external stimulation and zero ESD. One of the most striking effects of all signal delays (both internal and stimulus) is the effect on the peak firing rate. For even small lateral delays (e.g. 1 msec) the unit response peak drops. This is due to the delays desynchronising the peak response to external stimulus and peak neighbourhood feedback. Consider a network with lateral delays only. All the units in the network will still produce peak responses at the same time (i.e. at the termination of external stimulus). With no lateral delays, this would also be the time that maximum feedback from neighbouring units arrives. However, by introducing lateral delays, this peak feedback occurs at a later time, no longer concurrently adding to the peak response. Thus the response of all units is reduced.

The effect of the ESD is similar, except it reduces the unit's firing rates by desynchronising the responses to the external stimulus. The ESD has a smaller effect on the peak firing rate than the LD, as units that are close to each other see very little temporal differences in the external stimulus. It is units that are close to each other that most strongly influence each other (as a result of the Gaussian weights). Thus for the central unit (unit 250) only the weak distal feedback is desynchronised which weakly reduces its response.

A second observation is that all the half-height response widths (except for the last one listed) are very similar for both the 1 msec and 5 msec delays. Although delays may have potentially extended response width (due to providing more feedback during the exponential decay phase of a unit response), this was counterbalanced by the drop in peak response. A lower firing rate (as a result of the delays) naturally reduces the response width (less distance to decay). Thus the extra feedback that occurs during the response decay simply extends the decay to near that which would be achieved by the larger response peak. If the feedback is delayed too much, a thinner response width would be expected. This is likely to be the case of the much reduced response width observed in the mixed ESD and LD 5msec simulation result.

Two main conclusions may be drawn from these simulation results. Firstly, the effect of delays (for small to medium values) primarily affects the peak firing rate, rather than the duration of firing rate for a given unit. Secondly, for delays that are very large a significant reduction in response duration should be observed.

### 5.3.3 Summary

For a dynamic network that lies prior to the point of bifurcation we may still expect significant effects from weak lateral connections. In particular, the large number of connections cause the model STh to generate more pronounced responses to simulated brief cortical stimulation. Furthermore, the response times to such input are consequentially faster. This is still found in networks with significant delays in lateral connectivity or spread of excitatory innervation.

## 5.4 Postbifurcation System

In the system given by parameters that generate postbifurcation behaviour we have the possibility of a disturbing phenomenon: the state of *hysteresis*<sup>4</sup>. This is where each unit in the network is receiving sufficient input from its neighbouring units so that all units are effectively fully active. Thus, even without external input the complete network is in a massively self-sustained excited state. Analytically we have called this the high active state. In the postbifurcation model the occurrence of hysteresis is certainly possible. Moreover, from the prediction of system parameters (for example, large interconnectivity) the existence of this state is likely. Clearly, in many respects hysteresis is undesirable. If all units are at their peak firing rate they cannot respond to excitatory (for example, cortical or thalamic) input. Secondly, it is unlikely a neuron can physiologically sustain firing at near 500Hz for long periods of time. More importantly, this behaviour is simply not observed in the STh (for example, see Fujimoto and Kita 1993, or Kitai and Deniau 1981). We therefore have the situation that if the system exists such that these states are possible, then the model is failing to capture vital aspects of STh processing.

Before we address the full consequences of possible states of hysteresis in the model, we should further explore the system behaviours using numerical integration. This may lead to isolating under what conditions such states occur. Further, in a similar manner to the prebifurcation system, we will investigate the effect of connection delays on the system's functional behaviour.

### 5.4.1 Example 1

There are three primary parameters that determine whether a system in the low state makes a transition to the state of hysteresis. These are: the sigmoid threshold,  $y_0$ , the weight parameter,  $w$ , and the magnitude of the external input. The weight parameter,  $w$ , plays a direct role in the condition for bifurcation (see Equation 5.24). However, the

<sup>4</sup>For a discussion on the use of this term in this context, see the Glossary.

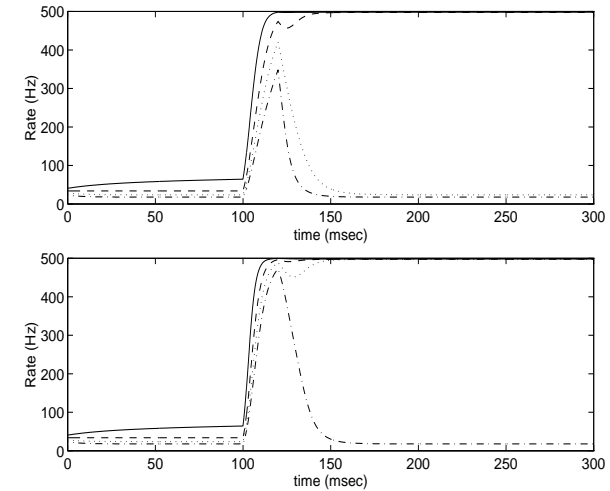


Figure 5.7: A. The top plot illustrates responses of unit 250 in four different 500 unit networks. The networks vary in their sigmoid threshold parameter,  $y_0$ . Excitatory input is presented to the system at  $t = 100$ msec and terminated at  $t = 120$ msec. The input has a Gaussian distribution centred about unit 250 (peak effect 15mV). B. The lower plot illustrates the same systems exhibiting responses to stronger input (peak 20mV). Solid line:  $y_0 = 15$ , dashed line:  $y_0 = 16$ , dotted line:  $y_0 = 17$ , dash-dot line:  $y_0 = 18$ . Other parameters,  $b = 0.2$ ,  $Z_{max} = 500$ Hz, weight Gaussian peak  $w = 0.4$ .

parameter  $y_0$  is largely obscured in the analytical results as it is contained in the term  $\bar{\sigma}(1 - \bar{\sigma})$  (see Equation 5.2). As we have already mentioned, large variations in  $y_0$  tend to produce a single stable state postbifurcation system (Section 5.2). Here we will consider small changes in this parameter using techniques of numerical integration. Figures 5.7A,B illustrate simulation results of four systems each with different values of  $y_0$ . All of the systems are initially at rest in the low state. Excitatory input is presented at  $t = 100$ msec for a duration of 20msec. As all of the systems have parameters that yield postbifurcation behaviour, excitatory input may push the systems from the low state to the hysteresis state. Figure 5.7A illustrates that systems with low values of  $y_0$  are more easily pushed into hysteresis. In systems with higher  $y_0$  the excitatory input only generates a transient response and the systems return to rest in the low state. Stronger ex-

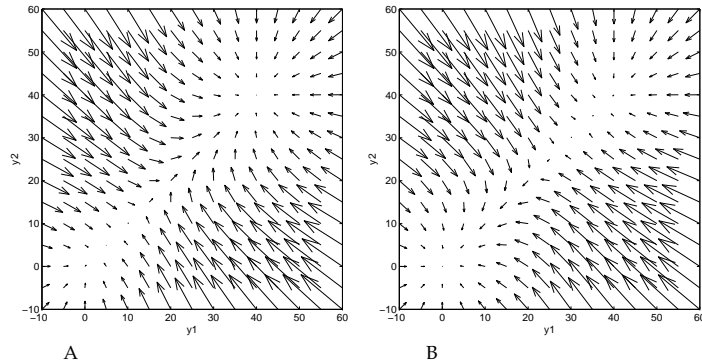


Figure 5.8: **A.** Phase plane for low  $y_0$  revealing a large attractor for the hysteresis stable point. **B.** Phase plane for high  $y_0$  revealing a reduced attractor size for the hysteresis stable point, and increased size for the low state.

citatory input is required to drive systems with high sigmoid threshold values into hysteresis (Figure 5.7B).

We may interpret these results in terms of phase plots from the two-unit system. Figures 5.8A,B illustrate two phase planes of a two-state postbifurcation system. The parameter sets of these phase planes differ only in their sigmoid threshold values. There is a region about each stable equilibrium point within which the system will permanently reside unless acted upon externally. Moreover, in our case, within this region the system will converge onto the stable equilibrium point. These regions are called *attracting sets*<sup>5</sup>. The systems exhibited in Figures 5.8A,B both have two attractors. A change in the  $y_0$  parameter affects the respective size of the two attractors. For low  $y_0$ , the hysteresis attractor is large whereas for high  $y_0$  it is reasonably small. Consequently, larger excitatory input is required to place the system into the hysteresis attractor (where it will then remain indefinitely) for larger sigmoid threshold.

Another interesting phenomenon observed in Figures 5.7A,B is the effect that the sigmoid threshold has on the low equilibrium point. As  $y_0$  is decreased, the low state equi-

<sup>5</sup>For a more formal definition, see *attractor* in the Glossary.

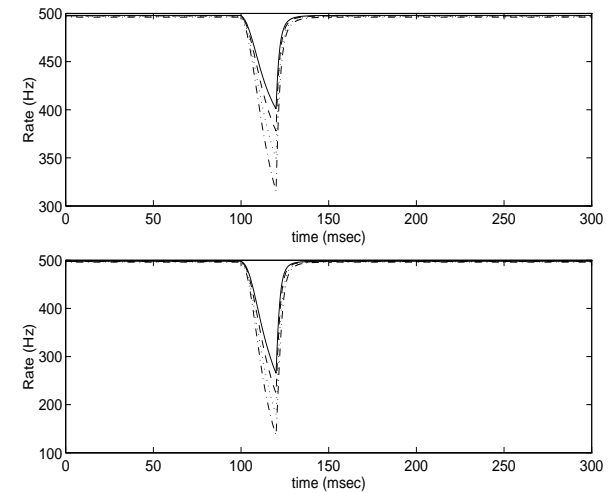


Figure 5.9: **A.** The top plot illustrates responses of unit 250 in four different 500 unit networks. The networks vary in their sigmoid threshold parameter,  $y_0$ . Inhibitory input is presented to the networks at  $t = 100$ msec and terminated at  $t = 120$ msec. The input has an identical Gaussian distribution to the excitatory input of Figure 5.7, but with a peak effect of  $-20$ mV. **B.** The lower plot illustrates the same systems exhibiting responses to stronger input (peak  $-25$ mV). Other parameters and key are given in Figure 5.7.

librium point is progressively increased. For example, the network with  $y_0 = 15$ mV rests at a high firing rate of 75Hz. As  $y_0$  is decreased further, the low equilibrium point eventually becomes unstable and the system goes into permanent hysteresis (for example, see Figure 5.4C).

The transition *from* hysteresis back to the low state takes a completely different form. Hysteresis is a stubborn state. Once the system has reached the state of hysteresis it is very difficult for localised inhibitory input to return the system to a low state. As Figures 5.9A,B demonstrate, both large inhibitory input and changes in the sigmoid threshold cannot push the system out of the state of hysteresis. Figure 5.10A illustrates the effect of localised inhibitory input over an entire network. The input given to this system has the same distribution and magnitude (although, now negative) that induced hys-

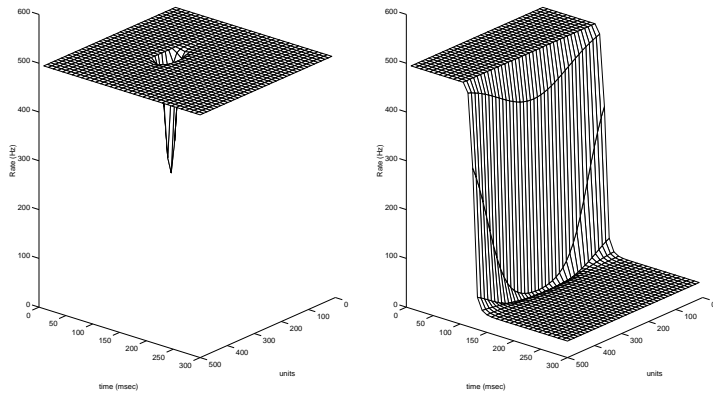


Figure 5.10: Response plots for all units over time. **A.** The left plot illustrates the stubbornness of hysteresis. The strong inhibitory input distribution given in this case is the same as the excitatory one that led to hysteresis. **B.** A widespread inhibitory input distribution where each unit receives a significant inhibition. In both plots, the responses of all 500 units are not shown, rather the responses of individual units chosen at regular intervals are shown to clarify the diagram.

teresis in the networks illustrated in Figure 5.7B (the input distribution is the same as that presented in the 3D network display in Figure 5.6). The reason why hysteresis is such a stubborn state is revealed in the system Equations 4.5

$$\tau \dot{y}_i = -y_i + \sum_{j=0, j \neq i}^N w_{ij} \sigma_j + e_i \quad (4.5)$$

In the low state the net input from the rest of the network ( $\sum w_{ij} \sigma_j$ ) is small compared to the external input ( $e_i$ ). However, in the state of hysteresis this term is exceedingly large. Localised inhibitory input cannot compete against the significant population of fully active excitatory neighbouring units. Since the weights ( $w_{ij}$ ) are large enough to support the postbifurcation behaviour (i.e. the generation of the hysteresis state from the low state), then a system in the hysteresis state will have a massive neighbourhood support and thus will be resistant to localised inhibitory input. Only by increasing the *distribution* of the inhibitory input, so that it covers the entire network can hysteresis be externally terminated (Figure 5.10B).

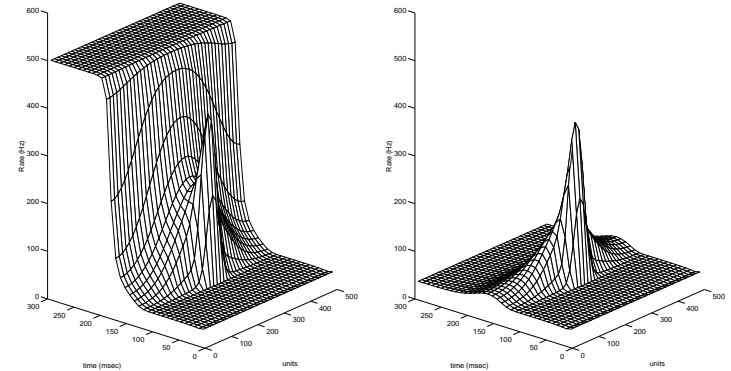


Figure 5.11: Response plots for all units over time. Note the inverted time and unit scales that yield a clearer view. **A.** The left plot illustrates a network where each lateral connection has a delay of 3msec. Although the build up to hysteresis takes longer, the final state of hysteresis still occurs. **B.** If the delay is increased to 4msec, the state of hysteresis is prevented. Other parameters,  $b = 0.2$ ,  $Z_{max} = 500\text{Hz}$ ,  $y_0 = 16\text{mV}$ , weight Gaussian peak  $w = 0.4$ .

## 5.4.2 Example 2

We will consider here the effect of lateral connection delays on the postbifurcation system (similar to the LD condition of Section 5.3.2). As we have demonstrated, parameters such as  $y_0$  affect the transition of the network to the state of hysteresis. Connection delays also have a dramatic effect on this transition. Small connection delays (1–3 msec for  $y_0 = 16\text{mV}$ ) lengthen the time the network takes to rise to the hysteresis state<sup>6</sup> (Figure 5.11A). However, as the connection delays are increased (for example,  $\geq 4$  msec for  $y_0 = 16\text{mV}$ ) the transition to hysteresis is prevented (Figure 5.11B). The reason for this is the same as for the dramatic peak response decrease observed in the prebifurcation system (see page 92). The delays desynchronise the neighbourhood feedback which in turn reduces the  $\sum w_{ij} \sigma_j$  term in the system equations. Each unit has passed its own peak

<sup>6</sup>Note the specific time taken for the entire network to reach the stable hysteresis state depends on other system parameters such as  $w_{ij}$ ,  $y_0$ , and the driving input strength and distribution.



response to the input when it receives the peak response from its neighbours. Therefore for large connection delays, the transition to hysteresis becomes more difficult. As long as connection delays are not too large we expect an effect similar to that observed for large sigmoid threshold ( $y_0$ ). As delays are increased, stronger excitatory input is required to force a transition to the hysteresis state. For very large delays hysteresis would only be possible with specially contrived input sequences that would resynchronise the responses.

### 5.4.3 Summary

There are a number of important observations that arise from the analysis of the postbifurcation system, and in particular, of the state of hysteresis. Firstly, the sigmoid threshold ( $y_0$ ) plays a crucial role in determining the size of the attractors about each equilibrium point. Larger values of  $y_0$  lead to a larger attractor about the low state and a smaller attractor about the hysteresis state. Conversely, smaller  $y_0$  increases the attractor size about the hysteresis state. Secondly, hysteresis is a stubborn state. Once it has been reached by a system it is very difficult for localised inhibitory external input to push the system to the low state. Only inhibitory input that influences the entire network can drive the system out of the hysteresis state. Finally, lateral connection delays in the network can reduce the effect of (in the extreme case, completely prevent) excitatory external input in driving the system to hysteresis.

## 5.5 Discussion

The dynamic network model of the STh can exhibit two distinctly different behaviours, classified as prebifurcation and postbifurcation. It is the primary parameters of the model, in particular  $b$ ,  $w$ , and  $Z_{max}$  that determine which behaviour is exhibited by the system. We are therefore left with the question, “where does the system that more

correctly models the STh lie — prebifurcation or postbifurcation?” From the mathematical analysis of the  $N$ -dimensional system (Section 5.1.2) and the parameter constraints on the system (Chapter 4) we cannot deny that the model should solely exhibit postbifurcation behaviour. A strong argument for this arises from the term

$$(N - 1)w b Z_{max} \quad (5.25)$$

in the condition for bifurcation (see Equation 5.24). If this term is large, the system has an unstable point and resides in the postbifurcation region. STh neurons have a characteristically high firing rate (large  $Z_{max}$ ). The transition to high firing frequencies is reasonably steep (large  $b$ ). Finally, and what is most convincing, is the extent of intranuclei connectivity (large  $(N - 1)w$ ). Even for reasonably weak weights the profuse connectivity found from the geometric simulations makes this term very large. Together these parameters yield a system that lies within the postbifurcation region.

Despite this, we would not expect the hysteresis attractor to be large. For reasonable lateral delays and sigmoid threshold, hysteresis will be the less dominant state. However, once this state is entered, as the simulations demonstrate, returning to the low state is more difficult.

The dynamic network model under the conditions of postbifurcation behaviour predicts widespread responses across the entire network. This concurs with experimental observations of widespread responses in the STh after cortical stimulation (Fujimoto & Kita, 1993). However, the observed neuron responses are more complex than the simple high frequency response exhibited by the model units. Neurons are generally observed to produce two high frequency responses separated by a brief silent period (see Figures 3 and 4 in Fujimoto and Kita, 1993). The current model cannot exhibit this complex bi-response behaviour. The consideration of a more detailed model of the STh neuron and neighbouring structures such as the GPe will begin to address these differences (see below).

A second experimental observation that should be considered is the recording of spontaneous activity in pairs of neighbouring STh neurons (Ryan et al., 1992). Cross-correlation

analysis does not reveal evidence for short term intranuclei interactions between neighbouring neurons. Although the dynamic network model predicts some degree of non-synchronous correlation in unit responses, it should primarily be observed at peak or hysteresis like activity. The neighbourhood sigmoidal function (Equation 4.2) significantly reduces expected correlations at the resting firing rate. Thus the model would predict an increased degree of non-synchronous correlations during periods of high activity rather than at rest.

Finally, sustained hysteresis exhibited by the model is not observed in the STh (Fujimoto & Kita, 1993). Thus, with consideration of the more complex behaviours that are observed, this leads us to the question “What aspects of the STh is the model failing to capture that would limit or prevent the hysteresis state?”. We suggest two possible candidates. Firstly, an inhibitory feedback system and secondly, intrinsic membrane properties. These will both be discussed in the following two subsections.

### 5.5.1 Inhibitory Feedback System

As outlined in Chapters 2 and 3, the STh is recurrently connected to the external segment of the globus pallidus (GPe). The GPe is largely GABAergic and thus inhibitory (see Section 2.4). This structure could prevent hysteresis in two different ways. Firstly, it could provide some tonic inhibition to all STh neurons. If this tonic inhibition is strong enough it may prevent transitions to the hysteresis state. However, this is possibly not the case, since STh neurons rest with high firing rates and can easily fire at their maximum firing frequencies. Secondly, the GPe could respond with a massive wave of inhibition *as a consequence* of the STh entering hysteresis. Thus states of hysteresis will be entered only briefly. Figure 5.12 illustrates this type of recurrent feedback response. The problem of the stubbornness of hysteresis is avoided here, since it is the massive widespread hysteresis itself that initiates the GPe response. We would therefore expect a widespread response in the GPe consequently providing inhibition across a large region of the STh.

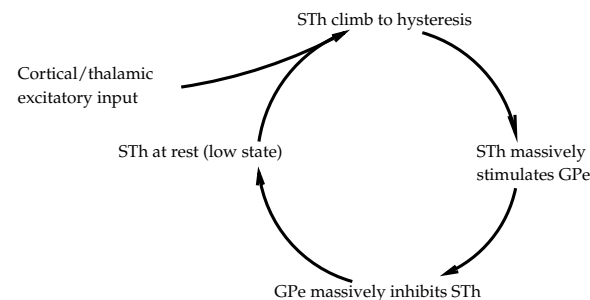


Figure 5.12: A diagram illustrating how the recurrent connection with the GPe could act to suppress states of hysteresis.

The idea of inhibitory feedback carries with it a serious consequence — the possibility of Hopf bifurcations. A Hopf bifurcation is the transition from a stable equilibrium point into some stable *oscillatory* behaviour (or limit cycle). In the current system comprising the STh only, a Hopf bifurcation is not mathematically possible as the eigenvalues of the linearised matrix cannot become imaginary<sup>7</sup> (compare with similar systems that can undergo a Hopf bifurcation, for example, Marcus and Westervelt 1989). However, by introducing a pallidal feedback system stable oscillatory states become a real possibility. Figure 5.13 illustrates how the inhibitory feedback system could lead to stable oscillations. Such stable oscillatory behaviour is not experimentally observed across large populations of STh neurons. However, oscillations are only one of the asymptotic states a joint GPe  $\iff$  STh system may produce. Moreover, as we expect the hysteresis state to be a small attractor, the system may act as a damped oscillator, leading to oscillations that are only transient.

It would be unlikely that the GPe did not play a role in controlling hysteresis. However, to discern its role, an analysis of the GPe similar to that undertaken in this and the previous chapters would be required. As the GPe is not the focus of this thesis, this will be left for future investigation.

<sup>7</sup>The parameters,  $w$ ,  $Z_{max}$ , and  $b$  are all positive by definition, and the term  $\bar{\sigma}(1 - \bar{\sigma})$  will also always be positive. Thus, for example, the terms  $q$  and  $r$  in the calculation of the eigenvalues of the two-unit system (Equations 5.5) are positive and consequently the eigenvalues are real (see Equation 5.8).

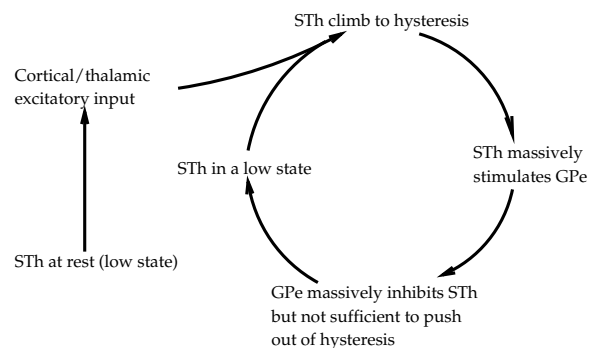


Figure 5.13: A diagram illustrating how the recurrent connection with the GPe could lead to stable oscillations of the combined GPe  $\leftrightarrow$  STh system.

### 5.5.2 Intrinsic Membrane Properties

In addition to the possible role of the pallidum in limiting states of hysteresis, the model formulation may also be excluding certain intrinsic properties of STh projection neurons. The simplification of a neuron used in the network model may overlook many intrinsic membrane processes that could also prevent hysteresis. In order to address this we need to consider the various channels that are involved in the primary behaviour emergent from single STh neurons. As we have seen in Chapter 2, very little detail is known about intrinsic STh membrane properties. However, the following two chapters demonstrate that with carefully constrained compartmental modelling techniques we may begin to discern the intrinsic membrane properties and their underlying mechanisms. From this we can then consider their effect on the network dynamics as a whole.

## Chapter 6

# The Computation of Single Neurons

### 6.1 Introduction

It is the operation, function and interaction of membrane channels that primarily define a neuron's response to its environment. To a large degree, channel dynamics and composition within a membrane define the neuron as a certain physiological and pharmacological type. Accurately capturing the computational behaviour of a particular neuron requires the consideration of these underlying mechanisms.

A membrane channel is essentially a protein, or collection of proteins that traverse the cellular membrane, often creating a selective pore or pathway for ions to travel through. Neuronal membranes, for most eukaryotic cells, are primarily composed of a lipid bilayer. The hydrophobic tails of lipids collect together forming two layers (Figure 6.1A). This formation of lipid bilayers is energetically favoured as it reduces the possibility of hydrophobic regions coming into contact with water in the intracellular and extracellular fluids. The lipid bilayer prevents the movement of most ions and molecules into or out of the cell. Only a few chemical types, such as steroids, are able to diffuse through the lipid membrane. The consequence of this impermeability is that the movement of most ions and molecules across the membrane may be selectively controlled by channels.

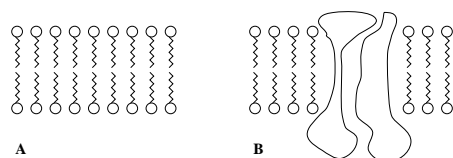


Figure 6.1: **A.** The hydrophobic tails of the lipids collect together to form a bilayer. Such a bilayer is a major structure of the cell membrane. **B.** Proteins traverse the lipid bilayer creating a pore that may allow, under certain conditions, selective ions or molecules to cross the membrane.

Not only can channels be differentiated by the ions they selectively allow to cross the membrane, but other factors such as responses to specific external or internal molecules (ligands) or to the potential difference across the membrane can also play a significant role in channel functioning. Channels that respond to external ligands are often referred to as receptors. There are some channels that act as continuously open pores, but most are referred to as being “gated”. Generally, gated channels may be in one of two states, either open or closed<sup>1</sup>. Their tendency to being in a particular state depends on the channel type. For example, some voltage gated channels have a much greater probability of being open under conditions of membrane depolarisation, than under resting membrane conditions. Similarly ligand activated channels may have a higher probability of being open in the presence of higher concentrations of the particular activating ligand.

A single channel on its own would contribute little to changes in membrane depolarisation or internal ionic concentrations. Neurons have large populations of channels distributed across the membrane which act together to induce significant changes in the neuron’s state. For example, a density of 100 – 400 Na channels per  $\mu\text{m}^2$  is common for unmyelinated axon of the vertebrate skeletal muscle (Hille, 1992). It is therefore not computationally practical to model individual channels within the membrane as a means to understanding the behaviour of the neuron as a whole. A classical approach to modelling the interaction of populations of channels, and one that is still in use today, is based on the assumption that an electrically excitable membrane involving a variety of channels may be described by a simple electrical circuit. Moreover, it is assumed that

<sup>1</sup>Some channels, for example the Acetylcholine-activated channels from cultured rat muscle, also have substates lying between fully open, and closed (Nicholls et al., 1992; Hille, 1992).

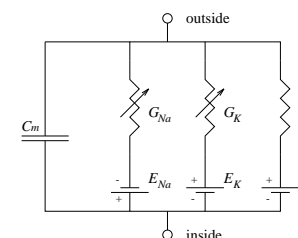


Figure 6.2: Electrical circuit diagram of the 1952 Hodgkin and Huxley model of action potentials in the squid giant axon.  $G_{Na}$ ,  $G_K$  and  $G_L$  are the sodium, potassium and leak conductances respectively.  $E_{Na}$ ,  $E_K$ ,  $E_L$ , are similarly the respective equilibrium potentials.  $C_m$  is the membrane capacitance. Adapted from (Hodgkin & Huxley, 1952b).

channels can be classified into distinct types, and populations of each type of channel may be modelled as measurable membrane conductances. The technique of using an electrical circuit to describe the properties of membranes was employed as early as 1905 in descriptions of action potential movement along axons (Herman, 1905 cited in Hille, 1992). In this early description, the passive spread of an action potential was assumed to be along a conducting cylindrical cable. Later investigation using the squid giant axon (Cole and Curtis, 1939, and Hodgkin and Huxley 1939) demonstrated that a significant membrane conductance increase occurred with an action potential. It was further observed that the membrane itself appeared to generate the net inward currents of the action potential. The electromotive force of this inward current was correctly postulated to arise from a change in membrane permeability to sodium ions (Hodgkin & Katz, 1949). This would drive the potential difference of the membrane towards the sodium equilibrium potential. For a discussion on the historical development of this view see Hille (1992).

By 1952, Hodgkin and Huxley had summarised the model for action potential generation in the squid giant axon with the electrical circuit illustrated in Figure 6.2. They demonstrated that changes in the membrane permeability to specific ions are both voltage and time dependent. Given characterisations of this dependence, the model demonstrates how these changes in the specific membrane permeabilities (reflected as changes in specific conductances) can generate an action potential. Primary assumptions of this

type of model include assuming that ionic conductance is a measure of the proportion of channels that are open and that channel currents obey Ohms law<sup>2</sup>. Furthermore, using this model Hodgkin and Huxley were not only able to demonstrate how an action potential may be generated by selective membrane conductance changes, but were also able to develop an empirical description of the channels themselves by assuming simple first order kinetics.

The assumption that the membrane conductance to a particular ionic species was proportional to the number of open channels selective to that ion allowed a particular ionic conductance to be given by

$$G_A = \bar{G}_A p \quad (6.1)$$

where  $G_A$  is the membrane conductance to the particular ionic species  $A$ ,  $\bar{G}_A$  is the maximum conductance the membrane reaches for the particular ion  $A$ , and  $p$  is the proportion of channels in the open state ( $0 \leq p \leq 1$ ). By assuming first order kinetics it was possible to give some theoretical basis to the proportion of channels that were open, and how the proportion changes under different conditions. A first order kinetic equation may be given by

$$1 - p \frac{\alpha}{\beta} p \quad (6.2)$$

where  $\alpha$  and  $\beta$  are rate constants. Alternatively, it may be written

$$\frac{dp}{dt} = \alpha(1 - p) - \beta p \quad (6.3)$$

or

$$\frac{dp}{dt} = \frac{p_\infty - p}{\tau_p} \quad (6.4)$$

where  $p_\infty$  is the proportion of channels open in the equilibrium state

$$p_\infty = \frac{\alpha}{\alpha + \beta} \quad (6.5)$$

and  $\tau_p$  is the time constant

$$\tau_p = \frac{1}{\alpha + \beta} \quad (6.6)$$

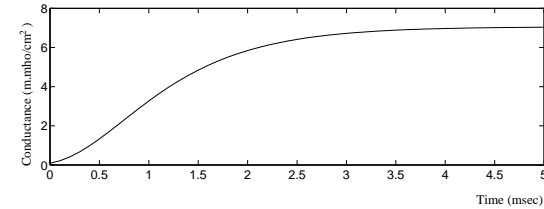


Figure 6.3: A curve fitted to the experimental data of the potassium conductance change associated with a membrane depolarisation of 25mV in squid giant axon (Hodgkin & Huxley, 1952a).

It is useful to express  $p$  in terms of the voltage dependent  $p_\infty$  and  $\tau_p$ , as empirical equations for these terms may be fitted to data from voltage clamp experiments (for a description of the voltage clamp technique see Nicholls et al., 1992). For example,  $p_\infty$  is the steady state proportion of channels open for a certain voltage. For potassium selective channels (i.e. potassium conductance) this can be directly measured from  $G_K/\bar{G}_K$  where  $G_K$  is the measured potassium conductance at a particular voltage and  $\bar{G}_K$  is the maximum observed potassium conductance (see Hodgkin and Huxley, 1952a). However, the rise in the potassium conductance to an asymptotic level for a certain clamped voltage does not follow a simple exponential as the assumed first order kinetic equation specifies (Figure 6.3). The increase in potassium conductance associated with a voltage clamp induced depolarisation follows an S-shape curve. This may still be accounted for using the first order kinetic equation by assuming that more than one independent kinetic reaction must take place for a channel to open. The classical explanation given by Hodgkin and Huxley (1952a) supposes that a number of similar particles must *each* be correctly placed in the membrane in order for the channel to open. Hodgkin and Huxley chose four hypothetical particles in order to sufficiently capture the experimental data. However, as they noted, higher numbers (e.g. 6) allowed the experimental voltage clamp data to be fitted more accurately. Using four independent kinetic processes equation 6.1 becomes

$$G_K = \bar{G}_K n^4 \quad (6.7)$$

<sup>2</sup>Although Ohms law is an adequate assumption for many channel types, channels selective for ions with an extremely small concentration on one side of the membrane (for example, calcium) do not have linear (or near linear) current voltage relations. See Hille (1992) and Section 6.2.3.

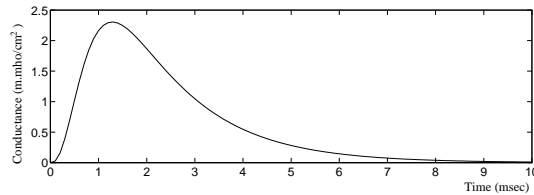


Figure 6.4: A curve fitted to the experimental data of the sodium conductance change associated with a membrane depolarisation of 26mV in squid giant axon (Hodgkin & Huxley, 1952a).

where  $n$  plays a similar role to  $p$  in equation 6.1, but here may be intuitively considered as the proportion of particles in a certain membrane position appropriate for channel opening.

Sodium conductance changes upon depolarisation take on a very different form to that of potassium conductances. A membrane depolarisation causes a rapid rise in sodium conductance, followed by a slower decrease in the conductance back to the resting level (see Figure 6.4). Unlike potassium conductance, the sodium did not reach a sustained asymptotic level proportional to the membrane voltage. Hodgkin and Huxley (1952b) proposed two mechanisms to empirically describe this data: an activation similar to the potassium activation, and an independent inactivation responsible for the transient nature of the conductance. They gave the sodium conductance as

$$G_{Na} = \bar{G}_{Na} m^3 h \quad (6.8)$$

where  $m$  is the activation variable that plays a similar role to  $n$  in equation 6.7 (for the sodium conductance, three independent variables were found to sufficiently capture the empirical data) and  $h$  is the inactivation variable that follows a simple exponential (directly given by first order kinetic equations of the form of Equation 6.3). Inactivation generally has a slower time course than activation, so that upon membrane depolarisation, Na channels activate, then quickly inactivate, yielding a collective conductance curve of the form shown in Figure 6.4. As inactivation is voltage dependent, channel reactivation (removal of the inactivation) occurs as the membrane becomes repolarised.

Variables,  $n$ ,  $m$  and  $h$  may be fitted to experimental data (for example, voltage dependent expressions for  $h$  are determined by fitting curves to experimental measurements of  $h_{\infty}$  and  $\tau_h$ ), leading to expressions for conductances  $G_K$  and  $G_{Na}$  calculated from Equations 6.7 and 6.8 respectively. If we assume the equivalent electrical circuit (Figure 6.2) represents an isopotential patch of membrane, so that the spatial current spread can be ignored, then the membrane potential ( $V$ ) may be given by

$$\frac{dV}{dt} = \frac{-1}{C} [G_{Na}(V - E_{Na}) + G_K(V - E_K) + G_L(V - E_L)] \quad (6.9)$$

Here  $G_L$  is the leak conductance,  $C$  is the membrane capacitance, and  $E_{Na}$ ,  $E_K$ ,  $E_L$  are the sodium, potassium and leak equilibrium potentials respectively. The leak conductance ( $G_L$ ) is generally considered to be voltage independent and is primarily responsible for the resting membrane potential of most cell membranes. Hodgkin and Huxley (1952b) used this approach to accurately describe many of the observed electrical phenomena of the squid giant axon. This procedure is still commonly used for describing and exploring the interdependent effects of many channel types in generating the electrical behaviours of excitable cells.

## 6.2 Modelling Neurons of the Subthalamic Nucleus

We follow the same approach in constructing a model of individual subthalamic nucleus neurons. However, the detail on which the model of the squid giant axon was derived is much more sparse in the case of the STh. There are as yet no direct observations of the individual channels nor specifications of their possible kinetics. Moreover, we do not have a clear indication of the various channel types distributed throughout the STh projection neuron membrane. Immediately, one of the goals of modelling individual channel types, that of characterising possible kinetic properties of channels, is not achievable here. However, by drawing on the known properties of certain channel types from other neuron populations we can begin to consider a required channel composition that effectively and efficiently characterises observed STh neuron behaviour. A model is useful here as it allows us to bring together very complex channel types into a hypothetical STh

neuron and explore their accumulative effects. Equally, due to the nature and power of multiple parameter differential circuits, any model using these techniques is so powerful that it can render results useless and arbitrary. One of the dangers of modelling is to bend very powerful models to characterise any arbitrarily desired function. Therefore, most of this chapter deals not only with the construction of the single neuron model, but also with finding methods of constraining the model to reduce its power and explore a more restricted parameter domain.

### 6.2.1 Morphological Considerations

As briefly introduced in Chapter 2, the STh seems to have two types of projection neurons. The two types have been distinguished morphologically on the basis of the presence of internal axon collaterals, and dendritic tree branching characteristics (Kita et al., 1983a; Carpenter, 1981). However, other authors have not found such a clear distinction in the STh projection neuron types (Afsharpour, 1985a; Yelnik & Percheron, 1979). For the purposes of investigating the internal STh processing dynamics, we will presently consider data from the observations of the morphology of STh neurons that have internal axon collaterals. Since currently, the STh in rat is the most studied (both anatomically and physiologically) all referenced data is drawn from studies of the rat unless otherwise specified.

#### The Soma

Most STh neurons have been classified as Golgi type I, with some variation in soma size and shape. Somata are generally polygonal or oval with mean diameter  $14.9\mu\text{m}$  in the shortest axis, and mean  $22.7\mu\text{m}$  in the longest (Kita et al., 1983a). We may approximate this by idealising the soma to a spheroid. This may be described as an ellipse with two primary axes, one of which is used as an axis of rotation to produce a three dimensional object. Two types of object may be obtained, depending on whether the smaller or larger axis is chosen as the rotation axis. If we assume the axis diameters are given

by the means above, the surface area of an oblate spheroid (rotation about the smaller axis to yield a disk like approximation) yields a surface area of  $1130\mu\text{m}^2$ . If the rotation is about the longer axis (prolate spheroid) a cigar shaped approximation is obtained and the surface area is  $950\mu\text{m}^2$ . These calculations place average bounds on the surface area of the soma. For simplicity, the idealised neuron is assumed to have a perfectly spherical soma. Assuming an average diameter of  $18.8\mu\text{m}$ , this yields a reasonable surface area of  $1110\mu\text{m}^2$ , which resides between the two average spheroid limits. This calculation fits very closely with the mean soma cross-sectional area of  $290.4\mu\text{m}^2$  observed by Afsharpour (1985a). Given an ideal circle with diameter  $18.8\mu\text{m}$  the calculated cross-sectional area that should be observed in the plane is  $287\mu\text{m}^2$ .

#### The Dendritic Tree

Kita et al. (1983a) observed that most STh neurons have 3–4 primary dendrites. The diameters of the primary dendritic trunks ranged from  $1.4$ – $3.0\mu\text{m}$ . The mean longest dendrites extended from  $200$ – $800\mu\text{m}$  with a mean of  $543\mu\text{m}$  from the soma (Kita et al., 1983a). Distal portions of the primary or secondary dendrites had pedunculated spines, although they were relatively sparsely covered (Afsharpour, 1985a). Kita et al. (1983a) found a significant difference in the number of dendritic tips of the two postulated STh projection neuron types (differentiated by the presence of internal axon collaterals). The mean dendritic branching ratio (number of dendritic tips per primary dendrite) for a neuron with intranuclear axon collaterals was 7.0, while the mean for neurons without internal collaterals was 4.1. By assuming binary branching we may simplify this distinction to two types of branching structures as illustrated in Figure 6.5. Here we do not show where the points of branching occur, rather the number and shape of the branches themselves. These two branching morphologies yield close approximations of the branching ratios observed. To maintain a binary branching structure (an assumption that is useful for later calculations) the ratio for a Type 1 tree is slightly less than the observed branching ratio. In the present construction of an idealised STh neuron model we will consider only dendritic trees of Type 1. These are more dense than Type 2 and primarily increase the total dendritic surface area assumed in the model.

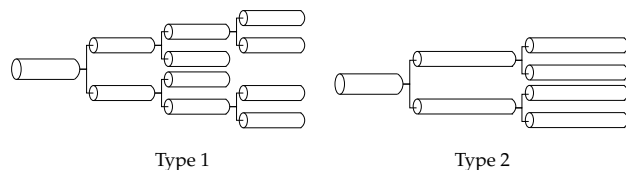


Figure 6.5: A significant distinction is found between STh neurons that have intranuclear axon collaterals, and those which do not. The Type 1 morphological layout contains a denser branching structure from a primary dendrite (the first/parent cylinder) capturing the larger number of dendritic tips observed in neurons that have intranuclear axon collaterals. The Type 2 layout illustrates a less dense branching structure used to represent a branch in the dendritic tree of STh neurons without intranuclear collaterals.

Afsharpour (1985a) observed that the bifurcation of primary dendrites occurred 3–90 $\mu\text{m}$  from the cell body. Kita et al. (1983a) calculated the mean length of primary dendrites before branching to be 40 $\mu\text{m}$ . Secondary dendrites were observed to bifurcate within 18–100 $\mu\text{m}$  from the cell body (Afsharpour, 1985a). This implies that bifurcation of primary and secondary dendrites occurs within a reasonably small distance from each other (mean distance < 60 $\mu\text{m}$ ). We assume that secondary branching occurs at least another 40 $\mu\text{m}$  from the first branch point. We further assume that tertiary branching (for the upper and lower branches only of the Type 1 structure illustrated) occurs at a point 50% along the remaining dendritic length. The total lengths of all branch paths are calculated so as not to exceed 500 $\mu\text{m}$ . In the observations by Kita et al. and Afsharpour, individual dendrites extended well beyond 500 $\mu\text{m}$ ; however the mean longest was 543 $\mu\text{m}$ .

We now construct an idealised STh neuron based on the morphologies derived from the mean observations above. If we assume that an idealised neuron has three primary dendrites, a morphological model of the branching structure as illustrated in Figure 6.6 may be constructed.

In order to reduce the complexity of the model, for both tractability of simulation and for simplifying the analysis, we assume that there are two primary dendritic trees such that each can be reduced to equivalent electrical cylinders. In Figure 6.6 this is illustrated by only two primary dendrites emerging from the soma. One dendrite leads to a single Type 1 dendritic tree, while the other bifurcates into two Type 1 trees, approximating

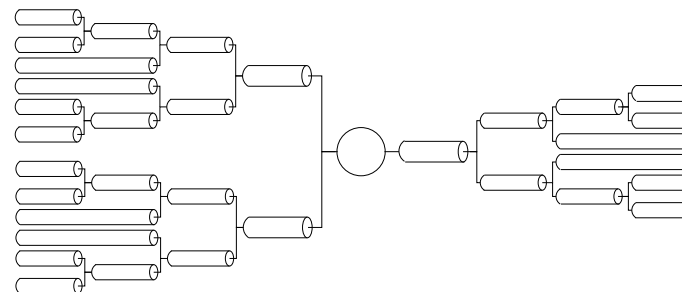


Figure 6.6: A schematic diagram of the morphological simplifications made for the idealised STh projection neuron. Each branch is not drawn to any scale; rather this diagram illustrates the branching structure alone.

three primary dendritic trees in total. In order to reduce both of these dendritic structures into two equivalent cylinders a number of assumptions are required. In particular, as described by Rall (1989,1960), we require the following assumptions:

1. The membrane resistance  $R_m$  ( $\Omega\text{cm}^2$ ) and the internal cytoplasmic resistance  $R_i$  ( $\Omega\text{cm}$ ) are the same for all branches.
2. All terminal branches end with the same terminal boundary condition. Hence we assume a sealed end.
3. All terminal branches end at the same electronic distance from the trunk origin.
4. At every branch point the diameter of the two daughter branches must be such that the sum of their  $3/2$  power values equals the  $3/2$  power of the parent branch diameter.

Conditions 1, 2, and 4 are reasonable assumptions which are not weakened by current physiological and morphological findings. For our purposes, all of these conditions impose two important domain limitations for the model. The first arises from condition 3, requiring that all trunk to terminal paths have identical electronic lengths. This imposes a dendritic tree morphology where each dendritic tip is roughly the same length from



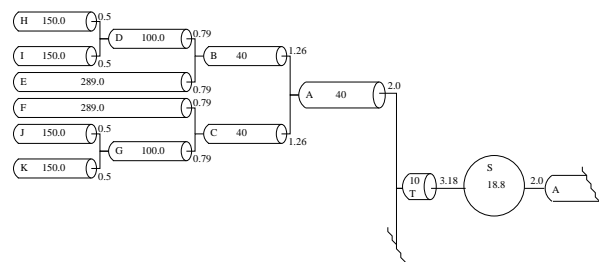


Figure 6.7: A diagram illustrating the lengths and diameters of the idealised STh projection neuron branching structure. Only one of the Type 1 branches is shown, as each of the three primary branches are given the same dimensions. All dimensions are given in  $\mu\text{m}$ . The naming convention A–K, T, S are used in calculations in the text.

the soma<sup>3</sup>. Secondly, a further constraint is introduced as a consequence of reducing the tree structures to equivalent cylinders:

- Proportional inputs must be delivered to all corresponding locations on each branch path of a dendritic tree such that an equal input voltage time course would be generated at all electronically equidistant locations along each path.

For example, if we were considering a synaptic EPSP at the top terminal branch of the right dendritic tree in Figure 6.6, we must assume for the equivalent cylinder that equivalent EPSP's occur simultaneously at the same electronic distance down each branch path of the right hand tree. Both this assumption and that of equal electronic lengths are direct consequences of reducing a dendritic tree into a single cylinder and prevent any investigation of differential synaptic inputs to different lengths down a single tree, or to inputs occurring on different tree branches.

Given these conditions, we propose a dendritic morphology, illustrated in Figure 6.7 that reduces to an equivalent and simpler model shown in Figure 6.8. Only one of the Type 1 dendritic trees is shown in Figure 6.7, as each of the three trees is assumed to have the

<sup>3</sup>This occurs from the conditions of restricted diameters (condition 4), equal passive membrane properties (condition 1), and a symmetric Type 1 branch structure.

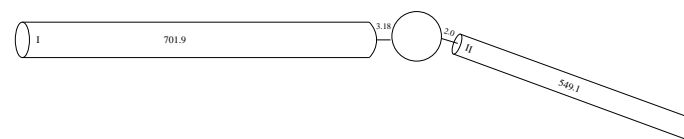


Figure 6.8: A diagram illustrating the two equivalent cylinders that are used to simplify the dendritic trees given in Figure 6.6. All dimensions are given in  $\mu\text{m}$ .

same dimensions. The diameters of each branch were chosen following the  $3/2$  power rule (condition 4) such that the base branch of the Type 1 tree had a diameter of  $2.0\mu\text{m}$ . This gave terminal branches for the most distal bifurcations with diameters of  $0.5\mu\text{m}$ . Afsharpour (1985a) found the diameter of primary dendritic trunks ranged between  $1.4\text{--}3.6\mu\text{m}$ . Both primary trunks in the simplified model were within this range ( $3.18\mu\text{m}$  and  $2.0\mu\text{m}$ ). Secondary branch diameters were usually found to be less than  $1.8\mu\text{m}$  (Kita et al., 1983a) which is maintained in the model as a consequence of the  $3/2$  rule. Branch lengths were chosen so that each trunk to terminal path had the same electronic length.

Given the conditions 1–5, we may calculate equivalent electrical cylinders for the 2 branches. An equivalent cylinder has the same electronic length as the equivalent part of the dendritic tree, and a diameter the same as the tree trunk diameter. The two trees on the left of the soma in Figure 6.6 reduce to an equivalent cylinder of diameter  $3.18\mu\text{m}$  and length  $701.9\mu\text{m}$ . The single tree to the right of the soma reduces to an equivalent cylinder of diameter  $2.0\mu\text{m}$  and length  $549.1\mu\text{m}$  (see Figure 6.8). One of the consequences of the assumptions made is that the surface areas of the complex trees and the equivalent cylinders should be the same. For the larger equivalent cylinder (cylinder I) and the larger dendritic tree (left tree in Figure 6.6) the surface areas are both  $7,000\mu\text{m}^2$ . The smaller equivalent cylinder (cylinder II) and the smaller dendritic tree also have equal surface areas of  $3,450\mu\text{m}^2$ . This gives the total surface area of the idealised STh projection neuron as  $11,560\mu\text{m}^2$ .

In order to further simplify the equations and techniques used for modelling the idealised neuron shown in Figure 6.8, we will adopt a compartmental modelling technique. This involves dividing the idealised neuron into compartments that can be considered

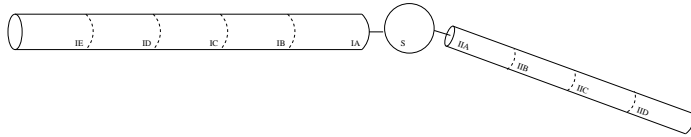


Figure 6.9: A diagram illustrating the division of the two equivalent cylinders into near isopotential compartments.

isopotential; that is, we will assume the spatial spread of current along the membrane surface is negligible *within each compartment*. Reducing the model to a series of compartments enables us to consider only temporal information (and not spatial) within a single compartment and dramatically reduces the complexity of the membrane equations (see Equation 6.9 for a single compartment/isopotential voltage equation). Ideally an isopotential compartment would cover virtually zero membrane surface area. However, for practical purposes we choose compartments that have sufficiently small electronic lengths. Rall (1989) shows that for dendritic trees that satisfy the equivalent cylinder conditions, and in particular for a “sealed end” cylinder, the following relation holds

$$G_{IN} = G_m A_D \frac{\tanh(L_D)}{L_D} \quad (6.10)$$

where  $G_{IN}$  is the input conductance,  $G_m$  is the membrane conductance,  $A_D$  is the surface area of the cylinder, and  $L_D$  is the electronic length of the cylinder. For sufficiently small electronic length

$$\tanh(L_D) \approx L_D \quad (6.11)$$

and hence,

$$G_{IN} \approx G_m A_D \quad (6.12)$$

For sufficiently small electronic length, the input conductance to a cylinder (or equivalent dendritic tree) is approximately equal to its particular membrane conductance ( $G_m A_D$ ). Intuitively, the voltage degrades negligibly across the length of the cylinder (see Rall, 1989). Thus for small electronic length the cylindrical compartment may be considered isopotential.

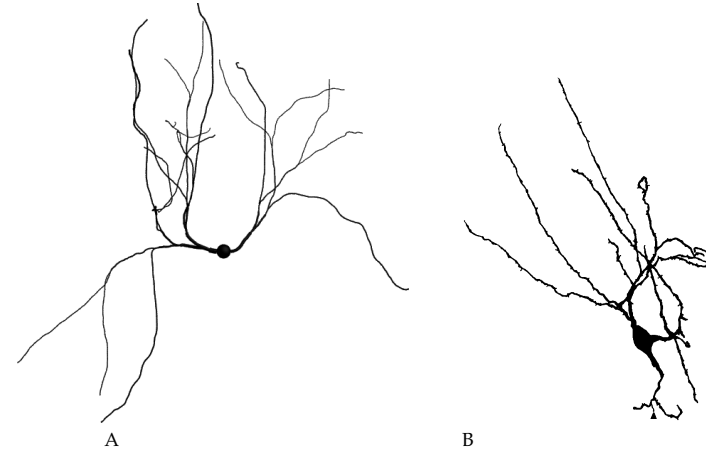


Figure 6.10: **A.** The morphology of the idealised neuron depicted in Figures 6.6 and 6.7 is projected as cylinders into a simulated 3D space. From this the gross morphological differences and similarities can be seen with a drawn rat STh projection neuron. The two dendritic trees were placed on either side of the soma, and branch separation angles were generated randomly (max  $\pi/2$ ). Curves in the long dendritic cylinders were also randomly generated (max curve of  $\pi/6$  per  $5\mu\text{m}$ ) and branch diameters are doubled in order to achieve higher definition. **B.** Reconstruction of a rat STh neuron taken directly from Afsharpour (1985a).

We can split the two equivalent cylinders (shown in Figure 6.8) into smaller cylinders/compartments so as to reduce the electronic length per compartment in order to sufficiently satisfy condition 6.11. Note that the total electronic length and properties of the original cylinder (or dendritic tree) remain the same. We calculate that cylinder I may be minimally divided into 5 compartments, and cylinder II into 4 (Figure 6.9). This gives

$$G_{IN_I} = 0.983 G_m A_I$$

$$G_{IN_{II}} = 0.975 G_m A_{II}$$

which were considered adequately isopotential.

### Summary of Morphological Simplifications

The dendritic tree structure illustrated in Figures 6.6 and 6.7 is a combination of a structure that can be reduced electronically to single cylinders, while capturing the salient features of STh projection neurons with Type 1 dendritic trees. As an illustration of both the coarse similarity and differences between what is morphologically simulated and the light microscope observations of real rat STh neurons, the simulated dendritic tree is given a random projection into a simulated 3D space. This allows us to then view the morphology in a form comparable with light microscope observations. Figure 6.10 illustrates both the simulated neuron and a reconstructed neuron taken from rat (from Afsharpour, 1985).

We can use this comparison to highlight some important differences. Firstly, as a consequence of the equivalent cylinder condition 3, all the trunk to tip path lengths are very similar in the model, whereas there is much more variation of branch lengths in the drawn neuron. The effect this may have on our simulations, particularly with multi-neuron simulations, is on the number and extent of lateral interactions. In the model the extent of lateral interactions could be larger and more diffuse, whereas in STh projection neurons it would be expected that a higher density of interactions would occur closer to the soma, and consequently limit the distal extent of lateral connections. Secondly, there is an absence of spines and filiform processes over the simulated dendritic trees. These will increase the effective surface area, and possibly alter the electrical properties in these regions.

### 6.2.2 Passive Electrical Membrane Properties

#### Capacitance

Both Cole (1968) and Hille (1992) suggest that neuronal membrane capacitance has a fairly consistent value of  $1\mu\text{F}/\text{cm}^2$ . We assume that this is the case for STh projection neurons.

### Membrane Time Constant

The time constant may be measured directly from the observed passive membrane properties. The time required for a (small) voltage decrease induced by terminating a current injection (i.e. capacitance discharge) to reach 37% ( $e^{-1}$ ) of its final value can be read directly as the passive membrane time constant. Induced voltage changes should be small to prevent non-passive conductances from being engaged. This direct measurement results from the RC circuit approximation, since the equation describing the ideal capacitance discharge

$$\frac{dV}{dt} = -\frac{V}{\tau}$$

can be directly solved, yielding

$$V = V_0 e^{-t/\tau}.$$

Kita et al. (1983b) have estimated the time constant for STh neurons as 6msec.

### Passive Membrane Resistance

We can calculate the membrane resistance using the time constant and capacitance described above. Since in an ideal RC circuit the time constant ( $\tau$ ) is equal to  $1/RC$ , the passive membrane resistance is calculated to be  $6000\ \Omega\text{cm}^2$ .

### Cytoplasmic Resistance

The cytoplasmic resistance may be calculated from both the input and membrane resistances. Kita et al. (1983a) found the *in vivo* input resistance of the STh neuron to be between 9 and  $28\text{M}\Omega$  (mean  $18\text{M}\Omega$ ). However, Nakanishi et al. (1987a) observed the *in vitro* input resistance to be around  $146\text{M}\Omega$ . A number of reasons are proposed in order to explain this discrepancy (for a more detailed discussion see Nakanishi et al., 1987a). For example, it is possible that the artificial *in vitro* extracellular fluid composition may

have contributed to the observed difference. As STh neurons have particularly large processes, differences may also result from severing some of these in *in vitro* preparation. It is also possible that tonic synaptic inputs are absent from the *in vitro* measurements. The idealised neuron can place a number of constraints on what the input resistance should be. Since input resistance, neuron morphology, cytoplasmic resistance, and membrane resistance are related, the model developed so far provides interesting insights into this difference. Following Rall (1989), we will consider this in terms of input conductance to a cell ( $G_{IN}$ ). In our idealised neuron, the input conductance is expected to take the form

$$G_{IN} = G_{IN_s} + G_{IN_i} + G_{IN_{ii}} \quad (6.13)$$

where  $G_{IN_s}$  is the soma input conductance, and  $G_{IN_i}, G_{IN_{ii}}$  are the input conductances of the two dendritic trees (Figure 6.8). The soma input conductance may be given by

$$G_{IN_s} = G_{shunt} + G_m S A_S \quad (6.14)$$

where  $G_m$  is the soma membrane conductance per unit area,  $A_S$  is the soma surface area, and  $G_{shunt}$  is the predicted conductance as a consequence of electrode penetration. Since the dendritic trees may be reduced to equivalent cylinders, the input conductance to each tree is given by (Equation 6.10)

$$G_{IN} = G_m A_D \frac{\tanh(L_D)}{L_D} \quad (6.10)$$

where  $L_D$  is

$$L_D = \frac{l_D}{k\sqrt{d_D}}, \quad k = \sqrt{\frac{R_m}{4R_i}}$$

$l_D$  and  $d_D$  are the length and diameter respectively of the equivalent cylinder,  $R_m$  is the membrane resistance, and  $R_i$  is the cytoplasmic resistance. Given these equations, the morphological model shown in Figures 6.6, 6.7, and 6.8, and the passive membrane properties determined so far, the only two free variables in Equation 6.13 are the input and internal cytoplasmic resistances. Assuming a very broad range for possible cytoplasmic resistance ( $10\Omega\text{cm} < R_i < 400\Omega\text{cm}$ ), for a low input resistance (as the *in vivo* study indicates) we must assume a large  $G_{shunt}$  in order for  $R_i$  to remain within the above bounds. In contrast, for a high input resistance (e.g.  $140M\Omega$ , as observed in the *in vitro*

study), then even with zero soma shunt, the cytoplasmic resistance does not remain in the above reasonable bounds. The morphological restrictions tend to imply that the input resistance should ideally lie relatively evenly between the two *in vitro* / *in vivo* values. For example, for an input resistance of  $R_{IN} = 68M\Omega$ , and a small shunt of  $0.2 G_{IN_s}$ , the cytoplasmic resistance has a medium value of  $R_i = 123\Omega\text{cm}$ .

We chose the cytoplasmic resistance to be  $123\Omega\text{cm}$  (from the above example of  $R_{IN} = 68M\Omega$ ) as a fairly average resistance value. However, it is clear that this choice is to a large degree unconstrained as it is based primarily on a “typical” neuron cytoplasmic resistance. We could not tie this parameter to a particularly limited range of values, as the input resistance observations were so diverse.

### Summary of the Passive Membrane Properties

Table 6.1 lists the passive membrane properties used for each compartment type of the model. A simple membrane equation that utilises these passive properties is of the form

$$\frac{dV_i}{dt} = \frac{-1}{C} \left[ G_{L_i}(V_i - E_L) + \frac{V_{i-1} - V_i}{r_{i-1,i}} + \frac{V_{i+1} - V_i}{r_{i,i+1}} \right] \quad (6.15)$$

where the subscript,  $i$ , is the compartment index,  $V_i$  is the membrane voltage of compartment  $i$ ,  $G_{L_i}$  is  $1/r_{m_i}$ , and  $r_{a,b}$  is the cytoplasmic resistance between compartments  $a$  and  $b$ . This equation directly follows from two simple electrical principles. Firstly, the current that flows through the membrane of a compartment must equal the cytoplasmic current entering and exiting the compartment (Kirchoffs current law)

$$\dot{i}_{m_i} = \dot{i}_{i-1,i} - \dot{i}_{i,i+1}$$

Secondly, following Equation 6.9, the membrane current may also be specified in terms of membrane capacitance and voltage changes.

In the model, dendritic tips were assumed to be electrically sealed ends, such that no cytoplasmic current leaves the tips. From this simple specification of the compartmental model of passive properties, and the parameters given in Table 6.1, the model generates a

Table 6.1: A summary of the general passive membrane properties and the specific properties for each compartment type in the idealised neuronal model. The specific values are calculated using the compartments particular surface area and the general values.

General Properties			
Membrane resistance	$R_m$	6000.0	$\Omega\text{cm}^2$
Cytoplasmic resistance	$R_i$	123.0	$\Omega\text{cm}$
Input resistance	$R_{IN}$	68.0	$\text{M}\Omega$
Membrane capacitance	$C_m$	1.0	$\mu\text{F}/\text{cm}^2$
Membrane time constant	$\tau$	6.0	msec
Soma Compartment			
Surface area	$A_S$	1110.0	$\mu\text{m}^2$
Membrane resistance	$r_{m_S}$	540.5	$\text{M}\Omega$
Cytoplasmic resistance	$r_{i_S}$	0.0556	$\text{M}\Omega$
Membrane capacitance	$c_S$	11.104	pF
Dendrite I Compartment			
Surface area	$A_I$	1400.0	$\mu\text{m}^2$
Membrane resistance	$r_{m_I}$	428.5	$\text{M}\Omega$
Cytoplasmic resistance	$r_{i_I}$	21.82	$\text{M}\Omega$
Membrane capacitance	$c_I$	14.00	pF
Dendrite II Compartment			
Surface area	$A_{II}$	862.6	$\mu\text{m}^2$
Membrane resistance	$r_{m_{II}}$	695.6	$\text{M}\Omega$
Cytoplasmic resistance	$r_{i_{II}}$	53.77	$\text{M}\Omega$
Membrane capacitance	$c_{II}$	8.626	pF

membrane response to current injection as shown in Figure 6.11. The main observation to be gained from this illustration is that the passive membrane properties exhibit the expected fast time constant of 6msec.

Passive membrane properties play a vital role in the electrical operation of the neuron. However, the interaction of the active membrane properties (for example, voltage dependent channels) is the basis of much of the information processing performed. The active membrane properties resulting from the membrane channel composition will be considered next.

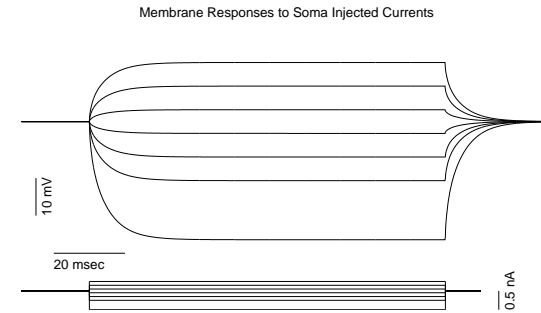


Figure 6.11: Passive electrical properties of the multi-compartmental simulated neuronal membrane. Current injection occurred at the soma compartment, and is also recorded from the soma compartment. No active membrane channels were included in order to illustrate the passive electrical properties. The upper figure is the recorded soma membrane response, while the lower figure depicts the current injected.

### 6.2.3 Membrane Channel Composition

Little is known about the exact channel composition of STH neurons. We will therefore speculate about the channel classes that may be present using physiological and pharmacological observations. Since we will be predicting not only the channel types, but also their functional forms, we emphasise that this is only one possible characterisation and useful only as a broad outline of the type of computation expected at the single neuron level. Nevertheless, by carefully constraining how we choose parameter values and fitting the model as closely as possible to the known physiology, this model will prove useful in piecing together the function and computation of the STH as a whole.

#### Fast $\text{Na}^+$ and $\text{K}^+$ Currents

First we assume that STH neurons have sodium and potassium channels appropriate for the generation of action potentials. The currents generated by these two channel types are given by

$$I_{Na} = \bar{G}_{Na} m^3 h (v - E_{Na}) \quad (6.16)$$

$$I_K = \bar{G}_K n^4 (v - E_K) \quad (6.17)$$

where

$$\dot{m} = \alpha_m(1 - m) - \beta_m m \quad (6.18)$$

$$\dot{h} = \alpha_h(1 - h) - \beta_h h \quad (6.19)$$

$$\dot{n} = \alpha_n(1 - n) - \beta_n n \quad (6.20)$$

as described in Section 6.1. The voltage dependent variables,  $\alpha_m, \beta_m, \alpha_h, \beta_h, \alpha_n, \beta_n$  have a shape essentially drawn from observations made of hippocampal neurons (Pongrácz et al., 1992), but slightly modified (by a procedure outlined below) to capture the fast firing rates and high resting potentials observed in STh neurons (see Table 6.3).

#### Calcium LVA Current

Nakanishi et al. (1987a) have demonstrated the presence of various  $\text{Ca}^{2+}$  currents in rat STh neurons. Two types of calcium dependent depolarisations may be observed after intracellular stimulation. They term these “slow depolarising potentials” (SDP) and “slow action potentials” (SAP). Neurons exhibit these behaviours under different conditions. When neurons were hyperpolarised to less than  $-65\text{mV}$  and then stimulated, the slow action potential was observed (Nakanishi et al., 1987a). This took the form of an all-or-none action potential with a duration of around 30msec. It could be induced by a simple release of hyperpolarising currents (see Nakanishi et al. 1987a) and was abolished with the addition of  $\text{Co}^{2+}$  to the superfusing medium. The slow action potential often led to a burst of fast action potentials. We postulate that one of the main underlying currents producing the slow action potential would be the low voltage activated (LVA) calcium T-current (Fox et al., 1987; Crunelli et al., 1989). This current was chosen for a number of reasons. Firstly, it is the only currently identified calcium mediated current with a sufficiently fast inactivation to account for the slow action potentials time course. Secondly, it is a low threshold activated current, characteristically initiating from hyperpolarised states, and often partially inactivated at rest (Fox et al., 1987). This fits well with the observed activation from hyperpolarised states of the slow action potential.

We modelled the calcium mediated T-current following Wang et al. (1991)

$$I_T = \rho_{T_{\max}} r^3 s \xi(v) \quad (6.21)$$

Here  $\rho_{T_{\max}}$  is the maximum permeability of  $\text{Ca}^{2+}$  ions through a homogeneous membrane of a specific surface area. Although this is not practical to measure directly (as membranes are not homogeneous), it may be fitted in a similar way to the maximum conductance variables based on physiological findings (see below for the general fitting procedure). The activation and inactivation variables,  $r$  and  $s$  respectively, are given by

$$\dot{r} = \alpha_r(1 - r) - \beta_r r \quad (6.22)$$

$$\dot{s} = \alpha_s(1 - s - d) - \beta_s s \quad (6.23)$$

$$\dot{d} = \beta_d(1 - s - d) - \alpha_d d \quad (6.24)$$

Notice that the inactivation variable  $s$  is given by two coupled differential equations. This describes a three-state inactivation model to account for the slow recovery from inactivation observed in the T-current of rat thalamic neurons (Wang et al., 1991). We assume the T-current in subthalamic neurons has essentially the same form<sup>4</sup>. For a detailed discussion on the form of this T-current model, see Wang et al. (1991). The function  $\xi(v)$  is derived from the Goldman–Hodgkin–Katz (GHK) equation that compensates for the nonlinearities of the current–voltage relation of the calcium mediated currents. The nonlinearities result from the extreme internal/external calcium concentration differences (see Hille 1992 for a review and derivation of this function). The function is given by

$$\xi(v) = z_{\text{Ca}}^2 \frac{EF^2}{RT} \frac{[\text{Ca}]_i - [\text{Ca}]_o \exp(-z_{\text{Ca}}(FE/RT))}{1 - \exp(-z_{\text{Ca}}(FE/RT))} \quad (6.25)$$

where  $z_{\text{Ca}}$  is the valence of the calcium ion (2+),  $F$  is Faradays constant,  $R$  is the universal gas constant,  $T$  is the temperature in Kelvin,  $E$  is the membrane potential for calcium ions, and  $[\text{Ca}]_i, [\text{Ca}]_o$  are the internal and external calcium concentrations respectively.

It should be stressed that  $\rho_{T_{\max}}$  is the maximum membrane permeability to the  $\text{Ca}^{2+}$  ion for a given membrane surface area. In order to separate different calcium channel types, the maximum permeability for a particular channel type is assumed to be the permeability of a membrane with all channels of that particular type open, and no other types

<sup>4</sup>The issues of drawing channel types from different neuron populations or even from different species will be discussed in Section 6.2.4.

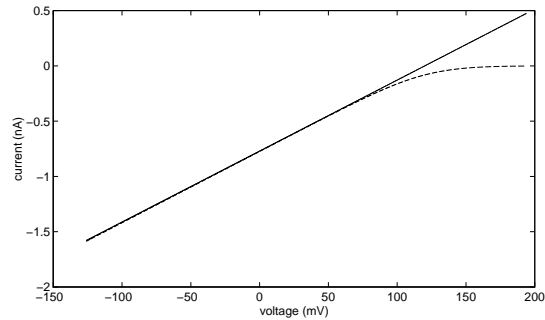


Figure 6.12: An example of the nonlinearities introduced by using the GHK equation (dotted line) compared with the linear Ohms law (solid line). These nonlinearities are most prominent for non-physiological membrane potentials. In this example,  $\rho_{T_{\max}} = 0.3 \times 10^{-12} \text{ cm}^3/\text{s}$  and the equivalent linear conductance,  $G_T = 6.5 \text{ nS}$ .

open. As previously stated, we are assuming a homogeneous membrane with this specific permeability, as necessary for the GHK equation. As this is fitted to physiological findings in a similar manner to the maximum conductances, this introduces no major unconstrainable parameter into the model. Rather, as the nonlinearities can have a significant effect on a calcium current, it allows us to capture more accurately the gross characteristics of these currents. Figure 6.12 illustrates the GHK and the Ohms law equivalent for a permeability/conductance used for the T-current.

### Calcium HVA Current

The SDP can be characterised as a long lasting calcium dependent depolarisation (often lasting well beyond the stimulus), generally supporting spikes. As it occurs under stimulus conditions that depolarise the cell more than the SAP we suggest that the high voltage activated channel types (HVA) may be involved in the SDP. Certainly, the co-occurrence of different calcium channel types is often found in CNS neurons (Hille, 1992). The two most characterised HVA calcium currents are the L- and N-types. However, both of these have only limited kinetic characterisations and are generally grouped together

as a single HVA type. For this reason, we model the activation kinetics of the L- and N-types together, and the N inactivation kinetics independently. This approach allows the model to be constrained by the physiological findings. The HVA current is then given by

$$I_{HVA} = (\rho_{L_{\max}} + \rho_{N_{\max}} u) q^2 \xi(v) \quad (6.26)$$

$\rho_{L_{\max}}$  and  $\rho_{N_{\max}}$  are the maximum permeabilities of  $\text{Ca}^{2+}$  ions through a equivalent homogeneous membrane for L- and N- channel types respectively (see  $\rho_{T_{\max}}$  above).  $q$  is the activation variable for the combined HVA channels and  $u$  is the inactivation variable for the N-type channels only. Both variables have the kinetic form

$$\dot{q} = \frac{q_{\infty} - q}{\tau_q} \quad (6.27)$$

$$\dot{u} = \frac{u_{\infty} - u}{\tau_u} \quad (6.28)$$

$q_{\infty}$  and  $\tau_q$  are taken from a description of HVA kinetic activation properties of rat sensorimotor pyramidal neurons (Brown et al., 1993). The N-type specific inactivation kinetic variables ( $u_{\infty}$  and  $\tau_u$ ) are drawn from characterisations of cultured chick dorsal root ganglia cells (Fox et al., 1987). The equations of these are given in Table 6.3.

### Calcium Activated Currents

One further observation made by Nakanishi et al. (1987a) was a calcium dependent post-response hyperpolarisation. It is likely that calcium dependent potassium channels may, at least in part, underlie this phenomenon (Hille, 1992). We therefore include a calcium activated potassium channel type (K(Ca), sometimes referred to as calcium dependent AHP). Following Pongrácz et al. (1992), the activation kinetics of this channel are dependent only on the internal calcium concentration and have no inactivation. This potassium current is given by

$$I_{K(Ca)} = \bar{G}_{K(Ca)} e (v - E_K) \quad (6.29)$$

where the activation variable  $e$  is given by

$$\dot{e} = \alpha_e (1 - e) - \beta_e e \quad (6.30)$$

See Table 6.3 for the calcium dependence of  $\alpha_e$ .

The complex processes that influence and maintain the internal calcium concentration, such as ionic pumps, buffers, and diffusion, are approximated with a single parameter system (Traub et al., 1991; Pongrácz et al., 1992). In particular, the relative internal concentration

$$f = \frac{[\text{Ca}^{2+}]_i}{[\text{Ca}^{2+}]_{i,\max}}$$

was given by (Pongrácz et al., 1992)

$$\dot{f} = \frac{1}{[\text{Ca}^{2+}]_{i,\max}} \frac{C_{\text{Ca}}}{A\delta} I_{\text{Ca}} - \beta_{\text{Ca}} f \quad (6.31)$$

This is a fixed exponential decay with a time constant of  $\beta_{\text{Ca}}$ . The influx of calcium is simply converted from the total calcium current ( $I_{\text{Ca}} = I_T + I_{\text{HVA}}$ ) into relative internal concentration under a fixed membrane shell of surface area  $A$  and depth  $\delta$  ( $= 0.2\text{nm}$ ).  $C_{\text{Ca}}$  is the conversion constant ( $1/2Ne$ ,  $N = \text{Avogadro's number}$ ,  $e = \text{elementary charge}$ ).

### Maximum Conductances

In each of the current equations a maximum conductance or permeability must be specified. As corresponding experimental measurements are not yet available we will consider these parameters as “free”, in that they must be robust to variations (see Section 6.2.4). However, values are also kept within known characteristic ranges from other cell populations (e.g. hippocampus and thalamus). Table 6.2 lists the values used in the simulations, although small variations are found to have little effect on model behaviour.

### Rate Functions

It can be clearly seen that all the channels have kinetics given in a “Hodgkin Huxley” (HH) type form. The voltage and calcium–concentration dependence of the kinetics is completely determined by the rate functions of each equation (e.g.  $\alpha_m$ ,  $\beta_m$ ,  $\alpha_h$ ,  $\beta_h$ , etc.). These functions (listed in Table 6.3) reveal the complexity and parameter abundance of

Table 6.2: Maximum conductances and permeabilities used in the current equations 6.16, 6.17, 6.21, 6.26, 6.29. For each permeability the equivalent conductance is also given.

Soma Compartment				
$\tilde{G}_{Na}$	10	mS/cm <sup>2</sup>		
$\tilde{G}_K$	4	mS/cm <sup>2</sup>		
$\rho_{T,\max}$	$0.02 \times 10^{-12}$	cm <sup>3</sup> /s	(0.05	mS/cm <sup>2</sup> )
$\rho_{L,\max}$	$0.01 \times 10^{-12}$	cm <sup>3</sup> /s	(0.02	mS/cm <sup>2</sup> )
$\rho_{N,\max}$	$0.06 \times 10^{-12}$	cm <sup>3</sup> /s	(0.13	mS/cm <sup>2</sup> )
$\tilde{G}_{K(Ca)}$	4	mS/cm <sup>2</sup>		
Dendrite I Compartment				
$\tilde{G}_{Na}$	1	mS/cm <sup>2</sup>		
$\tilde{G}_K$	4	mS/cm <sup>2</sup>		
$\rho_{T,\max}$	$0.28 \times 10^{-12}$	cm <sup>3</sup> /s	(0.5	mS/cm <sup>2</sup> )
$\rho_{L,\max}$	$0.12 \times 10^{-12}$	cm <sup>3</sup> /s	(0.2	mS/cm <sup>2</sup> )
$\rho_{N,\max}$	$0.73 \times 10^{-12}$	cm <sup>3</sup> /s	(1.2	mS/cm <sup>2</sup> )
$\tilde{G}_{K(Ca)}$	4	mS/cm <sup>2</sup>		
Dendrite II Compartment				
$\tilde{G}_{Na}$	1	mS/cm <sup>2</sup>		
$\tilde{G}_K$	4	mS/cm <sup>2</sup>		
$\rho_{T,\max}$	$0.18 \times 10^{-12}$	cm <sup>3</sup> /s	(0.5	mS/cm <sup>2</sup> )
$\rho_{L,\max}$	$0.07 \times 10^{-12}$	cm <sup>3</sup> /s	(0.2	mS/cm <sup>2</sup> )
$\rho_{N,\max}$	$0.45 \times 10^{-12}$	cm <sup>3</sup> /s	(1.2	mS/cm <sup>2</sup> )
$\tilde{G}_{K(Ca)}$	4	mS/cm <sup>2</sup>		

this type of model. We must be very careful in how we select the parameters in the rate equations, as their choice and interplay could enable us to model *any* desired behaviour. How the parameters are chosen and constrained will be discussed in the following section.

### 6.2.4 Constraining Parameters

The more unconstrained the parameters are, the less useful the model is in providing an adequate explanation of the processes underlying observed physiological phenomena. However, HH-type model's have the advantage that many of the rate functions are descriptions of experimentally observed phenomena (e.g. voltage clamp experiments can reveal the voltage dependence and temporal characteristics of selected channel types). In this way we are able to gain more confidence in the model's emergent behaviour from



Table 6.3: All the rate functions used in the kinetic equations specifying the channel dynamics of the multi-compartmental model. See the individual kinetic equations and text for details. Parameters in the equations are given in milliseconds and millivolts as appropriate.

$$\begin{aligned}
 \alpha_m &= 0.55 \frac{-(51+v)}{\exp(-(51+v)/10) - 1} & \beta_m &= 1.4 \frac{v+12}{\exp((v+12)/4) - 1} \\
 \alpha_h &= 0.5 \exp(-(28+v)/8) & \beta_h &= \frac{2.1}{\exp(-(10+v)/4) + 1} \\
 \alpha_n &= 0.1 \frac{-(9+v)}{\exp(-(9+v)/5) - 1} & \beta_n &= 0.15 \exp(-(43+v)/28) \\
 \alpha_r &= \frac{1.0}{1.7 + \exp(-(23.8+v)/13.5)} & \beta_r &= \frac{\exp(-(58.0+v)/7.8)}{1.7 + \exp(-(23.8+v)/13.5)} \\
 \alpha_s &= \exp(-(155.3+v)/17.8) & \beta_s &= \alpha_s \left( \sqrt{0.25 + \exp((78.5+v)/6.3)} - 0.5 \right) \\
 \alpha_d &= \frac{1 + \exp((32.5+v)/30)}{240 \left( 0.5 + \sqrt{0.25 + \exp((78.5+v)/6.3)} \right)} & \beta_d &= \alpha_d \left( \sqrt{0.25 + \exp((78.5+v)/6.3)} - 0.5 \right) \\
 q_\infty &= \frac{1}{1 + \exp((15.4-v)/11.3)} & \tau_q &= \frac{1.25}{\cosh(-0.031(v-2.9))} \\
 u_\infty &= \frac{1}{1 + \exp((48+v)/12.5)} & \tau_u &= 98 + \cosh(0.021(22.1-v)) \\
 \alpha_e &= \max(0.00033 f, 0.010) & \beta_e &= 0.002
 \end{aligned}$$

the constituent channel components. There is a trade-off between introducing experimentally constrained phenomena (e.g. new channel types) and the number of unconstrained parameters that must also be introduced as a consequence (e.g. distribution of the channels over the neuron). Parameters may be unconstrained for many reasons. For example, certain experiments may not yet have been carried out. Further complications arise when experimental data comes from neuron types other than the ones being modelled and when experimental data is drawn from different species. All of these factors must be considered in the specification of the model, and an approach to minimise free or unconstrained parameters should be adopted.

In order to maximise the experimental constraints, and minimise the free parameters we adopt the following procedures:

1. Include only the minimal number of channel types that together capture experi-

mentally observed behaviour.

2. For each parameter type **maintain ALL parameters in the primary rate equations**, apart from voltage shifts, **at the values derived from their original experimental descriptions**. Furthermore, any voltage shifts made for a conductance must move all kinetic equations for that conductance by the same amount and in the same direction.
3. The model behaviour is robust to variations in the unconstrained parameters.

Procedure 1 enables us to reduce the number of free parameters by including only channel types which together are sufficient in reproducing known physiological phenomena. For example, the L- and N-type activations are lumped together in the same HVA kinetic equation since this is sufficient for the replication of observed physiology. Moreover, by grouping the activation of these two channel types together the system can be more confidently constrained as the joint HVA rate equations have a larger experimental investigation on which to draw<sup>5</sup>.

The consequences of this minimal channel approach is that the model may overlook some valuable channel type(s) that affect the neurons behaviour either in subtle ways, or under circumstances not experimentally tested. However, in order to limit the number of free parameters at present we adopt this minimal approach.

Procedure 2, that of using the rate equations exactly as experimentally fitted, is perhaps more important for minimising free parameters. Immediately, a majority of the parameters become constrained by experimental findings. Two exceptions to this approach are made. Firstly, voltage shifts of the rate equations were permitted. This was done as the 5Th projection neurons have a characteristically high resting potential and the rate equations are generally drawn from experimental observations of other neuron types. Voltage shifts of the channels were allowed so that the channel kinetics could be fitted to the higher resting potentials. The second exception is to exclude the fast Na<sup>+</sup> and K<sup>+</sup>

<sup>5</sup>This is partly because the separation of the HVA-type into components is a relatively recent occurrence (Fox et al., 1987), and further, the pharmacological separation of these constituents is not straightforward.

Table 6.4: The neuron type and species origin of the rate equation functions used in the model (see Table 6.3). [<sup>†</sup>Modified as described in text].

Channel	Neuron type	Species
fast Na <sup>+</sup>	hippocampus pyramidal <sup>†</sup>	rat
fast K <sup>+</sup>	hippocampus pyramidal <sup>†</sup>	rat
Ca(T)	thalamic	rat
Ca(HVA) act.	sensorimotor pyramidal	rat
Ca(N) inact.	dorsal root ganglion cells	chick
K(Ca)	hippocampus pyramidal	rat

kinetics from this constraint. This was done as no known channel kinetics could replicate the fast firing rates of the STh projection neurons. This has two-fold consequences. Firstly, it implies the fast Na/K channel dynamics of the STh projection neurons may be significantly different to many other neuron populations (for further discussion see Section 7.2). Secondly, we now cannot use the model to make strong conclusions about the operation, shape or form of the fast Na/K generated spikes. The fast Na/K channel rate parameter selections are based on hippocampal spike generation but with the activation and inactivation arbitrarily quickened to speed spike production. Apart from these two exceptions, we adhered strictly to this parameter constraint approach.

There are a number of important consequences that follow from adopting Procedure 2. We cannot expect the model to *perfectly* replicate STh projection neuron behaviour. As there is no known characterisation of channel kinetics in the STh, these must be drawn from other neuron populations. Wherever possible, we use kinetic descriptions from neurons of a single species. The majority of experimental work relevant to this model have been carried out in rat. Table 6.4 lists the neuron populations and species from which the rate equations are drawn for each channel type.

To a large degree the kinetics of a single channel type change little across neuron populations (Hille, 1992). The reasoning behind this is that there is a finite set of protein subunits that form the various channels. There certainly may be variations of a particular channel protein composition between different neuron populations (e.g. different subunits combinations, or alternate mRNA splicing). However, here we rely on the assumption that the primary structure of the protein subunits change little, and that their

collective function as a particular channel type shares a common core kinetic form across neuron populations. There is reasonable evidence for a common core kinetic characteristic of channel types across populations (Hille, 1992). It is more difficult to extend this reasoning across species as proteins will be generated from different gene pools. However, within mammals a striking similarity in certain channel type kinetics has been found (Wang et al., 1991). Therefore we can have confidence that at least the salient features of the channel types have a form similar to that expected of the equivalent types in STh projection neurons. However, until experimental kinetic investigations are carried out in the STh we cannot expect the model to duplicate in accurate detail channel interactions and the resulting behaviour. We may only count on the salient behaviours emerging.

Procedure 3 is designed to determine the extent to which the parameters that are not tied by either of the previous two constraints affect the overall system behaviour. Salient behaviours should be robust to small changes in these parameters. Parameter searches were performed using a two tier approach. Firstly, a complete single-compartmental model was developed (presented in Gillies 1996). This produced a model with significantly lower degrees of freedom and consequently allowed more effective parameter searches. Once the parameters were assigned explicit values (or valid ranges) generating behaviours of interest in the reduced model they were transformed appropriately for the multi-compartmental model<sup>6</sup> and used as guidelines for more restricted parameter searches.

What are the consequences of all of these parameter constraint procedures for the model? In particular, what sort of results do we expect to gain from the model, and how should these results be considered? If the model is found to replicate known STh projection neuron physiological behaviour we may have confidence that the chosen channel types are a likely combination underlying the STh neuron responses. Furthermore, we can also suggest, due to the enforced constraints, that these channels have kinetics not dissimilar to other neuron populations. More importantly, we can also expect to predict a relation between the channel-induced responses and their affect on the high level models of the

<sup>6</sup>Transformation of parameters to the multi-compartmental model generally involved recalculation of surface area specific parameters only.

earlier chapters. The results of this single neuron model are presented in the following chapter.

### 6.3 Summary: The Development and Specification of a Single Subthalamic Projection Neuron Model

By investigating the underlying processing of single STh projection neurons we are more able to constrain and predict how a network of these neurons may function. The relationship between the low level channel processing and high level network dynamics is a difficult one to form. However, it is this relationship that to a large degree determines how a network of neurons function as a whole. The approach we adopt is to consider both high level and low level models and consequently how they influence each other. In this chapter we have described in detail the development of a low level model of a generic STh projection neuron. The results drawn from this model (presented in the following chapter) will allow us to constrain the high level models and, moreover, gain a greater characterisation and perspective of subthalamic nucleus function.

The development of the multi-compartmental model in itself has proved useful in highlighting properties of single STh neuron function. Firstly, by using the HH-formalism, channels and their kinetics must be made explicit. The prediction of a certain group of channel types underlying the salient STh physiological behaviour have been presented: fast  $\text{Na}^+$ , fast  $\text{K}^+$ ,  $\text{Ca(T)}$ ,  $\text{Ca(L)}$ ,  $\text{Ca(N)}$ ,  $\text{K(Ca)}$ . The model indicates that channels underlying the fast action potential ( $\text{Na}^+$  and  $\text{K}^+$ ) are likely to be different (possibly significantly faster) from currently known or characterised channels of the same type. Furthermore, the model predicts a significant calcium permeability through the three  $\text{Ca}^{2+}$  selective channels. The effects of possibly large calcium influxes will be discussed in Chapter 7.

A second constraint that the model development introduces arises from the strong morphological considerations. For example, these cast a new light on the conflicting experi-

mental *in vitro/in vivo* findings of the input resistance. The model's morphological specification predicts that the *in vivo* measurements of Kita et al. (1983a) are more likely to be in the correct range (with large micro-electrode shunt). However, it is likely that the true input resistance sits at a value intermediate between those found *in vivo* and *in vitro*.

The morphological considerations also begin to formalise the two types of dendritic trees found. In particular, neurons with intranuclear axon collaterals and denser dendritic trees (Type II) further support the likelihood of a recurrent network type arrangement proposed in the high level model of Chapter 4. In particular the dendritic spheroid proposed as a simplification of the dendritic tree is likely to be a more accurate representation for neurons with internal collaterals. The larger surface area increases the accuracy of a uniform field assumption.

Apart from these interesting findings and constraints, a more detailed investigation of the single STh projection neuron function and its consequences for the STh as a whole are considered with the simulation results of the model presented in the following chapter.

## Chapter 7

# The Single Subthalamic Nucleus Projection Neuron

The subthalamic nucleus has been described as having “original electrical membrane properties” (Kita et al., 1983a). Certainly, firing at near 500Hz indicates some unique underlying channel dynamics. However, much of the other observed properties emerge from the small collection of channel types described in Chapter 6. In this chapter we present the simulation results of the multi-compartmental model presented in the previous chapter. We focus on the experimental observations made by Nakanishi et al. (1987a) and illustrate the model’s responses under similar simulated experimental conditions. All simulations in this chapter arise from the same parameter regime unless otherwise specified.

The simulations were performed using the same multi-level neural simulator, *Rorohiko*, described in Appendix A. The simulation design is much more complex in this case, reflecting the introduced complexity of the multi-compartmental model (for more details see Appendix A). However the hierarchical approach of the simulator allows the construction of artificial neurons at this more detailed level in a straightforward manner.

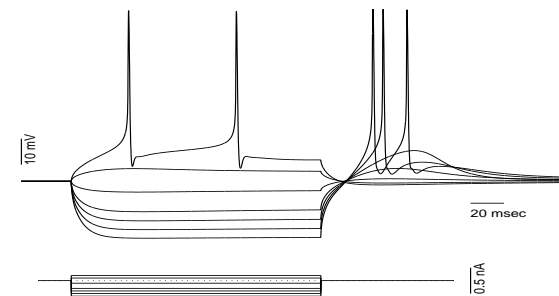


Figure 7.1: The response of the model to simulated current injections. The effect of the active channels on the passive properties can be seen (compare with Figure 6.11). Note in particular the slow rise in hyperpolarising currents, and the post hyperpolarisation spikes. Simulated current injections are at 0.1, 0.05, -0.05, -0.15, -0.2, -0.25, -0.30 nA.

All simulations were performed on a DEC *alpha* 3500S. A single simulation of 400msec involving current injection required 15–20 minutes on the *alpha*<sup>1</sup>. All graphical results presented are produced using the mathematical package MATLAB<sup>®</sup>. Results are presented in a form following the Neuroscience literature to allow an easy and direct comparison.

### 7.1 Passive Properties

It is often difficult to separate the passive membrane properties from active channel influences. Only in a model, where all parameters can be meticulously controlled, can we achieve perfect separation. For example, the passive properties shown in Figure 6.11 of Chapter 6 are from simulations where all channels (except the leak) are literally turned off. However, the investigation of passive properties with all active channels normally engaged can be equally revealing when a comparison with experimental data is sought. In this section we will introduce modelling techniques that have experimental analogues, and further demonstrate the effect the active channels have on the observed passive properties.

<sup>1</sup> A significant reduction in simulation time was achieved by hand optimisation of the code as described in in Appendix A.

The model STh projection neuron as described in the previous chapter has a resting potential of around -52mV. Very small positive current injections generally lead to spikes, demonstrating how close to threshold the model neuron rests (Figure 7.1). Hyperpolarising injections demonstrate the characteristic fast time constant. Two prominent features can be attributed to the active channels. Firstly an inward drift (towards rest) in both the depolarised and hyperpolarised potentials is observed. Under depolarised conditions the drift is a result of mild activation and subsequent inactivation of the Ca(T) and Na type channels (a “hump” can be seen more clearly in Figure 7.3). The drift under hyperpolarised conditions is considerably smaller. It results from releasing the large pool of inactivated Ca(T) channels allowing an increasing (albeit small) proportion to open spontaneously at the new hyperpolarised resting level. The cause of the hyperpolarising drift is seen more clearly in the isolated T-current (Figure 7.2).

Secondly, for significantly hyperpolarised potentials, post current injection spikes are generated. This also follows from the release of inactivated Ca(T) channels. At hyperpolarised potentials, a greater proportion of channels (compared to rest) become de-inactivated so that as the potential rises after the current injection a significant calcium current is produced. This pushes the neuron over threshold and one or more spikes are generated. Figure 7.2 shows an example Ca(T) current in response to a hyperpolarisation of 20mV.

The post-response spikes are observed experimentally (Nakanishi et al., 1987a). Although there are also drifts observed, it is by no means clear that these result solely from the mechanisms described above. As we have taken a minimal channel approach (Section 6.2.4) there are likely to be other processes occurring in a similar manner to the T-current drift.

To assess a wider range of passive responses (particularly depolarising responses) it is useful to abolish cell firing chemically. A common experimental approach is to use tetrodotoxin (TTX) which blocks a significant proportion of sodium channels thus eliminating the major driving force of action potentials (see Section 6.1). Application of TTX can be simulated in the model with a reduction in sodium conductance. The simplest method

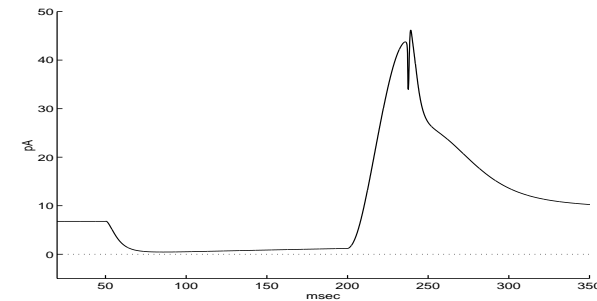


Figure 7.2: Hyperpolarisation (at 50msec) de-inactivates the calcium T channels. When repolarisation occurs (at 200msec) a significant calcium current is therefore generated before the channels again inactivate. Notice also a gradual positive current increase during the hyperpolarisation period. The increase underlies the voltage drift observed at hyperpolarised potentials. This result is taken from a proximal dendrite (1A) as the maximum Ca(T) channel permeability is larger than in the soma and provides a more influential current (see Figure 6.9 and Table 6.2).

is to replace  $\bar{G}_{Na}$  of Equation 6.8 with an appropriately reduced maximum conductance  $\bar{G}_{TTX}$

$$G_{Na} = \bar{G}_{TTX} m^3 h \quad (7.1)$$

$\bar{G}_{TTX}$  was chosen to be a 1% of  $\bar{G}_{Na}$ . Small variations in the conductance reduction had little effect on the passive properties. Figure 7.3 shows the model's passive properties under conditions of simulated TTX.

There is a degree of similarity between the passive properties exhibited by the model and those seen experimentally. From the passive simulations we have an indication that the calcium T-current is a major active channel perturbing the passive responses. It is primarily responsible for the small voltage drifts and the post hyperpolarising stimulus action potentials. As we shall see, the Ca(T) channels produce one of the major currents underlying many of the characteristic STh behaviours.

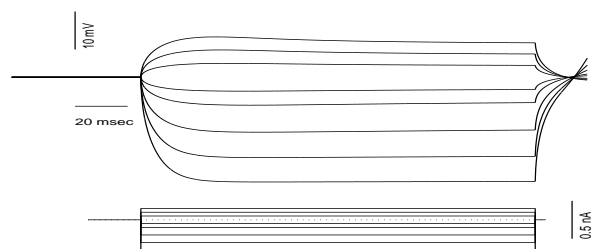


Figure 7.3: Passive properties under conditions of simulated TTX. In these simulations  $\bar{G}_{TTX} = 1\% \bar{G}_{Na}$ . A small “hump” produced at the beginning of the current injections can be seen in the depolarisations. In this case, it is solely the T-current generating this voltage hump as most of the sodium influence has been abolished. Simulated current injections are at 0.15, 0.1, 0.05, -0.05, -0.1, -0.2, -0.3, and -0.4 nA.

## 7.2 Fast Action Potential

As mentioned in Section 6.2.4 we can conclude very little about the fast action potentials themselves as the parameters underlying the active sodium and potassium conductances are illconstrained. However, the interspike intervals are largely dependent on other channel properties. Nakanishi et al. (1987a) observed a distinctive difference between the first and last spike intervals over a 150msec current injection. The interval between the second to last and last spikes could be over twice the interval between the first and second spikes. The difference also varied over stimulus strength. With constant current injection, the model exhibits a increasing interspike interval over time. There appears to be an initial cluster of spikes followed by a more regular firing pattern (see Figure 7.4). The initial clustering of spikes concurs with the observation that *very* small depolarising current injections may lead to a single spike generally immediately after the stimulus onset (see Figure 7.1 and Figure 2A of Nakanishi et al., 1987a). Both of these phenomena imply that there is a period at the beginning of the depolarising stimulus where there is a greater disposition for the cell to fire.

The mechanisms that are likely to cause the initial spike clustering may be found by again isolating the T-current in the model. With an increase in membrane potential, a

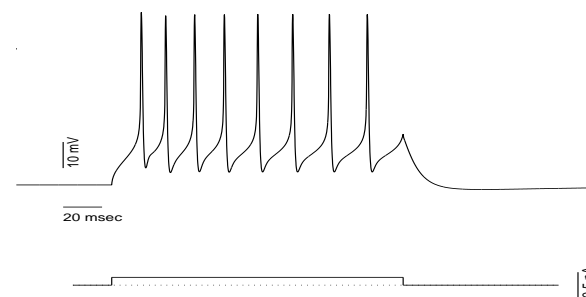


Figure 7.4: With a depolarising current injection (0.15nA above) regular spiking occurs in the model. There is a distinctive increase in interspike interval over the duration of the stimulus, with a characteristic initial clustering of spikes.

proportion of the Ca(T) channels that are not inactivated at rest will open, creating a small but significant calcium current (Figure 7.5). Normal Ca(T) inactivation terminates the current with a time constant of  $\sim 60$ msec. Thus in the model the initial clustering of spikes is a result of Ca(T) channel activation.

Other influences are also involved in the increasing interspike interval. High voltage activated calcium currents (Ca(HVA)) increase the internal calcium concentration over the period of cell firing. This in turn increases the activation of the calcium activated potassium current (K(Ca)). However, for a reasonable range of  $\bar{G}_{K(Ca)}$  this current was found to have only a small effect in comparison to the T-current spike clustering behaviour described above.

## 7.3 Slow Action Potential

Nakanishi et al. (1987a) observed that a “slow action potential” (SAP) could be generated from a depolarising stimulus under conditions where the cell is continuously hyperpolarised. The “all or none” action potential has a duration of around 30msec and is

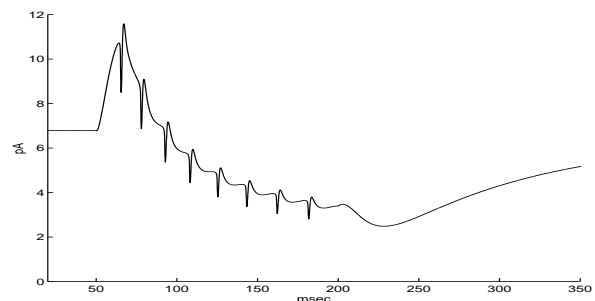


Figure 7.5: A small calcium current increase generated soon after the beginning of the stimulus is responsible for the initial spike clustering observed in the model. The decrease beyond the current resting level caused by Ca(T) inactivation also plays a role in the later increase in interspike interval (see Section 7.4).

generated from cells with membrane potentials more negative than  $-65$  mV (Nakanishi et al., 1987a). The SAP is abolished after application of  $\text{Co}^{2+}$  to the superfusing medium.

The model replicates these findings. It is primarily the Ca(T) channel that produces the distinctive SAP characteristics. Figure 7.6 illustrates simulations under conditions where the model neuron is continuously hyperpolarised and subsequently depolarised to various degrees. During the enforced hyperpolarised rest (via simulated current injection) a high proportion of the Ca(T) channels become de-inactivated (closed) and available for subsequent opening upon sufficient depolarisation.

The SAP can be seen more clearly under conditions of simulated TTX and TEA (tetraethylammonium). The TEA selectively blocks the potassium channels involved in the generation of fast action potentials and its effect is modelled in a similar manner to TTX (see Equation 7.1). Figure 7.7 illustrates the responses of the model under these conditions.

The processes underlying the SAP can be seen by observing the Ca(T) kinetic variables  $r$ ,  $s$ , and  $d$  (see Equations 6.22–6.24). Under normal resting conditions (with no current injection) the inactivation variable  $s$  (dashed line) sits very close to zero indicating that

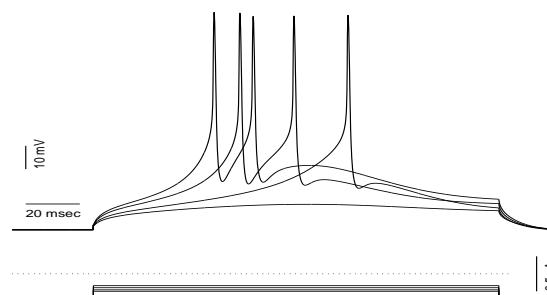


Figure 7.6: The slow action potential generated under different current injection conditions. The simulated neuron is given a continuous background current injection of  $-0.35$  nA. For the 50–200 msec period the current injection is reduced to values  $-0.25$ ,  $-0.2$ ,  $-0.17$ , and  $-0.15$  nA on different trials. This resulted in depolarisations and generally the initiation of the SAP. For the depolarising current injection of  $-0.15$  nA, no SAP is generated, illustrating its “all or none” nature.

a high proportion of channels are inactivated (see Figure 7.8A). However, under conditions where the simulated neuron is continuously hyperpolarised (via current injection), the inactivation variable is significantly increased, leaving a larger proportion of channels available to be open. Furthermore, the activation variable  $r$  (solid line) is significantly decreased under the hyperpolarised condition, indicating that very few channels are in the open state (see Figure 7.8B). Note that this reduction of open channels is amplified in the current equation by a cubic term.

$$I_T = \rho_{T_{\max}} r^3 s \zeta(v) \quad (6.21)$$

Following the release of the hyperpolarisation the activation variable  $r$  increases at a rate faster than the inactivation variable decreases (Figure 7.8C). This produces a net calcium current resulting in the SAP. The current is terminated following the time course of the  $s$  inactivation variable. The kinetic variable  $d$  plays little role here as its primary effect is in the return of the inactivation variable to its resting level.

Two processes are involved in producing the “all or none” type effect of the SAP. Firstly, the activation variable  $r$  has a kinetic description that produces a steep sigmoid type re-

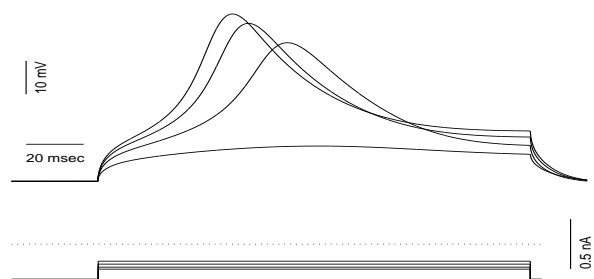


Figure 7.7: Simulated application of TTX and TEA reveals the shape and time course of the slow action potential.  $\bar{G}_{TTX} = 1\% \bar{G}_{Na}$  and  $\bar{G}_{TEA} = 1\% \bar{G}_K$ . The base simulated current injection used was  $-0.35\text{nA}$ . Depolarisations over the period of 50–200msec were produced from reduced injections of  $-0.25$ ,  $-0.2$ ,  $-0.17$ , and  $-0.15\text{nA}$ .

sponse. The variable  $r$  is generally in one of two states: on or off. Over many simulations we have observed that the flipping of  $r$  between the two states is the primary determinant of Ca(T) channel behaviour. Moreover, the steepness of this change makes the T-current a primary determinant in the cells behaviour. It is the flipping of this variable that produces the “all or none” SAP. Note from Figure 7.7 that a change in the current injection by  $0.02\text{nA}$  makes the difference between the SAP generation or a simple passive response.

The second process in the “all or none” response is the reported involvement of a rectifying potassium current (Nakanishi et al., 1987a). In the model, the potassium current involved in the fast action potentials is also engaged for the SAP (observed under conditions of simulated TTX only, not shown). However, the current is very small and only has a minor capping effect on the SAP. A larger potassium current could indeed provide a mechanism to produce a uniform SAP peak voltage independent of current injection as is observed experimentally. There is as yet no motivation to explore shifting the fast  $K^+$  channel response to observe if this effect actually occurs as this channel type is ill-constrained (see Section 6.2.3). Any effect resulting from a shift may be an artifact of the unconstrained channel definition. Such an investigation should wait until the fast  $Na^+$

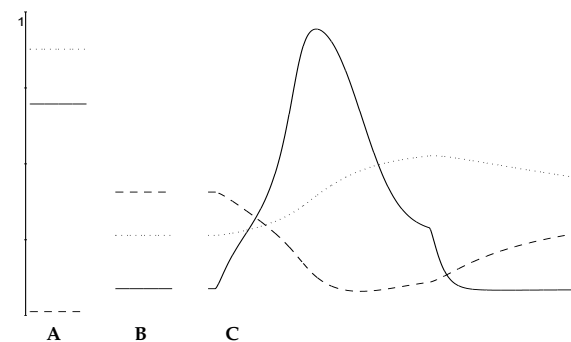


Figure 7.8: The kinetic variables  $r$  (solid line),  $s$  (dashed line), and  $d$  (dotted line) that describe the Ca(T) channel dynamics (see Equations 6.22–6.24). **A.** The variables under rest conditions. Note a high proportion of channels are inactivated ( $s$ ). **B.** The variables under conditions of maintained hyperpolarisation (from  $-0.35\text{nA}$  simulated current injection). Note that fewer channels are inactivated ( $s$ ), and significantly less are in the open state ( $r$ ). **C.** The change in variables under conditions of reduced hyperpolarising current injection (reduced to  $-0.2\text{nA}$ ) for 150msec. Fast action potentials have been eliminated using the simulated TTX and TEA protocols.

and  $K^+$  channel specifications for the STh projection neuron are characterised.

The only transformation made to the kinetic description of the Ca(T) channels (originally described for rat thalamic neurons, see Section 6.2.3) is a voltage shift of  $6\text{mV}$ . The essential features of the Ca(T) kinetics describe the STh projection neuron SAP with encouraging detail. Moreover, it is evident that the T-current plays an important role in many of the prominent STh neuron behaviours.

## 7.4 Post Response Quiet

Nakanishi et al. (1987a) observed a calcium dependent post-stimulus long lasting hyperpolarisation (250–500 msec). Similarly, *in vivo* experiments demonstrate a long lasting quiet period in STh neurons after considerable firing in response to cortical stimulation



(Fujimoto & Kita, 1993). Fujimoto and Kita (1993) found that the post-response quiescence (PRQ), which they call long lasting inhibition, was persistent after striatal, pallidal, and brainstem lesions. Unlike Nakanishi et al. (1987a), they did not find from their intracellular recordings an underlying membrane hyperpolarisation. However, other *in vivo* experiments do identify a post-response hyperpolarisation (Kitai & Deniau, 1981).

It is certainly clear that IPSPs are not the mechanism underlying this post-response behaviour (see authors above). Fujimoto and Kita (1993) propose disfacilitation of cortical input as a possible mechanism. This would parallel the proposal that disfacilitation of cortical input underlies a similar behaviour in striatal neurons (Wilson et al., 1983). There may indeed be some disfacilitation of excitatory inputs. However, since in the STn it is likely there is significant intranuclear connectivity (see Section 4.3.1) and moreover, that isolated brief cortical stimulation yields widespread responses (Fujimoto & Kita, 1993), an intrinsic membrane after-hyperpolarisation also could induce intranuclear disfacilitation. A post-response hyperpolarisation in cells that were recently coactive would lead to a mutually enforced quiet period resulting from a combination of reduced lateral excitation, and intrinsic hyperpolarisation.

The model predicts an intrinsic calcium-dependent post-response hyperpolarisation (Figure 7.9). A simulated calcium free medium is used to demonstrate the calcium dependence. In the calcium free simulations the maximum permeabilities for calcium conductances were reduced following

$$\rho_{A_{free}} = k\rho_{A_{max}}$$

where  $A$  is each of  $T$ ,  $L$ , and  $N$  (see Equations 6.21 and 6.26). Generally  $k$  was chosen to be zero or near. Small increases in  $k$  ( $k < 10\%$ ) had little effect on the elimination of the hyperpolarisation.

Two mechanisms are found to be primarily responsible for the post-response hyperpolarisation. First, a calcium activated potassium current (K(Ca)) is generated from the increased internal calcium concentration produced from action potential responses. This current outlasts a sufficient stimulus by 100–500msec thus contributing to the prolonged

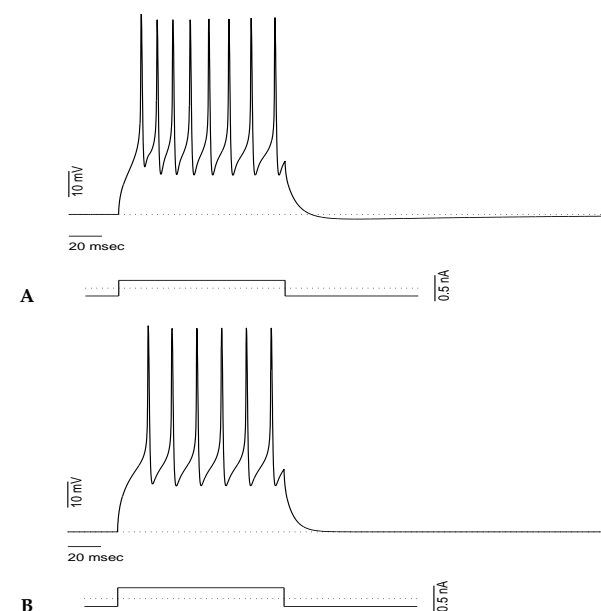


Figure 7.9: A. Post activity hyperpolarisation is observed after a current injection of 15nA (from baseline hyperpolarising current of  $-0.15\text{nA}$ ). B. The hyperpolarisation is eliminated in the calcium free system. It is also interesting to note that the spike clustering at the beginning of the stimulus is abolished in the  $\text{Ca}^{2+}$  free simulations.

after-hyperpolarisation. This is a common artifact of the K(Ca) channels, seen in many different neuron types (Hille, 1992). Its involvement is also in agreement with the calcium dependence experimentally found for this hyperpolarisation (Figure 7.9).

However, the K(Ca) current is not the major contributor to the PRQ. The model predicts that a very small proportion of Ca(T) channels can be open and not inactivated at rest<sup>2</sup>. This concurs with experimental findings in which the application of  $\text{Co}^{2+}$  to an *in vitro* superfusing medium results in an increase in input resistance (Nakanishi et al., 1987a).

<sup>2</sup>Note that we consider averaged dynamics over a large number of channels. We would predict from this that a small proportion of channels are spontaneously opening, inactivating, and closing at rest.

After a period of action potentials most Ca(T) channels are inactivated. This in turn produces a post-response hyperpolarisation as the small proportion of Ca(T) channels normally available to be open at rest are now inactivated. The de-inactivation period of Ca(T) channels is particularly long (Wang et al., 1991), producing a hyperpolarisation of 100-200msec.

We predict from the model a deceptive type of after-hyperpolarisation. Experimental analysis may not reveal a significantly decreased membrane resistance as would be expected if the K(Ca) were solely responsible for the PRQ. An opposing increase in membrane resistance should result from Ca(T) channel over-inactivation. However, both mechanisms have a common effect of producing a post-response hyperpolarisation. Taken together with the probability of disfacilitation of lateral excitatory inputs, the model predicts the PRQ will play a significant role in intrinsic STh projection neuron behaviour.

## 7.5 Discussion

The multi-compartmental model of the STh projection neuron was designed for a number of reasons. Firstly, as seen in Chapters 4 and 5, we require a formal method to further constrain the higher-level and more abstract models. Inclusion of all the detail of the multi-compartmental model would render the high level network models useless in both their mathematical and computational tractability. Furthermore, it is from their simplicity that the primary network behavioural dynamics emerge in a clear and unperturbed manner. However, further constraints are required (Section 5.5). The multi-compartmental model provides a means of incorporating many detailed experimental results into a single formalism. This model is constructed to include anatomical, pharmacological, and physiological findings. With the aim in mind of identifying *salient* features in order to constrain the more abstract models, a limited design approach was adopted; that is, a design which could reproduce many of the experimental findings yet with a reduced and limited composition in order to identify the salient behaviours

emerging from the single STh projection neuron. The multi-compartmental model presented achieves this goal.

Motivation for this model arose not only from the requirement to constrain more abstract investigations. A second and equally important goal is to provide an explanation of the possible mechanisms underlying observed physiological behaviour. Proposing channel mechanisms and compositions within a morphological framework from which physiological properties arise is an aim of multi-compartmental modelling in general. However, these models are notoriously under-constrained and generally have a large number of free parameters. Free parameters in such complex nonlinear dynamic systems dangerously undermine the power of this approach. This model was therefore designed to explore the channel compositions that could replicate observed physiology within a strict parameter constraint protocol.

Remarkably little is known about the STh in comparison to many other brain areas (for example, the hippocampus or even neostriatum). Subsequently, there is a requirement to use findings from research into other neuron populations in order to complete the model specification. For example, we can predict that a low threshold current is likely to be present in STh projection neurons. However, to include it into the model a complete kinetic specification is required. This is currently unavailable for STh projection neurons. We therefore make the decision to include kinetic specifications of channel types from characterisations made in other brain areas (see Table 6.4). However, we qualify this with the requirement that, apart from simple voltage shifts, these kinetic specifications should not be modified (see Section 6.2.4). The reasoning behind this is the assumption that there is a similarity between channel types across different neural populations. By not modifying the kinetic forms we constrain the model significantly. Foreign channel specifications would either reproduce the known STh physiology, or they would not. If they do not, we can draw no conclusions about the STh from this model. Altering the channel kinetics to achieve similarity would be equally uninformative as we have a massively powerful model simply bending to the required shape. However, if foreign channels do produce known STh physiology in the context of all the other STh model specifications, we have a constrained system illustrating possible mechanisms underlying

this physiology. We have found that the model with included foreign channel kinetics achieves this replication of salient STh physiology.

### 7.5.1 T Dominance

The Ca(T) channel emerges from the model as one of the dominant influences underlying many of the observed physiological phenomena. Each of the following behaviours have the T-current as their primary underlying mechanism

1. Passive perturbations.
2. Spike clustering.
3. Slow action potential (SAP).
4. Post-response quiet (PRQ).

There are two primary reasons that the T-current emerges as one of the central determinants in the behaviour of the STh projection neuron. Firstly, many of the interesting behaviours themselves are observed or generated from intracellular current injection experiments involving pre-hyperpolarisation of the cell or could be exaggerated by a pre-hyperpolarisation (see referenced authors through Sections 7.1–7.4). As we have described, Ca(T) is a low threshold activated channel and engages particularly energetically from hyperpolarised potentials. Thus it is expected that a low threshold current should be a contributor to some of the salient cell behaviours observed under these hyperpolarised conditions. This is in some sense a circular argument, as it is these very observations that led us to choose the Ca(T) as an underlying candidate. What is surprising is how well the T-current describes each of the behaviours providing convincing evidence of its dominant role.

The second reason why the T-current plays such a significant role in determining salient behaviour is revealed in its kinetic specification. As described in Section 7.3 the rapid flip

from near all on to near all off Ca(T) activation on a voltage decrease (or vice versa on a voltage increase) is sufficiently abrupt to jolt the cell into a new behaviour. In particular, the SAP and post hyperpolarising spikes are good examples of this dramatic response. This is possibly the very reason the Ca(T) induced SAP is referred to as an action potential in itself.

The fact that for a reasonable parameter search over maximum conductances/permeabilities ( $\rho_{L_{\max}}, \rho_{N_{\max}}, \bar{G}_{K(Ca)}$ ) the Ca(T) remained the dominant channel underlying responses was a surprise. For example, it was fully expected that the K(Ca), as in many other neuron types, would be primarily responsible for an after-hyperpolarisation. However, the finding that over-inactivation of Ca(T) also played a significant role<sup>3</sup> may explain the diverse findings regarding this behaviour (Fujimoto & Kita, 1993; Nakanishi et al., 1987a; Kitai, 1981). The T-current clearly stands out as the primary determinant in the reconstruction by the model of the physiological phenomena.

### 7.5.2 The STh Projection Neuron in Context

The results presented in this chapter replicate *in vitro* current injection experiments. The model does not illustrate possible responses that may occur to the major cortical, pallidal, and thalamic afferents. There are a number of experiments that investigate the effect of these major afferents (for example, Fujimoto and Kita, 1993; Ryan et al., 1992). These are difficult to include in the model and may be more appropriate in future model development. Consider, for example, modelling the results of Fujimoto and Kita (1993) and their investigation of the effect of cortical stimulation on the STh. Ideally the model would be required to include cortical neurons in order to capture the spread and type of activity generated from electrode stimulation in the sensorimotor cortex. Even if we could make acceptable assumptions about this<sup>4</sup> and then model the descending fibres

<sup>3</sup>The mix of these two mechanisms is the reason we call this behaviour PRQ rather than after-hyperpolarisation. Furthermore, disfacilitation may be involved on a network scale, encouraging the use of a more generic term.

<sup>4</sup>There is currently a debate as to the origin of the massive spread of activity observed in the STh from such cortical stimulation. In particular is the activity spread generated in the cortex or in the STh itself (see Fujimoto and Kita, 1993, and Section 8.1)? Resolving issues such as these would be required to model the corticosubthalamic pathway accurately.

only, there still remain issues such as the distribution and spread of synapses expected over a single large dendritic tree. As more anatomical information is being revealed, modelling this may indeed be fruitful. However, currently the assumptions required for this would deteriorate the model's ability to achieve the original goals.

This is not to say that the results as presented do not contribute to the understanding of the local circuit dynamics (see Figure 3.1 of Chapter 3). The features observed in the model can indeed be considered in the wider context. Certainly, the multi-compartmental model together with the more abstracted network models can provide a fuller explanation of the internal dynamics of the STh as a whole. As this is one of the aims of both models we will draw their results together and consider their joint conclusions in Chapter 8.

We now consider briefly the predictions from the model in the context of the primary STh afferents. Firstly, the major cortical and thalamic input provide an excitatory influence on the STh. Since the model neuron sits very close to threshold (Section 7.1) we expect that even limited corticosubthalamic or thalamosubthalamic activity will initiate some response. Fujimoto and Kita (1993) observed that very weak and isolated cortical stimulation yielded significant responses in the STh. Clearly, a neuron that rests very close to threshold may respond to even small afferent activity. The model further predicts that a PRQ should follow significant STh projection neuron firing (for further discussion on this see Chapter 8).

The STh response to cortical stimulation generally consists of two peaks of activity (Kitai, 1981). The intervening trough appears to be caused by IPSPs (Fujimoto & Kita, 1993) that are likely to originate from the major inhibitory pallidalsubthalamic pathway. The pallidum is not only known as an inhibitory afferent, but also a STh efferent site. It is a possibility that stimulation of the STh results in secondary stimulation of the external segment of the globus pallidus (GPe) which consequently then inhibits the STh. What is interesting is the strong response the STh regenerates after the inhibitory period. The model predicts that IPSPs will generally hyperpolarise cells (particularly with respect to

the high resting potentials observed in the STh) and should release a significant proportion of Ca(T) channels from inactivation. This, as demonstrated in the model, should lead to aggressive firing. Thus we can predict that the second wave of firing observed results primarily from the activation of Ca(T) channels. Consequently this should also involve a major calcium influx into the cell. Moreover, we may also expect the secondary response to be significantly reduced after the introduction of a selective Ca(T) antagonist. Currently, there is very limited experimental evidence to draw from for the support of these predictions. Although the two peak response is experimentally observed (Fujimoto & Kita, 1993) there is no indication of the mechanisms underlying its generation. The model presented above describes a possible mechanism which may easily lend itself to experimental verification.

However, there are behaviours exhibited by STh neurons that are not demonstrated by the current model. In particular, the "slow depolarising potential" (SDP) reported by Nakanishi et al. (1987a). This long lasting depolarisation can not be reproduced under the same parameter regime used throughout this chapter. Although this behaviour was exhibited only in some neurons, the model requires a significant modification in the characterisation of calcium channels to generate this phenomenon. This violates our parameter constraint regime, and thus the model cannot confidently reproduce this phenomenon. It is therefore possible that neurons with significantly different channel behaviours and distributions coexist within the STh. A further possibility is that calcium channels undergo mode changes resulting in the different behaviours (Delcour et al., 1993), introducing additional dynamic complexity. It is not possible at this stage to accurately model such heterogeneity.

Many of the responses observed in *in vivo* stimulation of afferent structures are understandably complex. As we have seen in Chapter 5 the response of a neuron in the context of the surrounding circuit may be very different to its isolated responses. Generally neurons cannot be considered in isolation when trying to understand the functioning of large structures. Therefore what will be important is forming a relation between this model and the earlier network level models. This will be considered in the following chapter.

### 7.5.3 Conclusion

In summary, this model provides a characterisation of possible mechanisms underlying the salient behaviours of individual STh projection neurons. In particular, the T-current has been shown to be a major component of almost all cellular responses explored. The effect of this and other mechanisms proposed by this model on the function of the STh as a whole will be explored in Chapter 8. It is one of the goals of this model that its results may be synthesised with other models and approaches into a coherent view of the STh.

## Chapter 8

# The Subthalamic Nucleus Pulse

In the previous four chapters we introduced techniques and analysis of STh dynamics from very different perspectives. The highly abstract dynamic network model allowed us to investigate large scale network processing, whereas the multi-compartmental model presented a more detailed account of the processing of single STh neurons. Can we draw the results of these differing approaches into a single coherent view of the subthalamic nucleus? Furthermore, how may such a coherent thesis fit with current theories of basal ganglia processing? We address these questions in the following sections.

### 8.1 The Subthalamic Nucleus Pulse Hypothesis

The dynamic network model revealed that states of hysteresis are not only possible in the network, but in fact likely. This is a matter of concern, since sustained hysteresis is an information-destructive state. However, the analysis of the network model also implied that the attractor around the hysteresis state is small. If there were a mechanism that could slow the firing rate once the hysteresis state is reached, then the system may escape the small attractor and sustained hysteresis would be prevented. Such a mechanism would be required for most neurons since hysteresis is resistant to localised

effects. The inactivation of the calcium T-current and the calcium activation of K(Ca) were demonstrated in the multi-compartmental model to be prime candidates for such a mechanism. As we have seen, the over-inactivation of the Ca(T) type channels allows an initial clustering of spikes followed by a reduced firing rate. We therefore propose that brief states of hysteresis are likely, but intrinsically controlled and terminated.

If this hypothesis is correct there are serious consequences for the processing properties of the STh and for the basal ganglia as a whole. Firstly, consider the STh response to cortical or thalamic input. If even localised input is reasonably influential, the network may be pushed to the state of hysteresis. The STh responses to excitatory input will therefore be widespread (encompassing much of the STh in rat) and extremely powerful. The hysteresis state resides near the maximum firing rate ( $Z_{max}$ ) and the nature of hysteresis is to push all neurons involved in the network into this state. However, hysteresis will then be quickly terminated by a combination of Ca(T) inactivation, GABAergic feedback from the GPe and K(Ca) activation. Consequently, *the subthalamic nucleus responds to sufficient excitatory input in the form of a massive uniform pulse*. Given the intrinsic properties of the STh, where the firing rate is characteristically high (near 500Hz) the pulse is likely to have an overpowering effect on STh target structures. However, the pulse will also be short lived, as a result of intrinsic mechanisms outlined above.

### 8.1.1 Intranuclear Consequences of the Pulse

The pulse hypothesis predicts that we should observe uniform and widespread responses in the STh after cortical or thalamic stimulation. This is indeed found in the rat STh (Fujimoto & Kita, 1993). However experimentally it is unclear whether the spread of activity is in the cortex or the STh itself. The model presented in Chapters 4 and 5 clearly indicate STh internal dynamics are sufficient to reproduce this phenomenon. This certainly does not rule out spread of activity in the cortex, or further, divergence of cortical input onto the STh. In fact, the geometric simulations of Section 4.3.1 emphasise that the large dendritic fields of STh neurons may encourage divergence of information. The enormity of the dendritic fields in a densely packed nucleus would allow many neurons

to be influenced by single fibres. Moreover, such divergence would increase the likelihood of pushing the system to hysteresis since the wider the input spread, the greater and more synchronous the net input contribution ( $\sum w_{ij}\sigma_j$ ) will be to each neuron involved. This increases the likelihood of hysteresis. Furthermore, divergence of cortical input concurs with the hypothesis that the primary purpose of the STh is some form of uniform widespread response, such as pulse generation. However, such divergence would make an experimental distinction between an intrinsic STh pulse and solely input driven activity difficult to achieve. This is because in both cases divergence of a single input source increases the expected synchrony of the response. If there were only lateral connections and localised input, experimentally we could expect a more asynchronous pulse generation (as a result of the lateral spread of activity, for example, see Figure 5.11). Due to the large dendritic fields, divergent input is likely and therefore increased synchrony is expected.

How widespread should we expect the uniform activity pulses to be throughout the nucleus? In the dynamic network model we used a Gaussian connectivity regime. Under these conditions, activity quickly spread over the entire network. If random volume intersection results are used as weight specifications (see Section 4.3.1) the spread of activity still encompasses the entire network. However it is possible to devise clustering of collateral orientations to restrict hysteresis to regions. Since collateral orientation and distribution within the STh is currently not known it is possible that pulses occur in isolated zones or regions. For example, such regions could correspond to distinct somatotopic zones representing "leg" or "arm". Such somatotopic divisions are more distinct in primates. For example, during normal movements in monkey, activity in large proportions of neurons segregated into a specific representation is observed (Wichmann et al., 1994). However, whether zones exist or not, we can still predict the essential features of hysteresis — a uniform pulse of activity with a fast rise time and intrinsic termination.

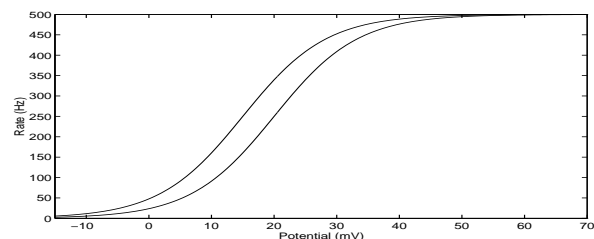


Figure 8.1: Two sigmoid functions as given in equation 4.2 with different threshold ( $y_0$ ) parameters. Parameters are  $b = 0.1$ ,  $y_0 = 15.0$  (left),  $y_0 = 20.0$  (right), and  $Z_{max} = 500$ . Resting potential is defined at 0mV.

### 8.1.2 The Long Term Effects of the Intrinsic Properties

The de-inactivation of the calcium T-current and the return of the K(Ca) to rest are both lengthy processes (in the order of 200msec). If these intrinsic properties are involved in the termination of the pulses we should expect long term effects after their activation in the STh. In the single neuron we observed a post activity hyperpolarisation as a consequence of these processes. However, what should be expected in the network as a whole? It is very difficult to translate such specifically defined entities like Ca(T) de-inactivation to the abstract properties of the network model. Simplifications, as we have experienced and emphasised in the previous chapters, wash many important details from the model. However, well constructed simplifications should capture core phenomena allowing us to explore salient effects. If we consider the joint consequence of Ca(T) over-inactivation and K(Ca) activation we have a hyperpolarisation that will not greatly change the resistance properties of the membrane. In the dynamic network model we may interpret this as an increase in the sigmoid threshold ( $y_0$ ); that is, the complete sigmoid function is shifted in the positive direction (see Figure 8.1).

We have observed in Chapter 5 (Figures 5.7 and 5.8) effects of increased threshold on the system, and in particular on the hysteresis state. Two primary features are observed. Firstly, the attractor around the hysteresis state becomes significantly smaller. Thus, as

expected, transitions to this state require greater excitatory drive due to the hyperpolarising effects of over-inactivation of Ca(T) and activation of K(Ca). Secondly, there is a significant reduction in the resting firing rate during this period. Experimentally, a post-response reduction in resting firing rate is observed in the STh (Fujimoto & Kita, 1993). Experimental observations reveal a time course for this post-response quiescence of around 200msec. This concurs with the time course of Ca(T) de-inactivation and K(Ca) deactivation predicted in the multi-compartmental model.

### 8.1.3 Are the Intrinsic Properties Sufficient?

One of the important questions to consider is whether the intrinsic properties outlined in Chapters 6 and 7 are sufficient to effectively terminate the state of hysteresis. Simulations demonstrate that small transmission delays in the lateral connectivity of the network increase the input required to drive the system to hysteresis. However, lateral delays also add to the “stubbornness” of hysteresis (see Section 5.4). This is because hyperpolarisation distributed across a neural population will have to be sufficiently sustained to affect the entire network. In the same manner that delay-induced desynchronisation of excitatory input reduces its accumulative effect, so does delay-induced desynchronisation of hyperpolarisation. Therefore for intrinsic hyperpolarisation to terminate hysteresis it would be required to last a sufficient duration. The intrinsic properties of Ca(T) and K(Ca) channels operate on timescales of the size required.

The reasonably high sigmoid threshold ( $y_0$ ) reduces the attractor size around the hysteresis state. Generally we expect the attractor around this state to be small, requiring only small changes in the firing rate to force a return to the low state. Moreover, as we have discussed, intrinsic properties, such as those of Ca(T) and K(Ca) channels, may concurrently reduce the firing rate and increase  $y_0$ . The dual effect of this will be to modify the attractor space reducing the pull of hysteresis while at the same time pushing the system away from the hysteresis state. Consequently, we propose that the intrinsic mechanisms involving the Ca(T) and K(Ca) channels play a significant role in the termination of the STh pulse.

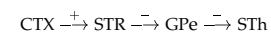
We have not yet mentioned the external segment of the globus pallidus in terms of the pulse theory of the STh. The GPe has a prominent role in STh processing through its recurrent connection (see Section 2.4). To investigate this interaction, a detailed analysis of the GPe would be required. However, we can speculate about the possible effects of this recurrent circuit on STh processing. Firstly it should provide inhibitory feedback to the STh. If portions of the STh generate a pulse of activity, we would expect areas of the GPe to reflect a similar increase in activity. In turn this should reflect an inhibitory pulse back towards the STh and inhibit widespread areas (for the same arguments of divergence resulting from large dendritic fields and those given in Section 5.5.1). This feedback mechanism may play an important role in pulse termination. However, we expect a more complex response than simple termination of activity in the STh. Hyperpolarisation of STh neurons is predicted to release the inactivation of a large proportion of Ca(T) channels (see Section 7.1). This is likely to generate a secondary response of STh neurons resulting from the Ca<sup>2+</sup> influx (consider the artificially hyperpolarised model illustrated in Figure 7.1). Such a secondary response is observed in experiments involving cortical stimulation of the STh (Fujimoto & Kita, 1993).

After the secondary response there will be significantly stronger K(Ca) activation and Ca(T) over-inactivation. This will increase the strength of the post-response mechanisms, but not their time course. The multi-compartmental model predicts that the secondary response should have a significantly reduced firing rate since the primary response would have already partially activated K(Ca) and inactivated a proportion of Ca(T) channels. We will discuss further interactions between the GPe and STh in Section 8.2.2.

#### 8.1.4 When Will Pulses Occur?

We have so far discussed the pulse generation process itself. Under normal conditions, when should we expect the pulse sequences to be generated? This will depend on the thresholding properties of the neurons and the strength of the cortical, thalamic, and pallidal input. The generation of pulses is not solely under cortical or thalamic control. In

the resting state the GPe, like the GPi, is spontaneously active (Ryan & Sanders, 1993; Chevalier & Deniau, 1990). This will produce a tonic inhibition over the STh. From the dynamic network model this will make the transition from the low state to hysteresis much more difficult. Consider the striatal control over the GPe:



Activation of zones in the striatum may inhibit the tonically active GPe and consequently disinhibit the STh. Therefore, the generation of pulses may only be able to occur with the coordinated striatal inhibition of the GPe and the cortical/thalamic excitation of consequently disinhibited regions of the STh. The generation of pulses may be under combined cortical and striatal control.

#### 8.1.5 Summary: Artifacts of Modelling

Although the previous sections describe how many of the features of STh physiology emerge from the joint consideration of the models, we must emphasise that these models can only be expected to reproduce salient features. During the development of the models we highlighted many limitations imposed by simplifications and parameter constraints. For example, the clustering and spread of collaterals could play a major role of restricting pulses to various isolated zones within the STh. As the collateral distribution is unknown the simplifications introduced will overlook (necessarily) such effects. Therefore we may only treat the models' conclusions as a prediction of coarse STh processing. However, it is very clear that a pulse of activity with a sharp rise (and possible sharp decline resulting from GPe feedback) is expected uniformly across large regions of the STh. This pulse is likely to be initiated by cortical and thalamic activity through the internal capsule and cerebral peduncle combined with striatal inhibition through the GPe. Consequently, the generation of pulses is likely to concur with activity in the corticospinal pathways. Indeed, in primates large proportions of cells associated with, for example, "arm" representations are observed to significantly increase activity immediately after arm movement onset (Wichmann et al., 1994). We need to begin to address the consequences of this type of STh processing in relation to the circuits and pathways of the basal ganglia as a whole. This will be considered in the following sections.



## 8.2 The Role of the STh in the Basal Ganglia

What role could a sharp uniform and widespread pulse play in basal ganglia function? Pulses that are likely to be generated concurrently with, or immediately after initiated movements. We use the framework of the current models of the basal ganglia, reviewed in Chapter 3 to explore these issues.

### 8.2.1 The Pathways: Braking Theory

As we have reviewed, the STh sits in a prime position to influence the basal ganglia output structures (GPi, SNr). Apart from the STh, these structures receive primarily inhibitory afferents (for example, from the GPe, or STR). Therefore, as mentioned in Chapter 3, as a result of the high resting frequency of STh neurons, STh activity may play a role in sustaining the tonic activity in SNr and GPi (Robledo & Féger, 1990). Consider now a corticospinal collateral initiated pulse. This will be in the form of a uniform fast rise in activity, to near 500Hz, followed by a dramatic fall (from GPe feedback). This pulse will be spread over a large region of the STh and is very likely to uniformly and massively excite large areas of the GPi and SNr. It is interesting that these two basal ganglia output structures will be excited by the pulse at about the same time. The STh → GPi pathway is physically longer than the STh → SNr route. However, it is found that the former pathway has a greater signal conduction velocity possibly compensating for the larger distance (Kita & Kitai, 1987). Therefore, from the pathways;

$$\begin{aligned} \text{CTX} &\xrightarrow{+} \text{STh} \xrightarrow{+} \text{GPi} \xrightarrow{-} \text{THAL} \\ \text{CTX} &\xrightarrow{+} \text{STh} \xrightarrow{+} \text{SNr} \xrightarrow{-} \text{THAL/SC} \end{aligned}$$

we expect a wave of widespread inhibition in the differing basal ganglia target structures, possibly at a common time.

Both GPi and SNr also receive inhibitory input from the striatum. How is this expected to interact with the effects of the excitatory pulse? It has been proposed that STh terminals

primarily terminate in the form of large boutons on the proximal dendrites and somas of GPi neurons, whereas striatal efferents are found to closely ensheath distal dendrites (Hazrati & Parent, 1992). This arrangement is very unusual, as it is more common to have inhibitory input on more proximal areas. However, conflicting results have identified these large boutons to be GABAergic and to originate from the GPe (Bolam et al., 1993). It is generally accepted that the striatal terminals ensheath the distal dendrites, but it is likely that the STh and GPe terminals share a more complex arrangement.

Although the distribution of STh terminals on neurons of the basal ganglia output structures is unclear, it is likely that during a pulse the STh can to some degree override other inputs. This has circumstantial support from the high firing rates achieved at the peak of the pulse. If the resting firing rate of STh neurons is sufficient to provide drive for the normal tonic activity in the target structures, a 10 fold increase is likely to have an overriding effect. However, when we consider the large GPe afferents the possible interactions become more complex. As the GPe is also likely to receive a pulse of excitatory activity from the STh the GPi and SNr may further receive a wave of inhibition in addition to the excitatory STh pulse. This will be discussed further in the proceeding section.

Considering the massive, and reasonably widespread pulse that may override other inputs to the basal ganglia output structures, a “braking” hypothesis may be introduced. By “braking”<sup>1</sup> we mean upon final invocation of a particular movement or movement sequence, the STh intercepts certain corticospinal signals that may generate an overriding pulse. The pulse may then terminate current processing in large areas of the GPi and SNr (via an overriding *excitatory* influence) and further lead to a uniform wave of inhibition in appropriate thalamic/SC areas. A braking role for the STh has been independently suggested from the observations of STh lesions (Wichmann et al., 1994). The idea of a widespread uniform pulse of activity provides further evidence for this theory. Since we do not understand what exact role the basal ganglia play in movement (or cognitive processes) the consequence of this inhibitory pulse on the target structures is unclear. For example, it may act like a reset mechanism in order to prepare for the next

<sup>1</sup>This term has a clearer interpretation in the context of disorders of the basal ganglia. See Section 8.3.

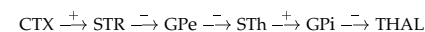
movement sequence (motor execution). Alternatively, it may be a signal to direct planning of possible future sequences, as the current ones have finally been initiated (motor planning). However, in all cases, the pulse has a form that implies the role of some form of “braking” — it generates widespread powerful inhibition in regions of basal ganglia output targets through the GPI and SNr.

### 8.2.2 The Pathways: Post Brake Window

As both the physiology and models presented demonstrate, the response of the STh is more complex than a single pulse. Generally pulses are interrupted by periods of inhibition resulting from GPe feedback. Furthermore, there is an intrinsic quiet period generated after the pulses. During this phase STh neuron firing rates are below their resting level. It is very difficult to deduce what consequences these observations have for basal ganglia processing. We consider the concepts of multiple pulses and STh quiescence separately.

Since the second pulse is predicted from the multi-compartmental model to have the Ca(T) activation as its primary driving force, further pulses are unlikely. If the GPe hyperpolarises the STh and releases Ca(T) channels which then aid in the generation of the secondary pulse, since Ca(T) de-inactivation is very slow, tertiary pulses are unlikely to occur. The Ca(T) resource will not be available to aid in their generation. Indeed, few, if any, three pulse sequences are observed in the STh after stimulation of the rat cortex (Fujimoto & Kita, 1993). Therefore, a generic two pulse sequence may be a characteristic phenomenon. In the interval between pulses large numbers of neurons are necessarily hyperpolarised (for Ca(T) activation), resulting in near zero firing rates. The effect of this on STh targets is to remove all excitatory drive from the SNr and GPI and induce a significant drop in their activity. This is likely to generate a disinhibitory pulse in regions of the basal ganglia output targets. Therefore, in addition to the braking effect, the pulse sequence is likely to generate a brief window of disinhibition.

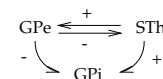
The GPe plays a primary role in this processing through the recurrent loop with the STh. However, there is a further pathway that is likely to influence this:



The GPe is under inhibitory control from the striatum. It is possible that there is a degree of interaction between striatal and subthalamic afferents in the GPe during a pulse sequence. Simulations are planned to explore this interaction<sup>2</sup> and it is possible that inhibitory striatal influences over the GPe may influence the *length* of the interpulse interval. If this is the case, it may be that in addition to some form of braking role the disinhibitory period between pulses may also play a crucial role in producing some time window for thalamic activity.

Following the second pulse we expect a period where the STh is particularly quiet. Any excitatory drive to GPI and SNr is therefore reduced. Consequently, it is expected that there will be widespread reduced inhibition over basal ganglia target structures. It is unlikely that the STh is the sole source of tonic activity in the GPI and SNr (Ryan & Sanders, 1993). In these circumstances the direct basal ganglia pathways should continue to affect the GPI and SNr yet with less contrast.

The possibility of STh generated pulses has forced us to examine some of the primary basal ganglia connectivity that is often overlooked in models due to their complexity. In particular, the recurrent GPe–STh loop, and the striatal influence of the GPe. Furthermore, it has been found that there is a direct pathway from the GPe → GPI (see Section 2.4). It is clear that the GPe, like the STh, sits in a prime position for mediating internal processing of the basal ganglia. In fact, the recurrent connection with the STh may indicate an intimate processing relationship between these two structures. Consider the complex arrangement;



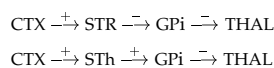
Since we can predict that the STh pulse should induce a recurrent pulse in the GPe, does this imply the GPI receives an excitatory–inhibitory pulse sequence, or will the interactions be more complex?

<sup>2</sup>A detailed model of neurons of the GPe will be required in a similar manner to the models presented of the STh.

Little is known about the processing in these complex pathways, and much experimental and theoretical work is required. A structure of particular interest is the GPe. In a similar manner to the STh, it lies in a position where it may significantly influence or modulate basal ganglia processing. The theory of STh pulse generation described here emphasises the importance of understanding this internal circuitry. Uniform and massive excitatory pulses may override other activity in large regions of GPe, GPi, and SNr. Alternative pathways, for example  $GPe \rightarrow GPi$ , will also have a significant effect considering the shape and form of the pulse. Furthermore, as outlined in the previous discussion, timing of events and temporal interaction of signals will play a defining role in the operation of the circuitry.

### 8.2.3 The Pathways: Contemporary Theories

How does the STh pulse theory integrate with the “focusing” or “scaling” theories discussed in Sections 3.1.4? The pulse theory does not belong to either of these camps; rather it may be interpreted by both as a useful phenomenon. Consider the focusing theory. If there is a widespread pulse of excitatory activity, we expect a wide area of GPi and SNr to be activated. If striatal inhibition could interrupt the overriding effect of the pulse (we have no models that can currently confirm or deny this) then we have a system that may simplify the focusing hypothesis. The pathways:



could effectively generate widespread uniform active zones in the GPi, apart from small inhibited regions under striatal control. Consequently regions of the thalamus may be widely inhibited yet contain tightly focused patches of disinhibition. However, the disinhibitory pathway



that is considered to partake in the generation of the focused thalamic disinhibition (see Section 3.1.4) is unlikely to do so given the STh pulse theory. The existence of widespread STh pulses does not concur with the sharply localised responses required in the focusing theory. This processing route therefore places limitations on the role of a pulse generating STh in the focusing theory.

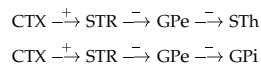
The pulse theory may also be applied to the scaling model. Consider the temporal windowing effect of the interpulse interval. The STh, under striatal control through the GPe, may provide a means of explicitly generating a window of thalamic disinhibition. With further consideration of the  $GPe \rightarrow GPi$  pathway, excitatory/inhibitory pulse sequences may be projected to the GPi. This would translate to inhibitory/disinhibitory sequences in the thalamus, leading to a distinct temporal separation of positive and negative scaling. The temporal interplay may ultimately be under striatal influence through the GPe.

The nature of the pulse generated in the STh, the possibility of controlling interpulse interval, and the effect of responses at target structures at a common time all indicate it has a role in temporal processing. Thus, some form of scaling model may provide a more adequate description of processing in this part of the basal ganglia. However, it has become clear, that further exploration of the complex recurrent and horizontal pathways in the basal ganglia is needed. These will certainly play a crucial role in temporal processing.

## 8.3 Disorders of the Basal Ganglia

### 8.3.1 The Braking Hypothesis

The theory of pulse generation and, in particular, its support of the Braking Theory fits well with the current interpretation of primary basal ganglia disorders. Consider the contemporary interpretation of the consequences of the loss of dopamine to the striatum as observed in Parkinson’s disease (see Section 3.3). Striatal efferents associated with the  $D_2$  dopamine receptor are considered to have increased activity. This should primarily affect the GPe and consequently the following pathways:



Firstly, increased inhibition of the GPe leads to disinhibition of the STh. From the dynamic network model, this will reduce the necessary cortical drive required to push the system to the hysteresis state. Thus, braking may occur more often, and outside direct striatal control. The striatum now tonically inhibits the GPe, reducing its specific influence over STh regions. Increased “braking” pulses, and inappropriately timed pulses may be involved in bradykinesia and the interrupted ability to initiate movements. A system with inappropriate braking will seriously disturb movement control.

Secondly, the direct GPe  $\rightarrow$  GPi connection under conditions of decreased GPe activity should lead to disinhibition of the GPi. Thus increases in tonic inhibition of basal ganglia targets would be expected. This may also be associated with Parkinsonism symptoms (see Section 3.3.2).

Recently, techniques that reduce the influence of the STh have been found to alleviate certain Parkinsonism symptoms (Benazzouz et al., 1993, 1995; Bergman et al., 1990). In particular, all these techniques reduce the STh tonic activity and the possibility of pulses. Benazzouz et al. (1993) use techniques of over-stimulation of the STh to produce long ( $> 100\text{sec}$ ) periods of silent activity. Such over-stimulation may push the entire STh into a hysteresis state, drain the Ca(T) resources, and significantly increase the internal calcium concentration in all affected cells. However, this in itself is not sufficient to explain the long durations of STh quiescence found. It is possible that the *network dynamics* lead to the generation of sustained quiet periods. If a region of neurons in the network are placed into a post-response parameter regime, in particular with altered  $y_0$  (see Section 8.1.2), then a short ( $\sim 200\text{msec}$ ) post-response quiet period is expected from the intrinsic properties. If this occurs in *all* neurons in the network, then following the return of  $y_0$  to normal resting conditions the system will not immediately result in the return of all neurons to the resting firing rate. This is because the primary determinant of the resting firing rate for each unit in the network is the term  $\sum w_{ij} \sigma_j(t)$  (see Section 4.2.1). The current resting level of all other units in the dynamic network determines the global

resting level. If all units have low activity resting states as a result of post activity hyperpolarisation (increased  $y_0$ ), after the intrinsic hyperpolarisation has terminated, the system may reside with a reduced firing rate for a longer duration. The more complete and dramatic the hyperpolarisation (for example, massive exhausting of the Ca(T) resources and  $\text{Ca}^{2+}$  build up) the longer the duration of network induced quiescence that is expected.

The models therefore propose a theoretical mechanism for the generation of these lengthy quiet periods. If there is another means apart from over stimulation or lesion, that can push the system into this laterally sustained quiet state then it could provide a means of reducing STh over-activity and over “braking” in Parkinsonism.

Under normal conditions, lesions of the STh lead to forms of ballism. This is characterised by massive uncontrolled flinging of the extremities (see Section 3.3). It can be reasoned that the absence of STh pulses used in “braking” may have dramatic effects reminiscent of ballism. As the pulses are hypothesised to cover large areas, have a uniform shape, and have an overpowering effect on STh target structures, their absence in normal (i.e. non-Parkinsonism) conditions is likely to lead to severe effects. The symptoms of ballism may reflect the loss of such a dominant braking system.

### 8.3.2 The Window Hypothesis

The more complex circuitry of the recurrent loop indicates that dual pulses may occur with a particular disinhibitory window affecting the basal ganglia targets (Section 8.2.2). What should we expect from this additional circuitry under conditions of Parkinsonism? Increased inhibition of the GPe is likely to deteriorate its ability to reflect a powerful inhibitory pulse back to the STh in response to pulse generation. Under these circumstances the interpulse hyperpolarisation is not expected to be so complete. We now have a system similar to that described in Section 5.5.1. Such a system could lead to sustained oscillation. However, considering the limited Ca(T) resource it is more likely damped oscillations will occur. The two pulse sequence is likely to be replaced by multiple damped

pulses. Increases in the numbers of oscillatory neurons in the STh is experimentally observed in MPTP lesioned primates (Bergman et al., 1994). Moreover, Bergman et al. (1994) suggest the frequencies of such oscillations coincide with the frequency of tremor observed in Parkinsonism. Until further analysis of the GPe is undertaken we can only predict the presence of oscillations as described in Chapter 5, and not their form. Observations such as these encourage us to investigate the GPe–STh interaction in the near future.

## 8.4 Summary

We have presented a synthesis of the different models described in the previous four chapters. Together this provides a unique view of the subthalamic nucleus operation. The theory of STh pulse generation provides a new perspective on the operation and malfunction of the basal ganglia. The network level model allows us to consider the cooperative operation of large numbers of neurons with simplistic properties, whereas the multi-compartmental model provides a theory of the operation of single neurons. Together they propose a mechanism which will intrinsically avoid states of hysteresis, yet use this “high” state in the generation of a uniform, widespread pulse. The consequences of STh pulses introduce a number of new concepts. Firstly, they provide a direct and powerful braking mechanism, supporting the braking theory of the STh. Secondly, the intrinsic generation of dual pulses (via GPe feedback and consequent activation of Ca(T) channels) introduces an interesting possibility of a window of disinhibition in the basal ganglia target structures. The duration of the window is possibly under direct striatal control. GPe feedback also introduces the possibility of oscillatory, or damped oscillatory behaviour under certain conditions. The current research has highlighted the need for further investigation of the GPe, as it appears to be intimately involved in STh operation. Together these structures are likely to greatly influence basal ganglia function. Many of the results outlined in this chapter indicate that these two structures are involved in operations of a temporal nature.

## Chapter 9

### Conclusion

We have presented a theoretical account of the type of processing expected of the subthalamic nucleus. This account is based on the observed anatomy and the predicted mechanisms underlying single neuron physiology. Geometric simplifications of the anatomical arrangement within the nucleus provides evidence that neurons within the STh are potentially massively interconnected. Considering the primary transmitter is found to be glutamate, we predict that the STh should act as a lateral excitatory network.

The analysis of a dynamic excitatory network model reveals a number of behaviour types that may emerge. A bifurcation analysis isolates the point of transition between the two primary types of behaviour (prebifurcation and postbifurcation). From a consideration of the connectivity, unit threshold, and voltage/firing-rate function, we predict that the STh should exhibit postbifurcation behaviour. This behaviour consists of two stable asymptotic equilibrium points: a low resting state and the state of hysteresis.

The state of hysteresis is primarily information-destructive for excitatory input, since every unit in the network resides at near its maximum firing rate. The primary determinant for the existence of the hysteresis state is the large interconnectivity predicted from the geometric model. A detailed single STh neuron model is developed to consider how this information-destructive state may be controlled.

Generally, the more detailed a model is, the greater the freedom in the choice of parameter values. To constrain the parameters in the single neuron model we introduce a strict parameter constraint procedure. This restricts the arbitrary choice of parameters and increases our confidence in the model. The low threshold calcium Ca(T) channel is found to play a primary role in generating the observed behaviours of the STh projection neurons. The dominance of the T-current in combination with the high resting potential of STh neurons explains much of the observed physiology. In particular, the slow action potential has the T-current as its driving force. Furthermore, initial spike clustering and the post-response quiescence are also strongly influenced by the Ca(T) channels. An interesting supplementary finding is that the Na<sup>+</sup> channel inactivation was required to be significantly faster than classical descriptions in order to generate the fast firing rates characteristic of the STh projection neurons.

The consideration of the intrinsic properties in the context of the dynamic network model reveals a novel mechanism for controlling hysteresis. The calcium T-current in combination with a calcium activated potassium current can ultimately prevent sustained hysteresis. Moreover, as they are intrinsic mechanisms, they overcome the stubbornness of hysteresis. Inhibitory feedback from the external segment of the globus pallidus is likely also to play a role in quickly terminating the hysteresis state. This leads to the theory of pulse generation. The large dendritic fields and profuse lateral connectivity provide a mechanism that, under sufficient excitatory input, will push the system to hysteresis. The hysteresis state is then quickly terminated resulting from the GPe feedback and intrinsic properties. Thus, a brief pulse of high activity spread over large areas of the STh is expected in response to sufficient excitatory stimulation. This type of activity is experimentally observed in rat STh after cortical stimulation (Fujimoto & Kita, 1993). It also, provides further evidence for the "braking theory" of the STh. A quick and powerful pulse of STh activity is likely to widely and quickly excite basal ganglia output structures producing a wave of inhibition over basal ganglia targets.

In addition to the support for the braking hypothesis, the intrinsic properties indicate that a more complex response should be expected. GPe inhibitory feedback is likely to provide a means for releasing Ca(T) channels which then will generate a secondary

pulse. A two pulse sequence is likely to provide not only a powerful inhibition on basal ganglia targets, but also a window of disinhibition as a result of interpulse hyperpolarisation of the STh. The temporal length of this window may be under direct striatal control. This supports the physiological experiments indicating that the STh may have a strong temporal processing role. The timing of the pulse generation, which may also be under striatal control (through disinhibition), and the generation of the disinhibitory window will play a significant role in global basal ganglia processing.

The "braking hypothesis" is supported primarily by observations from disorders of the STh. The condition of ballism indicates that there has been a loss of a mechanism of control or movement suppression. However, inferring functional roles for structures from observations of lesion generated behaviours is notoriously difficult. The current research provides a theoretical account of mechanisms that have the potential of generating a dominant controlling influence. The presented theory also concurs with current interpretations of Parkinson's disease. GPe over inhibition by the striatum leads to reduced inhibitory feedback to the STh. This means that pulses are under reduced striatal control, are likely to have increased duration, and are likely to occur more often and at inappropriate times. Furthermore, increased damped oscillatory behaviour of neurons may be expected with reduced GPe feedback.

We have characterised possible processing properties of the subthalamic nucleus. Additionally, this research has illuminated the intimate relationship between the STh and GPe. Like the STh, the GPe is an internal basal ganglia structure of which little is known. The models and analysis presented here highlight the need for further cooperative analysis of the GPe and its role in basal ganglia processing. This is an area where much future work could profitably be focused.

# Glossary

Many sources have been used to aid in the compilation of this glossary. However, all the terms have been rephrased or orientated to the contexts and meanings used throughout the thesis. Major sources are; Hille (1992), Hirsch and Smale (1974), Becker (1989) and Lipschutz (1968). Other useful references are given under specific entries.

**acetylcholine** A neurotransmitter commonly found in the central nervous system, neuromuscular junctions, and visceral nervous system.

**afferent** A physical input process to a neuron. Generally axons from other neurons/structures. Compare with **efferent**.

**after-hyperpolarisation** A slow hyperpolarising potential that occurs in some neurons after a train of action potentials.

**agonist** A molecule that *activates* a receptor or channel.

**akinesia** Literally means the absence of movement, however, more commonly the term is used to refer to a difficulty in the *initiation* of movement (see Lohr and Wisniewski, 1987).

**AMPA**  $\alpha$ -amino-3-hydroxy-5-methyl-4-isoxazole propionic acid. The selective agonist used to identify (and name) a specific excitatory channel that may more usually respond to glutamate.

**ansa lenticularis** Pallidothalamic fibres that “loop” (ansa) around the internal capsule and innervate the thalamus. A major output pathway of the basal ganglia.

**antagonist** A molecule that *prevents* the activation of a receptor or channel.

**anterograde** In the direction from the soma to the axon terminal.

**antidromic** Direction towards the cell body. In particular, **antidromic conduction** is an action potential moving in this direction.

**asymptotic behaviours** A behaviour of a dynamic system that will continue with the same form for all time (unless externally acted upon). There are a number of forms of asymptotic behaviour. For example, an equilibrium point, or **limit cycle** etc.. For a formal definition see Guckenheimer and Holmes (1983).

**athetosis** A characterisation of a movement disorder involving involuntary irregular movements, usually in the extremities. It is generally slower and more rhythmic than **chorea** (see Lohr and Wisniewski, 1987).

**attractor** A dynamic system of  $N$  variables can be represented as a point in  $N$ -dimensional space. If  $p$  is a point in this space visited infinitely often by the system (i.e. part of an asymptotic behaviour), then an **attracting set** is the set of all points arbitrarily close to  $p$  that once the system is in this set it remains in this set for all time. For a formal definition see Guckenheimer and Holmes (1983).

**autonomous system** A system of time differential equations

$$\dot{y} = F(y, \mu)$$

where the function  $F$  is *not* an explicit function of time.

**axoaxonic synapse** A synapse between two axons.

**axodendritic synapse** A synapse between an axon and a dendrite.

**ballism** A hyperkinetic movement disorder often involving wild flinging movements of the limbs. Generally more severe and stereotypical than **chorea**. It is one of the few movement disorders that is consistently associated with a particular region of the brain (the subthalamic nucleus) (see Lohr and Wisniewski, 1987).

**bicuculline** A molecule that blocks GABA<sub>A</sub> receptors.

**bradykinesia** Refers to the slowness of movement, in particular for repetitive tasks, their initial form appears normal but after repetitions the rate of movement progressively decreases. A characteristic shown to be independent of rigidity (see Lohr and Wisniewski, 1987).

**caudal** “Towards the tail”. In the direction of down the **neuraxis**.

**characteristic equation** If  $M$  is an  $N$ -square matrix and  $\lambda$  is an indeterminate variable then the matrix given by

$$\lambda I - M$$

is called the characteristic matrix of  $M$  ( $I$  is the identity matrix). The **determinant** of the characteristic matrix is called the characteristic polynomial of  $M$ . When this is set to zero it yields the **characteristic equation**.

**chorea** From the Greek for “dance” — a movement disorder characterised by involuntary rapid contortions of groups of muscles usually in the face and extremities (see Lohr and Wisniewski, 1987).

**CNS** Central Nervous System.

**convolution** A function ( $c(t)$ ) derived from two given functions (say,  $f(t)$  and  $g(t)$ ) by integration:

$$c(t) = \int_0^t f(v)g(t-v)dv$$

If the given functions can be represented in the frequency domain, then the function for the convolution in the frequency domain is simply the product of the given functions.

**coronal** A view of a planar section of the CNS as if cut perpendicular to the long axis of the **neuraxis**. Note that as the **neuraxis** bends, a coronal section of the forebrain in human is at 90° from a coronal section of the spinal cord. Sometimes referred to as the transverse plane.

**corticospinal tract** (pyramidal tract) A major pathway from the cortex to motor neurons and sensory neurons of the spinal cord. It forms a large part of the internal capsule.

**cyte** a cell, more common is **cytology** which is the part of biology that studies cells.

**delta function** (Dirac delta function) The function denoted by  $\delta(x)$  and defined to be zero for all non-zero  $x$  and infinite for  $x = 0$ .

**dendrodendritic synapse** A synapse between two dendrites.

**depolarization** A change in the membrane potential, usually becoming more positive (towards zero).

**determinant** For every square matrix  $M$ , there is a specific scalar assigned to it called the determinant of  $M$ . It is often denoted by  $|M|$ . In two dimensions the determinant of an arbitrary square matrix

$$M = \begin{bmatrix} a & b \\ c & d \end{bmatrix}$$

is given by  $|M| = ad - bc$ .

**diagonal matrix** A **diagonal matrix** is a square matrix (a matrix that has the same number of rows as columns) whose non-diagonal entries are all zero. For example

$$\begin{bmatrix} a_{1,1} & 0 & 0 & \cdots & 0 \\ 0 & a_{2,2} & 0 & \cdots & 0 \\ 0 & 0 & a_{3,3} & \cdots & 0 \\ \vdots & & & \ddots & \vdots \\ 0 & 0 & 0 & \cdots & a_{n,n} \end{bmatrix}$$

**disinhibition** A phenomena involving a spatial sequence of inhibition that ultimately leads to the reduction in final inhibition. For example,



If unit **A** is active, this inhibits unit **B**, preventing it from inhibiting unit **C**. Unit **C** is therefore **disinhibited**.

**dopamine** A neurotransmitter of the catecholamine family. Dopamine is produced in very few CNS neurons, generally clustered in nuclei of the brainstem. It is distributed to much of the brain through diffuse ascending fibre systems.

**dorsal** In the direction of “up” yet always with respect to the **neuraxis**. For example in a vertically standing human, a dorsal direction in the forebrain is towards the top of the head, whereas in the spinal cord it would be in the direction of the back of the human. From root *dorsum*, “back”.

**dyskinesia** Generally, any abnormality in movement. There are many forms, for example incoordination, or spasms.

**efferent** A physical output process from a neuron. Generally an axon conducting impulses. Compare with **afferent**.

**eigenvalue** If  $M$  is a linear operator over some  $N$  dimensional **vector space**  $V$  (for example, represented by some  $N$  dimensional matrix) then a scalar  $\lambda \in \mathcal{R}$  is called an eigenvalue of  $M$  if there exists a nonzero **vector**  $v \in V$  for which

$$M(v) = \lambda v$$

**eigenvector** If we have an **eigenvalue**,  $\lambda$ , of some linear operator  $M$  satisfying the equation

$$M(v) = \lambda v$$

then the **vector**  $v$  is referred to as an **eigenvector** of  $M$  belonging to **eigenvalue**  $\lambda$ .

**enkephalin** A neuropeptide of the opioid family. Neuropeptides are often released in conjunction with low molecular weight transmitters (for example, GABA).

**eukaryotic cell** A cell with a well defined nucleus. Generally part of a multicellular organism (compare with **prokaryotic** cell).

**excitatory postsynaptic potential** (EPSP) The potential change in a neuron (or muscle cell) produced by an excitatory neurotransmitter acting on the cell. Generally, the potential change is in the depolarizing direction.

**extrapyramidal motor system** A motor system largely independent of the direct **corticospinal tract**. The system involves the following; the cortex projects to the striatum which projects to the pallidum. The pallidum projects to the thalamus (VA, VL). These areas of thalamus project to the motor cortex. The substantia nigra and subthalamic nucleus are also part of the extrapyramidal motor system.

**GABA** ( $\gamma$ -aminobutyric acid) An inhibitory neurotransmitter.

**GABA<sub>A</sub> receptor** A neural receptor to the inhibitory neurotransmitter GABA which causes a rapid increase in chlorine conductance, usually resulting in hyperpolarization.

**GABA<sub>B</sub> receptor** A neural receptor to the inhibitory neurotransmitter GABA which blocks calcium channels, or activates potassium channels. Both actions lead to reduced membrane excitability. GABA<sub>B</sub> receptors exert their inhibitory effects via second messenger systems.

**Gaussian function** A function that exponentially and symmetrically decays from a centre peak in both positive and negative directions.



**glia** From the Greek for “glue”. Non-neuronal cells of the central nervous system. For example schwann cells (see myelin). Also referred to as neuroglia.

**glutamate** An excitatory neurotransmitter.

**histology** The anatomical study of cells. Generally cells are stained and studied with the light microscope.

**Hopf bifurcation** A bifurcation, or change in asymptotic behaviour, of a dynamic system from a stable equilibrium point to oscillatory behaviour. See Guckenheimer and Holmes (1983) for a formal definition.

**horizontal** A view of a planar section of the CNS as if cut parallel to the long axis of the **neuraxis** and perpendicular to the **dorsal-ventral** plane.

**horseradish peroxidase** An enzyme that is useful for determining connectivity between brain areas. It can be transported from axon terminals to the cell body (**retrograde transport**).

**hydrophobic** Repels water. A hydrophobic molecule generally has a non-polar structure.

**hyperkinetic disorders** Movement disorders characterised by an excess of abnormal movements. **Ballism** is an example of such a disorder.

**hyperpolarization** A change in the membrane potential, usually becoming more negative. This generally reduces cell excitability.

**hypokinetic disorders** Movement disorders characterised by a slowness of movement and often increased muscle tone. Parkinsonism is a prototypical hypokinetic disorder.

**hysteresis** A diversely used word. Originally from the Greek, *hysteros* meaning “coming later”. Generally, a phenomena exhibited by a system whose state depends on its previous history. Most commonly used in reference to the magnetisation of a ferromagnetic material such as iron. The magnetic induction of the material lags behind the inducing field. In the neural network literature, it is generally used to refer to a system of units who mutually sustain each others activity. The origin of this may arise from the analogy to the magnetic system. As a magnetic field increases, the magnetic induction of the substance also increases. However, if the magnetic field is subsequently reduced to zero the substance has a sustained residue induction. A reverse magnetic field is then needed to bring the magnetic induction back to zero. There is a clear analogy with the hysteresis state of the dynamic network described in Chapter 5.

**inhibitory postsynaptic potential (IPSP)** The potential change in a neuron (or muscle cell) produced by an inhibitory neurotransmitter acting on the cell. Usually the potential change is in the hyperpolarizing direction.

**lenticular fasciculus** Pallidothalamic fibres that “cross” the internal capsule and innervate the thalamus. A major output pathway of the basal ganglia.

**ligand** Communication between cells is often via extracellular chemical messengers called **ligands**. When the chemical messenger originates from the endocrine system it is called a hormone. When it originates from a nerve terminal it is referred to as a neurotransmitter (see Hille 1992).

**limit cycle** A dynamic system of  $N$  variables can be represented by a single point in  $N$ -dimensional space. If the asymptotic behaviour of the system follows a 1-dimensional closed loop of such points then this asymptotic behaviour is referred to as a **limit cycle**.

**linear** A function, transformation, or mapping,  $f$ , from some **vector space**  $V$  to vector space  $U$ , is **linear** if it satisfies the following criteria

- for any  $v, w \in V$ ,  $f(v + w) = f(v) + f(w)$
- for any  $k \in \mathcal{R}$ , and any  $v \in V$ ,  $f(kv) = kf(v)$

For example, note that the **sigmoid** function is **nonlinear**. For a stricter definition see a standard linear algebra text (e.g. Lipschutz, 1968).

**lipid** A diverse group of compounds defined by their solubility in nonpolar (and not polar) organic solvents (for example chloroform).

**MPTP 1-methyl-4-phenyl-1,2,3,6-tetrahydropyridine**. A neurotoxin that is considered to induce similar conditions to Parkinsonism in some animals.

**myelin** A sheath encompassing the axons of some neurons. It is made from layers of cell membranes of particular **glia** cells (for example, schwann cells). Myelinated axons have increased signal conduction rates.

**neuraxis** An axis through the CNS used as a positional reference (e.g. see **rostral**, **caudal** etc.). The axis runs from the forebrain (its beginning) to the the lower end of the spinal cord (its end).

**neuropil** From Greek, *neuro* + *pilos* meaning “wool” or “hair”. The dense mesh of neural fibres and glia that constitute the substance of the central nervous system.

**nonlinear** A function, transformation, or mapping that does not satisfy the criteria for **linearity**.

**oblate spheroid** The object obtained by rotating an ellipse about its smaller axis. This may be visualised as a “disk” shaped object.

**orthodromic** Direction towards the axon terminals. In particular, **orthodromic conduction** is a potential change moving in this direction.

**perikaryon** The part of nerve cell that contains the nucleus (*pl perikarya*).

**prokaryotic cell** A unicellular organism. It particularly lacks a nuclear membrane. For example, bacteria are **prokaryotes** (compare with **eukaryotic** cell).

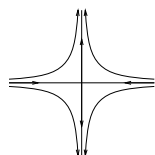
**prolate spheroid** The object obtained by rotating an ellipse about its larger axis. This may be visualised as a “cigar” shaped object.

**retrograde** In the direction from the axon terminal to the soma.

**rigidity** A movement disorder that generally involves increased muscle tone (e.g. muscles are more contracted than normal when at rest). There are many subclassifications of rigidity and the distinctions between them can be subtle (see Lohr and Wisniewski, 1987).

**rostral** "Towards the beak". In the direction of up the **neuraxis**.

**saddle** An unstable equilibrium point of a dynamic system whose phase plane in two dimensions  $(y_1, y_2)$  has the form



**sagittal** A view of a planar section of the CNS as if cut parallel to the long axis of the **neuraxis** and parallel to the **dorsal-ventral**.

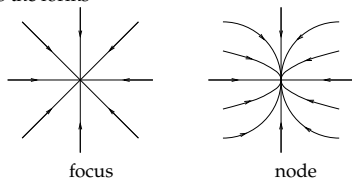
**scalar** The elements of  $\mathcal{R}$ , i.e. real numbers.

**second messenger** If an extracellular chemical messenger (e.g. neurotransmitter) does not have a direct effect on the cell, but rather is converted into some intracellular messenger, then this messenger is called a **second messenger**.

**serotonin (5-HT) 5-hydroxytryptamine**. A neurotransmitter of the indoleamine family.

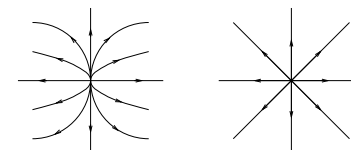
**sigmoid** A function that has an S-shape from. See Figure 4.1.

**sink** A stable equilibrium point of a dynamic system whose phase plane in two dimensions  $(y_1, y_2)$  has the forms



**soma** Cell body.

**source** An unstable equilibrium point of a dynamic system whose phase plane in two dimensions  $(y_1, y_2)$  has the forms



**spheroid** A solid object obtained by rotating an ellipse about one of its axes. If the rotation is about the smaller axis, the object obtained is called an "oblate" spheroid, whereas, rotation around the larger axis is called a "prolate" spheroid (Smith, 1966).

**synapse** A junction for signal transmission between two cells (usually neurons). For a chemical synapse, the presynaptic terminal releases some transmitter in response to depolarisation. The transmitter binds to receptor molecules in the postsynaptic terminal membrane which leads to a postsynaptic response.

**synaptic delay** The time required for the synaptic process to take place.

**tetraethylammonium (TEA)** A toxin that selectively blocks certain voltage activated potassium channels.

**tetrodotoxin (TTX)** A toxin extracted from puffer fish that selectively blocks voltage activated sodium channels.

**toroid** See **torus**.

**torus** A ring shaped surface or solid. In a one dimension array (or line), its end naturally connects to its beginning. In effect it has no end or beginning. In two dimensions it is obtained by rotating a circle (or one dimensional torus) about a coplanar line that does not intersect it.

**tremor** Involuntary movement consisting of rhythmical oscillations of part of the body about a fixed point. There are many subclassifications of tremor, however, they are more a continuum than distinct classes (see Lohr and Wisniewski, 1987).

**vector** A set of numbers, often treated as a point in some dimensional space. For example, if we have 3 numbers in the vector, then this can be interpreted as a point in 3-dimensional space.

**vector space** If a single  $N$ -dimensional vector can be treated as a point in some  $N$ -dimensional space, then a set of vectors can themselves define a space. For a more rigorous definition see a linear algebra text (e.g. Lipschutz, 1968).

**ventral** In the direction of "down" yet always with respect to the **neuraxis**. For example in a vertically standing human, a ventral direction in the forebrain is towards the neck, whereas in the spinal cord it would be in the direction of the front of the human. From root *venter*, "belly".

## Bibliography

- Afsharpour, S. (1985a). Light microscopic analysis of Golgi-impregnated rat subthalamic neurons. *J. Comp. Neurol.*, 236, 1–13.
- Afsharpour, S. (1985b). Topographical projections of the cerebral cortex to the subthalamic nucleus. *J. Comp. Neurol.*, 236, 14–28.
- Albin, R., Young, A., & Penny, J. (1989). Functional anatomy of the basal ganglia. *Trends in Neurosci.*, 12, 366–375.
- Alexander, G., & Crutcher, M. (1991). Parallel processing in the basal ganglia: up to a point. Reply. *Trends in Neurosci.*, 14, 56–58.
- Alexander, G., Crutcher, M., & DeLong, M. (1990). Basal ganglia–thalamocortical circuits: Parallel substrates for motor, oculomotor, prefrontal, and limbic functions. In Uylings, H., Van Eden, C., De Bruin, J., Corner, M., & Freenstra, M. (Eds.), *Progress in Brain Res. Vol. 85*. Elsevier Science, Oxford.
- Alexander, G., & DeLong, M. (1985). Microstimulation of the primate neostriatum: I physiological properties of striatal microexcitable zones. *J. Neurophysiol.*, 53, 1401–1416.
- Becker, E. E. (1989). *Churchills Illustrated Medical Dictionary*. Churchill Livingstone Inc., New York.
- Benazzouz, A., Gross, C., Féger, J., Boraud, T., & Bioulac, B. (1993). Reversal of rigidity and improvement in motor performance by subthalamic high frequency stimulation in MPTP-treated monkeys. *European Journal of Neuroscience*, 5, 383–389.
- Benazzouz, A., Piallat, B., Pollak, P., & Benabid, A. (1995). Responses of substantia nigra pars reticulata and globus pallidus complex to high frequency stimulation of the subthalamic nucleus in rats: electrophysiological data. *Neuroscience Letters*, 189, 77–80.
- Bergman, H., Wichmann, T., & DeLong, M. (1990). Reversal of experimental Parkinsonism by lesions of the subthalamic nucleus. *Science*, 249, 1436–1438.
- Bergman, H., Wichmann, T., Karmon, B., & DeLong, M. (1994). The primate subthalamic nucleus. II. Neuronal Activity in the MPTP model of Parkinsonism. *J. Neurophysiology*, 72, 507–520.

## Bibliography

185

- Bolam, J., Smith, Y., Ingham, C., von Krosigk, M., & Smith, A. (1993). Convergence of synaptic terminals from the striatum and globus pallidus onto single neurones in the substantia nigra and the entopeduncular nucleus. In Arbuthnott, G., & P., E. (Eds.), *Progress in Brain Res. Vol. 99*. Elsevier Science, Oxford.
- Breakfield, X., & Bressman, S. (1987). Molecular genetics of movement disorders. In Marsden, D., & Fahn, S. (Eds.), *Movement Disorders 2*. Butterworth & Co., London.
- Brotchie, P., Iansek, R., & Horne, M. (1991a). The motor functions of the monkey globus pallidus: cognitive aspects of movement and phasic neural activity. *Brain*, 114, 1685–1702.
- Brotchie, P., Iansek, R., & Horne, M. (1991b). The motor functions of the monkey globus pallidus: neuronal discharge and parameters of movement. *Brain*, 114, 1667–1683.
- Brotchie, P., Iansek, R., & Horne, M. (1991c). A neural network model of neural activity in the monkey globus pallidus. *Neurosci. Letters*, 131, 33–36.
- Brown, A., Schwindt, P., & Crill, W. (1993). Voltage dependence and activation kinetics of pharmacologically defined components of the high-threshold calcium current in rat neocortical neurons. *J. Neurophysiology*, 70, 1530–1543.
- Bunney, B., & Aghajanian, G. (1976). The precise localization of nigral afferents in the rat as determined by a retrograde tracing technique. *Brain Res.*, 117, 423–435.
- Cajal, R. (1911). *Histologie du système nerveux de l'Homme et des vertébrés*. Reprinted 1972, Cosogo superior de investigacions científicas Madrid.
- Cambell, G., Eckardt, M., & Weight, F. (1985). Dopaminergic mechanisms in subthalamic nucleus of rat: Analysis using horseradish peroxidase and microntophoresis. *Brain Res.*, 333, 261–270.
- Carpenter, M. (1981). Anatomy of the corpus striatum and brainstem integrating systems. *Handbook of Physiology — The Nervous System*, 2, 947–995.
- Chesselet, M., & Graybiel, A. (1987). Striatal neurons expressing somatostatin-like immunoreactivity: evidence for a peptidergic interneuronal system in the cat. *Neuroscience*, 17, 547–571.
- Chevalier, G., & Deniau, J. (1990). Disinhibition as a basic process in the expression of striatal functions. *Trends in Neurosci.*, 13, 277–280.
- Cole, K. (1968). *Membranes, Ions and Impulses. A chapter of classical biophysics*. Cambridge University Press, London.
- Cole, K., & Curtis, H. (1939). Electrical impedance of the squid giant axon during activity. *J. Gen. Physiol.*, 22, 649–670.
- Collin, C. (1995). Determining Constraints for Neurobiological Modelling. Master's thesis, University of Edinburgh.

- Crunelli, V., Lightowler, S., & Pollard, E. (1989). A T-type  $\text{Ca}^{2+}$  current underlies low-threshold  $\text{Ca}^{2+}$  potentials in cells of the cat and rat lateral geniculate nucleus. *J. Physiol.*, *413*, 543–561.
- Crutcher, M., & Alexander, G. (1990). Movement-related neuronal activity coding direction or muscle pattern in three motor areas of the monkey. *J. Neurophysiol.*, *64*, 151–163.
- Delcour, A., Lipscombe, D., & Tsien, W. (1993). Multiple modes of N-type calcium channel activity distinguished by differences in gating kinetics. *J. Neuroscience*, *13*, 181–194.
- DeLong, M., & Georgopoulos, A. (1981). Motor functions of the basal ganglia. *Handbook of Physiology — The Nervous System*, *2*, 1017–1061.
- Desiraju, T., & Purpura, D. (1969). Synaptic convergence of cerebellar and lenticular projections to the thalamus. *Brain Res.*, *15*, 544–547.
- DiFiglia, M., Pasik, P., & Pasik, T. (1982). A Golgi and ultrastructural study of the monkey globus pallidus. *J. Comp. Neurol.*, *212*, 53–75.
- DiFiglia, M., Pasik, P., & Pasik, T. (1976). A Golgi study of neuronal types in the neostriatum of monkeys. *Brain Res.*, *114*, 245–256.
- Elman, J. (1990). Finding structure in time. *Cognitive Science*, *14*, 179–212.
- Féger, J., Robledo, P., & Renwart, N. (1991). The subthalamic nucleus: new data, new questions. In Bernardi, G., Carpenter, M., Chiara, G., Morelli, M., & Stanzione, P. (Eds.), *The Basal Ganglia III*. Plenum Press, New York.
- Flaherty, A., & Graybiel, A. (1991). Corticostriatal transformations in the primate somatosensory system. Projections from physiologically mapped body-part representations. *J. Neurophysiol.*, *66*, 1249–1263.
- Fox, A., Nowycky, M., & Tsien, R. (1987). Kinetic and pharmacological properties distinguishing three types of calcium currents in chick sensory neurons. *J. Physiol.*, *394*, 149–172.
- Fujimoto, K., & Kita, H. (1993). Response characteristics of subthalamic neurons to the stimulation of the sensorimotor cortex in rat. *Brain Res.*, *609*, 185–192.
- Gerfen, C. (1992). The neostriatal mosaic: multiple levels of compartmental organization. *Trends in Neurosci.*, *15*, 133–139.
- Gerfen, C., Engber, T., Mahan, L., Susel, Z., Chase, T., Monsma, F., & Sibley, B. (1990).  $\text{D}_1$  and  $\text{D}_2$  dopamine receptor-regulated gene expression of striatonigral and striatopallidal neurons. *Science*, *250*, 1429–1432.
- Gerfen, C., & Young, W. (1988). Distribution of striatonigral and striatopallidal peptidergic neurons in both patch and matrix compartments: an in situ hybridization histochemistry and fluorescent retrograde tracing study. *Brain Res.*, *460*, 161–167.

- Gillies, A. (1996). Electrical properties of subthalamic nucleus projection neurons. *The Proceedings of the Fourth Annual Computation and Neural Systems Conference*, *4*, in press.
- Graybiel, A., & Ragsdale, C. (1983). Biochemical anatomy of the striatum. In Emson, P. (Ed.), *Chemical Neuroanatomy*. Raven Press, New York.
- Groves, P. (1983). A theory of the functional organization of the neostriatum and the neostriatal control of voluntary movement. *Brain Res. Rev.*, *5*, 109–132.
- Guckenheimer, J., & Holmes, P. (1983). *Nonlinear Oscillations, Dynamical Systems, and Bifurcations of Vector Fields*. Springer-Verlag, New York.
- Hammond, C., Shibasaki, T., & Rouzair-Dubois, B. (1983). Branched output neurons of rat subthalamic nucleus: Electrophysiological study of the synaptic effects of identified cells in the two main target nuclei, the entopeduncular nucleus and substantia nigra. *Neuroscience*, *9*, 511–520.
- Hammond, C., & Yelnik, J. (1983). Intracellular labelling of rat subthalamic nucleus with horseradish peroxidase: computer analysis and characterization of axon arborization. *Neuroscience*, *8*, 781–790.
- Hazrati, L., & Parent, A. (1992). Convergence of subthalamic and striatal efferents at pallidal level in primates: an anterograde double-labeling study with biocytin and PHA-L. *Brain Res.*, *569*, 336–340.
- Hikosaka, O. (1991). Basal ganglia — possible role in motor conditioning and learning. *Current Opinion in Neurobiology*, *1*, 638–643.
- Hille, B. (1992). *Ionic Channels of Excitable Membranes*. Second Edition. Sinauer Associates, Massachusetts.
- Hirsch, M., & Smale, S. (1974). *Differential Equations, Dynamical Systems, and Linear Algebra*. Academic Press, New York.
- Hodgkin, A., & Huxley, A. (1939). Action potentials recorded from inside a nerve fibre. *Nature*, *144*, 710–711.
- Hodgkin, A., & Huxley, A. (1952a). Currents carried by sodium and potassium ions through the membrane of the giant axon of *Loligo*. *J. Physiol.*, *116*, 449–472.
- Hodgkin, A., & Huxley, A. (1952b). A quantitative description of membrane current and its application to conduction and excitation in nerve. *J. Physiol.*, *117*, 500–544.
- Hodgkin, A., & Katz, B. (1949). The effect of sodium ions on the electrical activity of the giant axon of the squid. *J. Physiol. (Lond)*, *108*, 37–77.
- Ilinsky, I., Jouandest, M., & Goldman-Rakic, P. (1985). Organization of the nigrothalamocortical system in the rhesus monkey. *J. Comp. Neurol.*, *236*, 315–340.
- Jellinger, K. (1987). The pathology of Parkinsonism. In Marsden, D., & Fahn, S. (Eds.), *Movement Disorders 2*. Butterworth & Co., London.

- Jones, E., Coulter, J., Burton, H., & Porter, R. (1977). Cells of origin and terminal distribution of corticostriatal fibers arising from the sensorimotor cortex of monkeys. *J. Comp. Neurol.*, 173, 53–80.
- Juraska, J., Wilson, C., & Groves, P. (1977). The substantia nigra of the rat: A Golgi study. *J. Comp. Neurol.*, 172, 585–600.
- Karabelas, A., & Purpura, D. (1980). Evidence for autoapses in the substantia nigra. *Brain Res.*, 200, 467–473.
- Kimura, H., McGeer, P., Peng, F., & McGeer, E. (1980). Choline acetylcholinesterase containing neurons in rodent brain demonstrated by immunocytochemistry. *Science*, 208, 1057–1059.
- Kita, H., Chang, H., & Kitai, S. (1983a). The morphology of intracellularly labeled rat subthalamic neurons: a light microscope analysis. *J. Comp. Neurol.*, 215, 245–257.
- Kita, H., Chang, H., & Kitai, S. (1983b). Pallidal inputs to the subthalamus: intracellular analysis. *Brain Res.*, 264, 255–265.
- Kita, H., & Kitai, S. (1987). Efferent projections of the subthalamic nucleus in the rat: light and electron microscope analysis with the PHA-L method. *J. Comp. Neurol.*, 260, 435–452.
- Kita, H., & Kitai, S. (1988). Glutamate decarboxylase immunoreactive neurons in cat neostriatum: Their morphological types and populations. *Brain Res.*, 447, 346–352.
- Kitai, S. (1981). Electrophysiology of the corpus striatum and brain stem integrating systems. *Handbook of Physiology — The Nervous System*, 2, 997–1015.
- Kitai, S., & Deniau, J. (1981). Cortical inputs to the subthalamus: intracellular analysis. *Brain Res.*, 214, 411–415.
- Kitai, S., & Kita, H. (1987). Anatomy and physiology of the subthalamic nucleus: a driving force of the basal ganglia. In Carpenter, M., & Jayaraman, A. (Eds.), *The Basal Ganglia II—Structure and Function: Current Concepts, Advances in Behavioral Biology Vol 32*, pp. 357–373. Plenum Press, New York.
- Künzle, H. (1975). Bilateral projections from precentral motor cortex to the putamen and other parts of the basal ganglia. An autoradiographic study in *macaca fascicularis*. *Brain Res.*, 88, 195–209.
- Künzle, H., & Akert, K. (1977). Efferent connections of cortical area 8 (frontal eye field) in *macaca fascicularis*. A reinvestigation using the autoradiographic technique. *J. Comp. Neurol.*, 173, 147–164.
- Lehmann, J., & Langer, S. (1983). The striatal cholinergic interneuron: synaptic target of dopamine terminals. *Neuroscience*, 10, 1105–1120.
- Lipschutz, S. (1968). *Theory and Problems of Linear Algebra*. McGraw-Hill Inc., New York.
- Lohr, J., & Wisniewski, A. (1987). *Movement Disorders. A Neuropsychiatric Approach*. John Wiley & Sons, New York.

- Marcus, C., & Westervelt, R. (1989). Stability of analog neural networks with delay. *Physical Review A*, 39, 347–359.
- Marsden, C. (1982). The mysterious motor function of the basal ganglia: The Robert Wartenberg lecture. *Neurology*, 32, 514–539.
- McClelland, J., & Rumelhart, D. (1988). *Explorations in parallel distributed processing: Volume 3*. MIT Press, Massachusetts.
- McGeorge, A., & Faull, R. (1989). The organization of the projection from the cerebral cortex to the striatum in the rat. *Neuroscience*, 29, 503–537.
- Mensah, P. (1977). The internal organization of the mouse caudate nucleus: Evidence for cell clustering and regional variation. *Brain Res.*, 137, 53–66.
- Moriizumi, T., Nakamura, Y., Okoyama, S., & Kitao, Y. (1987). Synaptic organization of the cat entopeduncular nucleus with special reference to the relationship between the afferents to entopedunculothalamic projection neurons: An electron microscope study by a combined degeneration and horseradish peroxidase tracing technique. *Neuroscience*, 20, 797–816.
- Nauta, W., & Mehler, W. (1966). Projections of the lentiform nucleus in the monkey. *Brain Res.*, 1, 3–42.
- Nakanishi, H., Kita, H., & Kitai, S. (1987a). Electrical membrane properties of rat subthalamic neurons in an in vitro slice preparation. *Brain Res.*, 437, 35–44.
- Nakanishi, H., Kita, H., & Kitai, S. (1987b). Intracellular study of rat substantia nigra pars reticulata neurons in an in vitro slice preparation: electrical membrane properties and response characteristics to subthalamic stimulation. *Brain Res.*, 437, 45–55.
- Nauta, W., & Feirtag, M. (1986). *Fundamental Neuroanatomy*. W. H. Freeman and Co., New York.
- Nicholls, J., Martin, A., & Wallace, B. (1992). *From Neuron to Brain*. Sinauer Associates, Inc., Sunderland, MA.
- Pantelis, C., Barnes, T., & Nelson, H. (1992). Is the concept of frontal-subcortical dementia related to schizophrenia?. *British Journal of Psychiatry*, 160, 442–460.
- Parent, A. (1986). *Comparative Neurobiology of the Basal Ganglia*. Wiley, New York.
- Parent, A. (1990). Extrinsic connections of the basal ganglia. *Trends in Neurosci.*, 13, 254–258.
- Parent, A., & Hazrati, L. (1993). Anatomical aspects of information processing in the primate basal ganglia. *Trends in Neurosci.*, 16, 111–116.
- Park, M., Falls, W., & Kitai, S. (1982). An intracellular HRP study of the rat globus pallidus: I. Responses and light microscope analysis. *J. Comp. Neurol.*, 211, 284–294.
- Percheron, G., & Filion, M. (1991). Parallel processing in the basal ganglia: up to a point. *Trends in Neurosci.*, 14, 55–56.

- Pert, C., Kuhar, M., & Snyder, S. (1976). Opiate receptor: Autoradiographic localization in rat brain. *Proc. Natl. Acad. Sci. USA*, *73*, 3729–3733.
- Pongrácz, F., Poolos, N., Kocsis, J., & Shepherd, G. (1992). A model of NMDA receptor-mediated activity in dendrites of hippocampal CA1 pyramidal neurons. *J. Neurophysiol.*, *68*, 2248–2259.
- Rall, W. (1960). Membrane potential transients and membrane time constant of motoneurons. *Exp. Neurol.*, *2*, 503–532.
- Rall, W. (1967). Distinguishing theoretical synaptic potentials computed for different soma–dendritic distributions of synaptic input. *J. Neurophysiol.*, *30*, 1138–1168.
- Rall, W. (1989). Cable theory for dendritic neurons. In Koch, C., & Segev, I. (Eds.), *Methods in Neuronal Modeling*. MIT Press, Massachusetts.
- Robledo, P., & Féger, J. (1990). Excitatory influence of rat subthalamic nucleus to substantia nigra pars reticulata and the pallidal complex: electrophysiological data. *Brain Res.*, *518*, 47–54.
- Rothwell, J., & Obeso, J. (1987). The anatomical and physiological basis of torsion dystonia. In Marsden, D., & Fahn, S. (Eds.), *Movement Disorders 2*. Butterworth & Co., London.
- Ryan, L., & Sanders, D. (1993). Subthalamic nucleus lesion regularizes firing patterns in globus pallidus and substantia nigra pars reticulata neurons in rats. *Brain Res.*, *626*, 327–331.
- Ryan, L., Sanders, D., & Clark, K. (1992). Auto- and cross-correlation analysis of subthalamic nucleus neuronal activity in neostriatal- and globus pallidus-lesioned rats. *Brain Res.*, *583*, 253–261.
- Servan-Schreiber, D., Printz, J., & Cohen, D. (1990). A network model of catecholamine effects: Gain, signal-to-noise ratio, and behaviour. *Science*, *249*, 892–895.
- Shamma, S. (1989). Spatial and temporal Processing in central auditory networks. In Koch, C., & Segev, I. (Eds.), *Methods in Neuronal Modeling*. MIT Press, Massachusetts.
- Smith, C. (1966). *Biostatistics*. Charles Griffin & Co. Ltd., London.
- Smith, P., & Bolam, P. (1990). The neural network of the basal ganglia as revealed by the study of the synaptic connections of identified neurons. *Trends in Neurosci.*, *13*, 259–265.
- Smith, Y., & Parent, A. (1988). Neurons of the subthalamic nucleus in primates display glutamate but not GABA immunoreactivity. *Brain Res.*, *453*, 353–356.
- Smith, Y., Wichmann, T., & DeLong, M. (1994). The external pallidum and the subthalamic nucleus send convergent synaptic inputs onto single neurons in the internal pallidal segment in monkey: Anatomical organization and functional significance. In Percheron, G., McKenzie, J., & Féger, J. (Eds.), *The Basal Ganglia IV*. Plenum Press, New York.

- Sturrock, R. (1991). Stability of neuron number in the subthalamic and entopeduncular nuclei of the ageing mouse brain. *J. Anat.*, *179*, 67–73.
- Sugimoto, T., Hattori, T., Mizuno, N., Itoh, K., & Sato, M. (1985). Direct projections from the centre median–parafascicular complex to the subthalamic nucleus in the cat and rat. *J. Comp. Neurol.*, *214*, 209–216.
- Tokuno, H., & Takada, M. (1993). Common structural organization of the two output nuclei of primate basal ganglia. *Trends in Neurosci.*, *16*, 308–309.
- Traub, R., Wong, R., Miles, R., & Michelson, H. (1991). A model of a CA3 hippocampal pyramidal neuron incorporating voltage-clamp data on intrinsic conductances. *J. Neurophysiology*, *66*, 635–650.
- Vogt, C. (1911). Quelques considerations générales sur le syndrome du corps strié. *J. Psychol. Neurol. (Leipzig)*, *28*, 479–488.
- Wang, X., Rinzel, J., & Rogawski, M. (1991). A model of the T-type calcium current and the low threshold spike in thalamic neurons. *J. Neurophysiology*, *66*, 839–850.
- Wichmann, T., Bergman, H., & DeLong, M. (1994). The primate subthalamic nucleus. I. Functional properties in intact animals. *J. Neurophysiology*, *72*, 494–506.
- Wickens, J., & Alexander, M. (1993). Analysis of striatal dynamics – the existence of 2 modes of behaviour. *J. Theoretical Biology*, *163*, 413–438.
- Wickens, J., Alexander, M., & Miller, R. (1991). Two dynamic modes of striatal function under dopaminergic/cholinergic control: Simulation and analysis of a model. *Synapse*, *8*, 1–12.
- Wilson, C. (1990). Basal Ganglia. In Shepherd, G. (Ed.), *Synaptic organization of the Brain (3rd Edition)*. Oxford University Press, Oxford.
- Wilson, C., Chang, H., & Kitai, S. (1983). Disfacilitation and long-lasting inhibition of neostriatal neurons in the rat. *Exp. Brain Res.*, *51*, 227–235.
- Wilson, S. (1914). An experimental research into the anatomy and physiology of the corpus striatum. *Brain*, *36*, 427–492.
- Yelnik, J., & Percheron, G. (1979). Subthalamic Neurons in primates: A quantitative and comparative analysis. *Neuroscience*, *4*, 1717–1743.

## Appendix A

# A Multi-level Neural Simulator: Rorohiko

### A.1 The Single Simulator Formalism

The development of multi-level models in order to facilitate the understanding of neural structures is one of the underlying aims of the presented research. Models which can be explored through computational simulation are chosen for their ability to clearly demonstrate responses and behaviours under different situations (varying input, parameters, etc.). However, using different models to explore the same structure from very different perspectives requires a generic simulation medium. We desired a simulator which could fulfill the following criteria

1. Provide a formalism which can describe an artificial neuron with an arbitrary level of detail.
2. Allow the primary description of the artificial neuron and associated parameters to reside in easily understandable and modifiable input files.

3. Encourage effective optimisation of the simulator in order to achieve high operational speeds.
4. Place an emphases on networks of neurons and communication between arbitrary numbers of neurons at any artificial neuron level of description.

Goals 1 and 4, which are vital to the concept of a multi-level simulator, are the most difficult to satisfy in a single formalism. Significant alterations of currently available simulations (such as GENESIS) would be required to achieve a cohesion of these. It was thought more appropriate to design a new simulator with these goals as its defining criteria. In this way, we could begin to explore the processing of the STh at different levels within a single formalism. This in turn facilitates integration and comparison between levels or approaches.

Over the last three years the simulator has developed a great deal, and currently is a very large, multi-functional program. We will therefore only briefly describe the single formalism developed and how the simulator achieves each of the 4 goals above. Other descriptions of the simulator in the context of the principles of neural modelling have also been presented (see Collin, 1995).

#### A.1.1 The Electric Brain

The generic formalism was developed in a single simulator named *Rorohiko*. In Maori (my second native language) new terms, in particular nouns, may be creatively constructed from old terms. The root word “roro” is literally translated to “brain”, and “hiko” literally translates to “lightning”. However, the modern interpretation of “hiko” encompasses the concept of electricity. Thus the noun “rorohiko” may be translated as “electric brain”. Indeed, sometimes this noun is used to refer to computers in general. However, we decided it was an apt name for what we were trying to achieve.

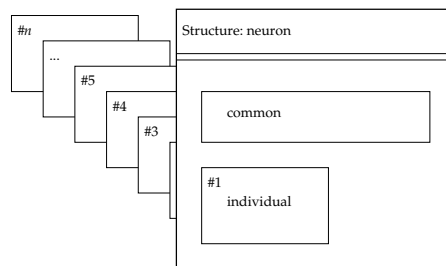


Figure A.1: Simple use of a single structure to create a network of  $n$  simple artificial neurons.

## A.2 The Arbitrary Structure

At the base of all simulations is the primitive building block from which both complex and simple artificial neurons can be built. It is simply named, a “structure”. One of the key aspects to structures is that they themselves hold all parameters and information. Thus *the building block itself is a user definable component*. Therefore, a particular model is defined by first designing the individual structures that are needed and then using the structures to build the entire model. This principle is best illustrated by using examples of the type of models presented in Chapters 4 and 6.

A single structure may be intuitively divided into two parts: *common* and *individual* (see Figure A.1). The *individual* component has an arbitrary depth,  $n$ , and contains specifications that may vary over  $n$  different instances of this structure. For example, if the structure represents a complete artificial neuron, the voltage associated with a particular unit must certainly be individual as there can be  $n$  variations of it. Conversely, the *common* component contains specifications that are common to all *individual* instances of this structure. Following the same example, a voltage–firing rate function may be common to all units. The common component also contains the relationship between instances (for example, weights) and further, the relationship between this and other structures. Thus, the simple model presented in Chapter 4 is represented in a single structure as

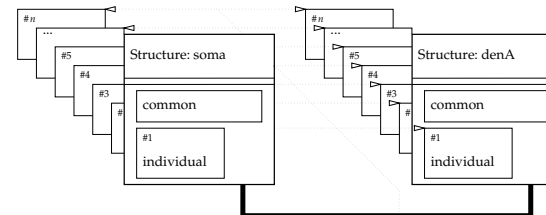


Figure A.2: Simple use of two structure to create a network of  $n$  two-compartment neurons. Each of the individual instances can be simply linked up to counterpart individual instances of other structures.

illustrated in Figure A.1. In this case we only require one structure as the model is relatively simple.

For more complex models multiple structures may be required. For example, a compartmental model with two compartments generally will require two structures, as there can be fundamental differences between compartments (See Figure A.2). However, this does not prevent us from continuing the extension into  $n$  instances. Since individual instances can be associated with instances in other structures we have a very easy way of constructing complex multi-compartmental models with  $n$  artificial neurons. Figure A.2 schematically illustrates a model containing an arbitrary number of artificial neurons, each described by two compartments. It is a straightforward extension to design the multi-compartmental model presented in Chapter 6.

## A.3 Afferents

For all structures only afferents are considered to exist (as opposed to efferents). A structure may be the origin of another structures afferent (in which case it has an efferent), but all inputs are solely viewed from the receiving point of view. Afferents may be considered as arbitrary input lines. Either other structures or *external inputs* may be attached to afferents. All structures have by default a base afferent. This is used, for example, in



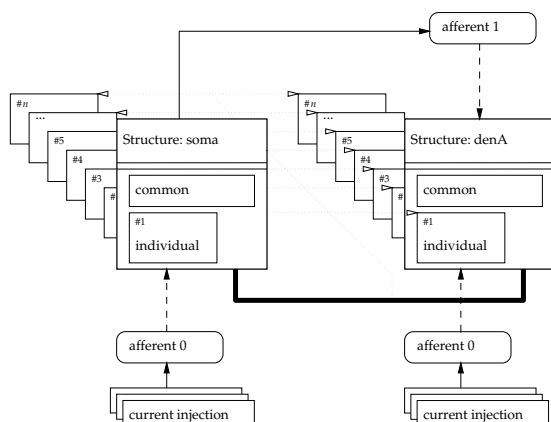


Figure A.3: An example of afferents in a model of  $n$  two-compartment neurons. Afferents are shown external to their structures for simplicity only. They are actually specified as part of the common component of a structure.

multi-compartmental neurons as the current injection source, and in more abstract models as an external input source. Any number of *external inputs* may be defined in addition to this. For example, in variations of the model presented in Chapter 4 an extra external input was created to represent inhibitory pallidal input. Finally, afferents may be associated with entire structures. For example, in the more abstract models, one structure representing the GPe may be an afferent source for another structure representing the STh. At more detailed levels, soma compartments may be afferent sources for dendritic or spine compartments (for example, see Figure A.3).

Afferents are considered within the *common* component of a structure, but their realisation is part of the *individual* component. As far as the primary setup of a structure is concerned it is sufficient to specify connectivity at the structural (rather than instance) level. For example, structure A has an afferent from structure B, despite the fact there may be arbitrary numbers of instances (e.g. units) in each structure. The simulator will automatically fulfill the instance connectivity. This, as with most simulator operations, can be overridden by the user (this is done through explicit weight files).

## A.4 Conductances

The specification and derivation of various conductances can be very complex. In simple models there may be no conductances. However, in more complex models multiple shared conductances may be used. Afferents may be associated with conductances (for example, an AMPA conductance may be defined and triggered by an afferent). Conductances are the soul of multi-compartmental models and may indeed be very complex. Briefly there are seven types of conductances currently provided

- *memory*: conductances that vary only with time, so that the functional form may be stored in memory (e.g. an AMPA conductance).
- *constant*: conductances that are constant for the duration of the simulation (e.g. leak).
- *active*: the specification of conductances via an explicit function which is to be convolved with afferents.
- *volmem*: conductances that vary only with voltage, so that the functional form may be stored in memory.
- *voltage*: a voltage dependent conductance specified by activation and inactivation surfaces (both stored in memory).
- *hh*: Hodgkin Huxley type specification of conductances. If this form is used the Hodgkin Huxley type equations can be specified and sufficient precalculations stored in memory. This is a specialised form of the generic *voltage* type.
- *calc*: the specification of conductances via an explicit function, without afferent convolution (e.g. the GHK calculation). This is a last resort approach as it is the least efficient of all types.

The variation in conductance types is orientated towards achieving simulation efficiency. It is assumed (generally correctly) that simulations that use multiple conductances require all methods of optimisation. Storing conductance functions in memory (if possible) significantly increases simulation speed.

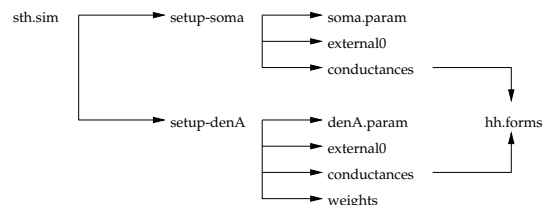


Figure A.4: Example input file structure that could be used for the two compartment model of Figure A.3. Each name represents a file, and pointers represent hierarchical reference. Notice the same Hodgkin Huxley channel specification file can be used by both compartments.

## A.5 Input Files

Almost all model specification is done through simulator text input files. These can be organised in many different ways, which is itself completely up to the designer (for example, conceptually different parts of the model design may be put into separate files or directories). The simulator requires a core setup file specifying how the model is to be setup. This may be given as an argument to the simulator program. The primary purpose of this file is to define basic simulation parameters (for example, the numerical algorithm to be used) and each structure in the model. For example, consider the two compartment model of Figure A.3. The structures may be setup using the commands

```

# ** structure locations:
#
structure      setup-soma
structure      setup-denA
  
```

This indicates that the file `setup-soma` contains all the specifications for setting up the soma structure. Each structure is given a reference number by the designer that can be used throughout the entire setup when reference to that particular structure is required. Figure A.4 illustrates a typical file hierarchy used in multi-compartmental models.

The simulator has a primitive text parser so that detailed information can be specified in an easy to interperate form. For example

```
link afferent 1 to structure 1
```

this statement links afferent 1 of the current structure being setup to the structure with reference number 1. Easy to interpret input files are invaluable in the construction of complex models.

The complete simulation configuration files of the model presented in Chapter 4 are included in Section A.7.

## A.6 Optimisation

Hand optimisation of certain parts of the C code is required. The specification of the primary equations defining the simulation currently must be given as a C function called `derivs`. Furthermore, the Hodgkin Huxley type equations must also be hard coded into the program. Generally this does not require a great deal of work, as all the major setup is done by the simulator and input files. The alternative would be to incorporate an equation interpreter into the simulator. However, these can never reach the optimisations gained by hard coding the primary equations. It was thus decided it would be a significant advantage to enforce the hand optimisation.

One of the major disadvantages of this approach is that it requires the model designer to understand the basics of the C language. For the purposes of the current project this was acceptable for achieving goal 3 of Section A.1. Further development of this simulator could follow a dual approach where hand optimisation becomes an option.

## A.7 Example Simulation

This example is for a specific simulation of the model presented in Chapter 4. The hierarchical file organisation is illustrated in Figure A.5

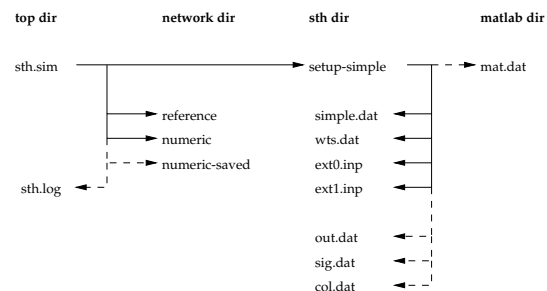


Figure A.5: The input file structure used in simulations of the model described in Chapter 4. Solid lines indicate an input file, dash lines indicate an output file.

### A.7.1 sth.sim

The main input file given as an argument to the simulator program. [Note that BIO3 and BIO3a are names of the simulator during its development.]

```

# BIO3 format simulation configuration file (sth.sim)
#
# ** maximum number of structures (used in memory control):
#
maximum structures    50
#
# ** structure locations:
#   NB in linear order
#
structure             network/sth/setup-simple
#
# ** report level (how much info for standard output):
#
report                80
#
# ** file to report too:
#   NB (default is stdout)
#
report file          sth.log
#
# ** location of the reference file:
#
reference file        network/reference
#
#
  
```

```

# ** standard form value (work in what value msec,sec...)
#
standard form         1.0e-00
#
#
# ** Numerical integration parameters:
#
start time            0.0
finish time           300.0
fixed step size       0.5
accusary              1.0e-7
first step geuss      1.0e-1
minimum step          1.0e-25
save at fixed or      0.0
#
# ** choice of numerical integrater (depends on derivs)
#   1 = fifth order adaptive Runge-Kutta (default)
#   2 = fourth order adaptive Rosenbrock (requires jacob)
#   3 = fifth order adaptive Cash-Karp Runge-Kutta
#
integrator            3
#
# numerical start file network/numeric
# numerical save file  network/numeric-saved
#
  
```

### A.7.2 reference, numeric, numeric-saved, and sth.log

None of these files will be included as they are all data files. The `reference` file is part of an automated reference system that gives each simulation a unique reference for cataloging. The `numeric` and `numeric-saved` files are optional beginning and endpoints of the numerical integration. Finally the `sth.log` file is where simulation messages and warnings are written (note its definition in the primary setup file example in Section A.7.1). If none is specified standard output is used.

### A.7.3 setup-simple

Setting up the structure for the simple model. In this case it is primarily used as pointers to other files.

```

# setup file for the subthalamic nucleus (STH)
# BIO3 format Simple Model
#
#
# ** structure reference number:
#
#   structure reference          1
#
#
# ** file locations:
#
#   parameters          network/sth/simple.dat
#   results             network/sth/out.dat
#   signal results     network/sth/sig.dat
#   collateral         network/sth/col.dat
#   weights            network/sth/wts.dat
#
# Common
#
#
# External Inputs
#
#   external0          network/sth/ext0.inp
#   external1         network/sth/ext1.inp
#
# Hodgkin Huxley stuff
# (a number specifies that it is to point the information to
# the specified structure reference);
#
#
# matlab parameter file
#
#   matlab             network/sth/mat.dat
#

```

#### A.7.4 simple.dat

This file contains the primary parameters for the structure (see the “parameters” line in the setup file of Section A.7.3).

```

# Subthalamic nucleus (STH) general parameters
# BIO3a format simple.dat file
#
# Setup file for the SIMPLE network
#
# ** number of units in this structure:

```

```

#
#   units                500
#
#
# ** number of differential equations that describe a neuron:
#
#   equations            1
#
#
# ** number of explicit equations used in a neuron description:
#   NB: not strictly necessary - see conductances.
#
#   explicit              0
#
# ** number of conductances in a neuron:
#   NB: in equations above, one is assumed for voltage,
#       the rest are dedicated to conductances, Any
#       conductances not associated with an equation are
#       assumed explicit.
#
#       (equations - 1) + explicit = conductances
#
#   conductances         0
#
#
# ** number of afferents to this structure:
#
#   afferents            1
#
#
# ** LINKING AFFERENTS
#
#   afferents can either come from other structures, or from
#   external inputs.
#
#
# ** link afferent 1 of this structure to structure (ref) 1
#   (neighbouring somas, i.e. receives inputs from
#   neighbouring somas)
#
#   link afferent 1 to structure 1
#
#
# ** AFFERENT EFFECTS
#
#   which afferents effect which conductances! the
#   conductances must not be constant, and any afferent
#   can effect any number of conductances.
#
#   afferent 1 effects conductance 1
#
#
# ** specify if the collaterals are regularly spaced
#
#   regular                1

```

```

#
#
# ** what percentage of units have collaterals
#
# percent collaterals      100.0
#
#
# ** normalise weights ?
#
# normalize weights        0
#
#
# ** get weights from a file (1=yes)?
#
# use weight file          0
#
#
# ** Gaussian beta width for each afferent
#
# Gaussian weight beta 1    0.0002
#
#
# ** Gaussian peak height for each afferent
#
# Gaussian weight peak 1    0.002
#
#
# ** SIMPLE network designs can take advantage of speedspace
#
# speedspace                1
#
#
# ** CONDUCTANCES
#
# ** EXTERNAL INPUTS
#
# background : constant background value for this external
#               input.
# type : type of external input;
#         current (0) = current injection.
#         discrete (1) = discrete piled input events.
#         sustained (2) = on, off sustained input.
#         [NB: background does not apply in discrete types]
# input file : where to get external input events from, it
#               may be an explicit file name or a reference
#               to a file listed in this structures setup
#               file.
# history : the number of timesteps required to capture
#               the firing form information.
#
#
# ** setup external 0 (always present, for current injection)
#

```

```

make external 0
  background      0.0
  type            current
  input file      external0
end
#
#
# ** initial voltage
#
# initial voltage      0.0
#
#
# ** voltage to reset to after a fire (only for voltage action 4)
#
# voltage reset        -55.0
#
#
# ** voltage reset delay, i.e. number of steps before reset
#   engaged (only for voltage action 4)
#
# voltage reset delay    0
#
#
# ** what to do when voltage hits threshold;
#   1: do nothing and use firing rate in conductance
#   convolutions
#   2: fire on threshold using calculated firing rate function
#   3: leave everything to conductances
#   4: fire, then subtract the voltage reset above.
#
# voltage action        3
#
#
# ** when a unit in this structure fires, perform a voltage
#   reset on the same unit in the structures specified here
#   - only for voltage action 4 and only useful for
#   compartmental models. The specified structure to trip
#   must also be voltage action 4, and will be reset to
#   *its* vreset!
#
#   here structures 2 and 3 will be reset with this structure
#
# voltage trip reset    2
#
# voltage trip reset    3
#
#
# ** make the initial voltage include a random fluctuation
#   (if > 0)
#
# voltage initial random      0.0
#
#

```

```
# ** maximum firing rate
# (used in calculating spike trains: zmax) units msec-1
# here, as tau is in msec, and ythres in mV.
#
# sigmoid max          0.5
#
#
# ** threshold in sigmoid threshold function (y0)
#
# sigmoid threshold    22.0
#
#
# ** beta in sigmoid function relating voltage to firing rate
# (zbeta)
#
# sigmoid beta         0.1
#
#
# ** offset in sigmoid function relating voltage to firing rate
#
# sigmoid offset       0.0
#
#
# ** global tau used for simple equations
#
# global tau           6.0
#
#
# ** delay on afferent 1 (in multiples of system dt)
#
# delay on afferent 1  0
#
#
# ** external background input
#
# external background  0.0
#
#
# ** special variables
#
# ** specialN variables
#
#
```

### A.7.5 All other files

The file `wts.dat` simply specifies override weights if the autogenerated ones are not sufficient. The weights and connectivity used in the simulation can be confirmed by

looking at `col.dat`. The files `ext0.dat` and `ext1.dat` specify the external inputs. The file `out.dat` is the primary simulator output file. For large simulations this can be large. Finally, `sig.dat` provides an alternative output format.

## Appendix B

# Automated Numerical System Solution Search

In order to provide a simple graphical approach to aid the understanding of how parameter changes affect the solutions of dynamical systems (for example, Figure 5.3) a small program was constructed to numerically calculate solutions over changing parameters. Here we do not want to numerically integrate the system as the solutions reached through this approach depend on the initial conditions. An extensive search would then be required to find all possible solutions. Rather, we adopt a simple phase analysis approach, where phase planes are computationally analysed in a simple manner to reveal approximate sinks and sources. This yields a reasonably quick algorithm which can locate stable solutions to a given accuracy.

### B.1 Recursive Depth Search

A recursive algorithm is used that divides a given solution space into sectors. Each sector is analysed for flow patterns. For example, Figure B.1 illustrates a simple division of a phase plane, and highlights a sector that contains a flow pattern of interest. In this

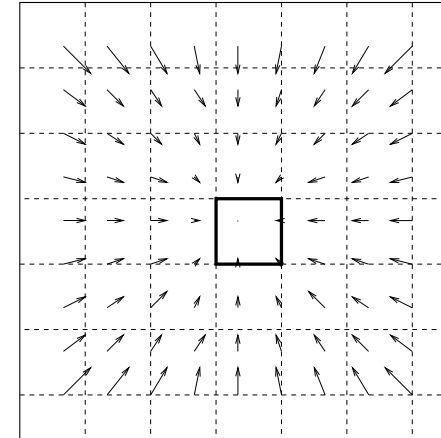


Figure B.1: A simple phase plane showing sector division and the highlighting of a sector with an identified flow of interest (in this case a sink).

example, the flow is a sink. The sectors identified with recognisable flows are then recursively analysed until the accuracy of a particular point is reached. For example, the sector highlighted in Figure B.1 can be recursively subdivided.

The choice of subdivision parameters plays an important role in the speed of search, furthermore, coarse parameters can miss points of interest. It is stressed that this is a numerical approximation approach designed to extract solutions of interest with minimal computational expenditure. Other more rigorous methods should be used if independence from search parameters is required. For our purposes, this algorithm has been a very useful tool in the analysis of system behaviours.

## Appendix C

# Geometric and Spatial Simulator

In order to gain some insight into the connectivity of neurons in the STh we introduce geometric approximations of the neurons dendritic and collateral fields. From these we would like to perform a number of different investigations. For example, given a regular 3D array of neurons each with dendritic fields of randomised orientation, how many of these will a completely immersed collateral intersect. For more advanced purposes we would like to simulate the complete geometric arrangement of the nucleus with random placement of the fields and collaterals (and example of this is illustrated in Figure 4.5). This would lead to a complete instance of connectivity given by the random placements. We therefore required a general simulator that could take arbitrary shapes as representative of dendritic and collateral fields, and place them in a user specified virtual 3D space (given density, orientations, etc.). For example, the user may wish to specify that all dendritic fields have a certain orientation (for example, an orientation parallel to that of the STh itself, as experimentally found) yet with a random variation given by a Gaussian mean and standard deviation.

As a result of the diversity of tasks required from the simulator, it was decided that a common library should be build to manipulate the 3D objects in a virtual space. A C library was constructed and is simply called "xyz". From the library a number of programs were built as useful tools in the analysis of the geometric models of the STh. Each of these programs will be briefly outlined in the following sections.

### C.1 Immersion

Given a neuron density, and prototypical dendritic and collateral fields, this program calculates the number of neurons needed to completely immerse the collateral, and generates virtual space composed of sufficient matter to accomplish this. Random variations in position, size of dendritic field and orientation may also be specified.

The output files created are:

- `pneurons.dat` contains raw data: for every dendritic field that had overlap with the collateral field the dendritic field reference and amount of overlap is given.
- `poverlap.dat` contains summary data: a file containing summaries of the numbers of dendritic fields for different percentage volume intersections.

A MATLAB<sup>®</sup> script which automatically plots results with appropriate scales is also included.

### C.2 Orientation Search

This program is a simple extension of the previous one. Given a neuron density and prototypical dendritic and collateral fields, the program calculates the number of neurons needed to completely immerse the collateral, and generates virtual space composed of sufficient matter to accomplish this. Each dendrite created has an orientation that is varied from  $0-\pi/2$ . This effectively calculates effects of different orientations of interaction between the dendritic and collateral fields.

The output files created are:

- `pmatrx.dat` contains summary data: for each general orientation (at a given orientation step) a summary of the dendritic/collateral field intercepts is given.

A MATLAB<sup>®</sup> script which automatically plots the 3D results is also included.



### C.3 Simulation

Given a neuron density, prototypical dendritic and collateral fields, and a specific number of neurons ( $N$ ), this program creates an appropriate geometric representation of those neurons in a virtual space. Random variations in position, size of dendritic field and orientation may also be specified. The program produces the positions of neurons, a record of the size and orientation of all dendritic fields, a weights calculation based directly on dendritic/collateral field overlaps, and the position of all the collaterals for each neuron (which may also be given random variations).

The output files created are:

- `pos.dat` unit positions: this file has  $N$  lines (i.e. a line for each unit). Each line holds the 3D position of the associated neuron soma.
- `denor.dat` dendritic field descriptions: this file also has  $N$  lines. Each line holds the orientation of the dendritic field (same order as in `pos.dat`) in the form of the two oblate spheroid axes positions (specified by 12 real numbers).
- `col.dat` collateral descriptions: This holds the positions of each collateral of each neuron. Each line holds one collateral, firstly the number of the neuron to which it belongs, then its start and finish points.
- `tw.dat` intersection file (weight file). A list of weights. Each line contains one weight. All weights are included, and are given in the same order as positions are in the `pos.dat` file. For example, if there are 1000 units, the first 1000 numbers and lines are the weights from unit 1 to all other 1000 units. The second 1000 are the weights of unit two etc.. In total there will be  $N \times N$  lines. The format of the file is such that it can be read directly into the *Rorohiko* simulator as explicit weights.

### C.4 Visualisation

As the conceptualisation of virtual 3D space containing complex object placement and interactions is difficult<sup>1</sup>, a visual tool was also developed. This not only provided a quick method of viewing a given geometric arrangement but also allowed the results of the programs above, and in particular the library, to be confirmed visually.

Since we are dealing with simple geometric forms, it was obvious the best visualisation of such objects and their interactions could be achieved using a Constructive Solid Object ray tracer (CSO). We choose the public domain ray tracer “Rayshade” for this purpose. Thus the task of the visualisation program is to translate the complex 3D virtual space used by the xyz library into the Rayshade CSO language. Once this was done, the ray tracer could be used to visualise the 3D space from any position, perspective, or lighting. Figure 4.5 is an example of the final output.

Two visualisation programs have been created. Firstly, a program to display and confirm the interactions in the geometric arrangements (for example, Figure 4.5). Secondly, a program designed to take the output of the *Rorohiko* simulator and display activity values of neurons in the virtual 3D space at any point in time. Activity values can either be displayed in terms of colour (for example, the “hot” scale) or size. This is only useful when simulations with clear geometric arrangements are being used (for example, with weights given by the geometric calculations, where specific activities will be effected by spatial position).

### C.5 Summary

The use of simple geometric volumes in approximations of anatomical arrangement provides a useful perspective on network interactions. However, one of the major disadvantages is that the geometric shapes are often too simple. It is hoped the these tools may be

<sup>1</sup>Note, this tool in fact was developed early to aid in the development of the other tools, as the manual confirmation of the complex 3D spaces was found too difficult.

developed further to allow the consideration of complex shapes. There is no reason why more dendritic-tree like structures may not be used in such network arrangement calculations. For example, the artificial neuron given in Figure 6.10A was constructed with similar techniques to some of those used in the xyz library. It would be very interesting to extend the library so that more complex dendritic trees may be explored.